NORTHWESTERN UNIVERSITY

Deformation and Fracture of Cross-linked Polymer Gels

A DISSERTATION

SUBMITTED TO THE GRADUATE SCHOOL
IN PARTIAL FULFILLMENT OF THE REQUIREMENTS

for the degree

DOCTOR OF PHILOSOPHY

Field of Materials Science and Engineering

By

Wei-Chun Lin

EVANSTON, ILLINOIS

December 2007

ABSTRACT

Deformation and Fracture of Cross-linked Polymer Gels

Wei-Chun Lin

Because soft materials, particularly polymer gels, are playing a greater role in industrial and biotechnological applications today, the exploration of their mechanical behavior over a range of deformations is becoming more relevant in our daily lives. Understanding these properties is therefore necessary as a means to predict their response for specific applications. To address these concerns, this dissertation presents a set of analytic tools based on flat punch probe indentation tests to predict the response of polymer gels from a mechanical perspective over a large range of stresses and at failure.

At small strains, a novel technique is developed to determine the transport properties of gels based on their measured mechanical behavior. Assuming that a polymer gel behaves in a similar manner as a porous structure, the differentiation of solvent flow from viscoelasticity of a gel network is shown to be possible utilizing a flat, circular punch and a flat, rectangular punch under oscillatory conditions. Use of

the technique is demonstrated with a poly(N-isopropyl acrylamide) (pNIPAM) hydrogel. Our results indicate that solvent flow is inhibited at temperatures above the critical solution temperature of 35^{o}C.

At high stresses and fracture, the flat probe punch indentation geometry is used to understand how the structure and geometry of silicone based gels affect their mechanical properties. A delayed failure response of the gels is observed and the modes of failure are found to be dependent on the geometry of the system. The addition of a sol fraction in these gels was found to toughen the network and play an important role at these large deformations. Potential mechanisms of fracture resistance are discussed, as is the effect of geometric confinement as it relates to large scale deformation and fracture. These results lay the groundwork for understanding the mechanical response of other highly, deformable material systems utilizing this particular geometry.

To my parents, Tong and Newman,

and my sister, Chau-Fang,

Thank you for believing in me.

ACKNOWLEDGEMENTS

It is often hard to predict where life will take you and who you will meet along the way. I was lucky in this sense to be able to pursue my graduate studies at Northwestern and meet a number of wonderful people who saw me through the endeavor. I would also like to recognize and thank the people from my past who have always been my cheerleaders.

First and foremost, I would like to send my gratitude to my advisor, Dr. Ken Shull. Ken has been a wonderful mentor and role model. He is one of the most patient people I have ever met and his patience and encouragement allowed me to grow into an independent, self-confident researcher over the years. His love for continued learning, dedication to his family, and his kindness are all qualities that I value and instill in my own life. As my advisor, he helped shape my current approach to problem-solving in all walks of life, teaching me to look at the big picture, and ask the appropriate questions. He truly looks out for his students and I must thank him for supporting me into my next endeavor. He is one of the reasons I will miss my time at Northwestern dearly – working with him has been a great experience.

Along with Ken, I would like to thank my collaborators, Dr. Herbert Hui and Dr. Claire Lin, who have been influential throughout my graduate career as well. I met Herbert during my first summer at Sandia National Laboratories and I want to express my appreciation to him for treating me as one of his own students. His uncontained enthusiasm over the years has been an endless source of inspiration and made research

a lot fun. He has been more than an academic mentor, providing me with sound advice on life in general, and impressing colleagues and students alike with his impressive athletic ability of being able to outrun most graduate students. I also want to acknowledge Dr. Claire Lin, whom I met at several conferences, for her thoughtful discussions on our research and for her perspective on being a female professor with a family in Taiwan and in the United States.

Additionally, Professor Shef Baker, my Cornell University undergraduate advisor, played a crucial role in my academic career. It was with Prof. Baker's encouragement that I decided to apply to and attend Northwestern. From the days of my freshman year in college, he has gone above and beyond his call of duty as an undergraduate advisor. His drive and ambition inspire me to always strive for the best in my life. To this day, Prof. Baker still provides guidance and advice regarding my career, even as I begin the journey to France to start the next chapter of my life. He is truly one of the most influential people in my life and it is for all this that I thank him.

I also wish to recognize my committee members and colleagues from Northwestern. The insight of my committee, which consisted of Dr. Monica Olvera, Dr. Phil Messersmith, Dr. Wes Burghardt, and Dr. Katherine Faber, was very helpful in preparing this document. Thank you to Dr. Faber for providing detailed commentary on my draft and to Dr. Burghardt for joining my committee at the last minute.

At Northwestern, I also had the opportunity to work with a number of collaborators and a number of talented people, many of them in the Shull group. In the beginning of graduate school, I collaborated on a few projects with Dr. Lonnie Shea

and a few of his students, as well as Dr. Phil Messersmith and his student, Dr. Bruce Lee. I was also able to work with a number of past Shull group members, who have now since graduated. These people include Dr. Rebecca Webber, Drs. Nelson and Michelle Nunalee, Dr. Chi-Yang Chao, Dr. Rachel McSwain, Dr. Peter Drzal, Dr. Elizabeth Martin, Raj Boya, and Dr. Rodney Guico. Furthermore, I would like to acknowledge the current Shull group members for their encouragement and help. These people include: Michelle Seitz, Dr. Anny Flory, Murat Guvenderin, Daniel Carvajal, David Brass, Rafael Bras, Andy Schoh, Aleta Hagman, Raj Boya, Katie Otim, Kevin Henderson, Kendra Erk, Yan Sun, and Marc Palmeri. I am especially grateful for crossing paths with Michelle Seitz, Anny Flory, Murat Guvenderin, and Drs. Michelle and Nelson Nunalee for their comments, critiques, and ideas throughout graduate school. Without their insight, I would not be where I am today and working on this dissertation would have been a more arduous task. *Merci beaucoup!*

My work at Northwestern would have been difficult to accomplish without the funding and support of Sandia National Laboratories. For the opportunity to work there, I want to acknowledge Dr. Phillip Cole, Dr. John Emerson, Dr. Joe Lenhart, and Dr. Mike Kelly. Phillip and Joe were continually supportive of my project from an academic standpoint and our discussions led to development of some of the ideas in this document. Furthermore, I met and worked with several people at Sandia, who were quite helpful in more ways than one. Kudos to: Scott Spanglar for acquisition of rheology data; Kevin Austin for assistance in setting up the R200; Duane Schneider and Jennifer Corona for the extraction data; John Schroeder for material inventory; G. Craig

Clark, Bob Winters, and Nina Baum for assistance in sample preparation; and Tony Romero for making all the new probes for the fracture tests with an unbelievable turn-around time. I hope to see Nina in the 2008 Olympics.

Outside of Northwestern, there were a number of people who truly opened up my mind and perspective during my time in graduate school. In New Mexico, I am especially grateful to have met and lived with Jo Ann and Colin Smith, who always made me feel like part of their family. Because of them, I had a great time in New Mexico and will always have wonderful memories of my stay there. I do not think they realize how much it meant to me when they were able to attend my hooding in Evanston. I would also like to thank Joyce Bogusky, who with two Ph.D.s taught me the value of patience and discipline, as well as the power of mind. It was only after studying several years of pilates, yoga, and mediation with her that has led me to a more open heart and greater learning. She is probably one of the most learned and spiritual people that I know. My gratitude also goes to Kim Schwartz, my yoga teacher in New Mexico, Fury Gold, my ballet instructor, and Dr. Carolyn Montford, my school counselor. These people taught me to step back and look at life from different points of view. It was through working with them that I developed a greater understanding of the patterns that we all live by, whether it be in our emotions, behavior, or movement. And, I will always be indebted to my friends/mentors at the Cornell Club of Chicago: Katherine Cornell, Jen Hernandez, Phyllis Richardson, Celia Rodee and Peter Cooper, Diane Baker, and Evelyn Taylor Pearson. The opportunities, advice, and support with which they have provided me made me feel much at home in a city where one could

easily feel lost. I would especially like to thank Celia, Diane, and Evelyn, whose teas and lunches, made me realize that it was possible to balance life and a career. These women have been a source of inspiration in my professional and personal life.

On a more personal note, I will never forget my close friends, some of whom I met at Northwestern and some of whom I have known from my past. At Northwestern, I am indebted to Feng Qu, Prakash Kolli and Nandini Koka, Larry and Melissa Aagasen, and my roommate, Rebecca Gray. I am not sure if I would have survived graduate school in one piece without you. I am also thankful for those of you, who injected fun and spontaneity into my life: Liz Kelly, Michelle Yu, and Melissa LoPinto as well as those who fed me, Chiew Hoon and Hon Sing Lee. Thank you also to Justin Kim for fond yet bittersweet memories of Chicago. And, of course, there are those people that I would never forget, the ones that I have known for many years, the ones that keep me smiling in good and bad times. My gratitude goes to Andrea Kmicikewycz, Herman Mak, Duane Wardally, Urbashi Poddar, Li-fen Chen, Miguel Valadez, Saba Deyheim, Tiffany Wong, Meredith Baum and George Tucker, and Jennifer and Chuck Tucker. I would never have gotten so far if they were not around to pick up my late phone calls and cheer me up at random times. True friends like them are hard to come by.

Most importantly, I want to thank my parents, Tong and Newman, and my sister, Chau-Fang, for their continuous love and support. Thank you for encouraging me to follow my dreams and to dream big. Because you believed in me, I believed in myself.

LIST OF SYMBOLS

a	Contact radius
A	Contact area
c	Concentration of polymer in solution
C	Compliance
c*	Critical concentration
d	Pore size of gel
D_C	Cooperative diffusion coefficient
D_p	Permeability of gel
E	Young's modulus
E_L	Longitudinal modulus
erf(f)	Error function
$F(t)$	Generalized function to describe time relaxation function
G	Shear modulus
G'	Storage modulus
G"	Loss modulus
G_e	Entanglement plateau modulus
G_x	Modulus due to cross-links
h	Sample thickness
J	Flux
k_B	Boltzmann's constant
L	Length of rectangular indenter
M	Molecular weight of polymer chain
M_e	Molecular weight between entanglements
M_x	Molecular weight between cross-links
N	Number of monomers
Δp	Pressure gradient
P	Load
P_ω	Load amplitude in oscillatory test
P_∞	Load at $t=\infty$ or long times for a single relaxation curve
P_0	Initial load at $t=0$ for a single relaxation curve
P_{ss}	Steady state load displacement
R	Universal gas constant
R_0	End-to-end distance for a self-avoiding walk
t	Time
T	Temperature

Y_∞	Load response for long times per unit displacement
$Y(t)$	Load response per unit displacement
Y_0	Initial load response per unit displacement
γ	Step strain
δ	Measured displacement
δ_0	Unit displacement
δ_{ss}	Steady state oscillatory displacement
δ_ω	Displacement amplitude
Δ	Phase angle
ϕ	Polymer volume fraction
η	Viscosity
λ	Fractional relaxation due to solvent flow
μ	Extension ratio
κ	Time normalized by indenter radius
ν	Poisson's ratio
ν_{eff}	Effective Poisson's ratio
ν_∞	Poisson's ratio at $t=\infty$ or long times
π	Pi
$\prod$	Osmotic pressure
ρ	Density
σ	Applied stress
σ_{avg}	Average engineering stress
τ	Relaxation time
ω	Frequency
ξ	Correlation length
Ω	Normalized frequency
$\Im$	Tearing energy
$\mathcal{E}$	Elastic strain energy

TABLE OF CONTENTS

LIST OF TABLES

CHAPTER 4

CHAPTER 5

LIST OF FIGURES

CHAPTER 2

CHAPTER 3

CHAPTER 4

CHAPTER 5

CHAPTER 1

INTRODUCTION

CHAPTER 1

INTRODUCTION

1.1 RESEARCH MOTIVATION

In the late 1980s to early 1990s, the mechanical properties of soft materials in biomedical applications attracted a great deal of media attention. The health and safety of an estimated one million to two million women were at risk [1]. Lawsuits were filed against several large companies, such as Dow Corning Wright, and the Food and Drug Administration began to question the ethics of scientific practices in business. A stir surrounding silicone gel breast implants inundated the country.

The cause of concern dealt with a lack of understanding on the mechanical and transport properties of materials used in the implants. A dearth of knowledge existed on the un-cross-linked silicone fluid that was used to fill the prosthetic and the cross-linked silicone elastomer shell in which it was encased. For over thirty years, no one had predicted that the fluid would diffuse readily into and through the elastomer, and that the swelling of the shell by the silicone fluid would adversely affect the mechanical properties of the shell [2]. Basic polymer science principles had been ignored.

As a result of the impending lawsuits and a number of women affected, the FDA called for a moratorium on the devices in 1992 that sparked several studies on the

prosthetics. Officials at Dow Corning, the manufacturer, maintained that the implants were safe. However, evidence in literature suggested otherwise [1]. Studies showed that swelling of the outer shells from the silicone oil led to an overall decrease in the mechanical strength and properties of the outer layer. These results suggested that the degradation of the silicone elastomer shell caused the high incidence of rupture in these devices [2]. Although the safety of these devices is still unresolved today, the results of this case study demonstrate the importance of studying soft materials over a range of deformations.

The silicone implant example is an extreme case of how the mechanical properties of a soft material can affect legal, health, and safety issues in a community. In our daily lives we often encounter situations of a similar nature, where prediction of the behavior in material is important to know as its physical properties change. Consider for example the diffusion of a solvent into a material. At a picnic, we opt for the paper plates that have the greatest strength when oil or grease diffuses into them. The same logic would apply to buying paper towels or even, a baby's diapers. Learning to control and predict such properties of materials over a large range of deformations becomes an important aspect of everyday life. This topic is particularly relevant as soft materials play a greater role in industrial applications and biotechnology.

1.2 OVERVIEW

The purpose of this dissertation is to encompass the elements necessary to explore the behavior of soft materials, particularly polymer gels, over a range of strains and at fracture. The thesis is divided into five chapters, following this introduction, and is summarized at the end to clarify the reader's understanding.

The fundamental principles and background necessary to understand this research are described in Chapter 2. Definitions of polymeric structures and an overview of the systems of interest are first introduced. A discussion describing the mechanics and dynamics of these systems follows. Chapter 2 closes with a review of an axisymmetric indentation technique, a method that is applied to all our experiments.

The experimental work of this thesis is discussed in Chapters 3-5. Each of these chapters focuses on the mechanical properties of our materials in three distinct regimes: at small strains, large deformations, and failure. Chapter 3 discusses the use of mechanics to predict internal transport behavior of polymer gels in the Hookean region. A novel indentation technique and model are presented to determine the solvent diffusion within a hydrogel system at small strains. Subsequently, Chapters 4 and 5 aim to understand the behavior of polymeric materials beyond the linear elastic regime. In these chapters, highly, deformable silicone gels are used as model systems. Characterization of these silicone materials over a range of stresses prior to fracture is the focus of Chapter 4. An understanding of the addition of sol fraction within these samples is detailed. Chapter 5 extends our knowledge to include fracture of these

systems. The mechanism of indentation fracture is described and related to the physical properties of these gels.

Conclusions of the presented experimental work are summarized in Chapter 6. The implications of our results are noted and further discussed as a vehicle to motivate future experiments in this area of research. The purpose of Chapter 6 is to serve as a bridge for future endeavors on this topic.

CHAPTER 2

BACKGROUND

CHAPTER 2

BACKGROUND

2.1 INTRODUCTION

Polymers, and their respective mixtures and solutions, are a class of materials that form a large subset of soft condensed matter. As with metals and ceramics, the properties of polymeric materials are intricately related to their chemical and physical characteristics. Despite the various ways that polymeric materials can be synthesized, there are universal characteristics that surface from the generic traits found in long, chain-like molecules. Because these commonalities are even more apparent when the string-like molecules overlap and create networks, an understanding of how and why they behave is crucial. Various polymer structures and classifications need to be discussed and the fundamental models and theories that govern their properties from a mechanical and dynamic perspective reviewed. Equally as important is the knowledge of how to characterize them. Such topics, which help to tie together the experimental work for this thesis, are examined in this chapter.

2.2 POLYMER STRUCTURES

The term, ‘polymer’, originates from Greek roots and its meaning can be translated as ‘consisting of many parts’[3]. In general, a polymer is a giant molecule

that is formed from a number of structural repeating monomer units that are covalently bonded in a long chain. The entire structure of a polymer chain is generated during polymerization, in which the chemical identity of the monomers determines the characteristics of the system. The properties of a polymer chain are also dependent on the way the atoms arrange themselves during the polymerization process. Depending on the type of monomer used for a polymer, polymeric materials can form a variety of architectures, ranging from linear[4] to ring[5] molecules, as well as star-branched[4, 6] and randomly branched[4, 5] archetypes, as shown in **Figure 2.1**. Such polymer architectures are the basis of more complex polymeric structures, such as polymer networks and gels.

2.2.1 Polymer Networks and Gels

When a high degree of cross-linking is available among polymer chains, such as in the case of randomly branched polymer strands, a three-dimensional polymer structure can form[4]. The formation of this structure can be a polymer network or gel, depending on the extent of reaction during polymerization[7]. A polymer network is formed when nearly all linear strands are attached to create a single, interconnected polymer, as seen in **Figure 2.2(a).** This large macroscopic molecule is created at a certain extent of reaction and is defined by infinite branching. Polymer gels, on the other hand, are a form of diluted polymer networks, where the diluent can be other

polymer chains or solvent. A polymer gel is a system that contains a network but is also permeated by a number of independent, unentangled and unlinked finite polymer strands[8], as seen in **Figure 2.2(b)**. This two component system is defined by its network and its continuous phase of polydispersed chains, or sol. It is formed when the extent of reaction is not reached for a molecule with infinite branching.

The formation of these three-dimensional systems is dependent on how the polymer chains are organized and linked. Chemically cross-linked networks are the result of chemical bonds between polymer strands, whereas physical networks are formed from physical bonds. Hence, polymer gels can be classified as either chemical or physical gels, depending on the nature of their network. **Figure 2.3** illustrates the types of bonding in these gels. Physical gels are characterized by temporary associations (**Figure 2.3(a)**), whereas chemical gels are covalently bonded (**Figure 2.3(b)**). These temporary associations can range from helical structures to nodules of block copolymers[8]. In a triblock copolymer gel, for example, the aggregation of endblocks due to the influence of a solvent is one type of physical bond that is possible in a gel system[9], as depicted in **Figure 2.3(a)**.

2.2.2 Systems of Interest

Within the above classifications, polymer networks and gels can be further grouped according to their physical properties and characteristics. A gel, for example,

can be defined according to its constituents, as in the case of aerogels and hydrogels. Aerogels are generally highly porous networks filled with air[10], whereas hydrogels are three-dimensional networks swollen with water[11]. A gel can also be classified according to their interchain interactions at elevated temperatures[12]. Thermosets and elastomers, for instance, degrade irreversibly because their structures are permanently cross-linked. In contrast, physically-bonded thermoplastics are reversible upon heating and cooling due to the ability of their chains to slide past each in their networks. Based on these classification schemes, we physically characterize hydrogels and elastomers, two systems of interest in our research.

The first class of materials that we study is hydrogels. Hydrogels are cross-linked networks formed by water-soluble chains dispersed in water[13]. They can contain over 90-99% water[13, 14] and are prepared by chemical polymerization or by physical self-assembly of man-made or naturally occurring building blocks[11]. In recent years, these types of gels have been increasingly studied for applications in biomedical applications, such as drug delivery[4] and tissue regeneration[14, 15] due to their properties and biocompatibility. One motivation behind these studies is that hydrogels provide suitable semi-wet, three-dimensional environments for molecular-level biological interactions[15-17]. Furthermore, a number of 'intelligent' hydrogels have been designed to change properties in response to externally applied triggers, such as temperature, ionic strength, solvent polarity, electric/magnetic field, light, or small bio-molecules [18-21]. However, a major limitation of novel materials like these is

that the barriers to use in medical applications are significant when the properties are not fully understood. Chapter 3 resolves one aspect of this issue by exploring the mechanical and transport properties of such materials. The particular gel chosen for our studies is a poly (n-isopropylacrylamide) (pNIPAM) system, one of these thermoreversible, 'intelligent' materials.

In the latter half of this dissertation, we focus on elastomeric systems. Elastomers, more commonly referred to as rubbers, are polymer networks that are characterized with glass transition and melting temperatures below room temperature. They degrade when heated, since cross-links are achieved in these networks by nonreversible chemical reactions[22]. Due to these bonds, such materials exhibit high extension ratios when stretched and easily recover their dimensions without losing their elasticity after the applied stress is released[23]. Because of these properties, elastomers have been favored in mechanical studies of polymer networks [24-26]. Studies in the past focused on understanding elastic models [27-29] and mechanisms leading to failure [30-32] of polymer networks. However, more recent research has concentrated on increasing the strength of elastomers by adding fillers in them [33] or by introducing them as part of an interpenetrating double-network system[34]. In Chapters 4 and 5, we extend these previous studies to include elastomeric gels at high stresses and fracture. The gels we use as model systems are based on silicone networks.

2.2.3 Polymer Structures and Porous Media

The architecture of a certain polymeric structures, such as gels or networks, lend themselves to being considered forms of porous materials. Like the voids and pores that form the "microstructure" of soil, the "microstructure" of a gel can be related to the pores formed when the solid network of a system is swollen with solvent[35]. As demonstrated by Scherrer, et al. [36], such pores remain relatively constant upon swelling and shrinking in inorganic gels. Evidence of an apparent pore structure in gel systems has been provided by scanning electron microscope images of silica aerogels[37]. As with inorganic gel systems, the microstructure of polymer gels can be related to the network and distribution of polymer chains within the solvent of the material.

2.3 CHARACTERIZATION OF POLYMER SYSTEMS

The characterization of polymer structures is commercially and academically important as a means to predict the performance of a particular system in a specific application. As discussed briefly in the above sections, the molecular properties and constituents of a polymer structure often contribute to its bulk properties. For example, the properties of polymer gels are highly dependent on their constituents and network structures. Forming these connections is essential to understanding the transport properties of gels, the focus of this work. In this section, we center our attention on the

relationship between the network and sol fraction of a gel from a mechanical and dynamic perspective, as a means to gain insight into its transport properties. The approach taken to understand these gels will be treated phenomenologically and in terms of molecular processes.

2.3.1 Entangled Rubber Elasticity

The mechanical behavior of polymer gels and networks can be described according to the theory of rubber elasticity[31]. The classical theory of rubber elasticity assumes that a perfect, homogeneous rubber is made up of network strands joined at cross-linked junctions that can fluctuate. Under deformation, each individual cross-link point moves in proportion to the deformation of the whole sample and does not interfere with neighboring chains. As the number of possible configurations is reduced when the chains are displaced under deformation, the properties of the network arise primarily from the change in entropy of the network strands.

An effective modulus can be determined from this theory if we assume that the energy contribution per network strand is on the order of k_BT. At a local level, the material behaves like a liquid: the bulk modulus is high and a first approximation of the material may be taken as incompressible[38]. However, cross-links in the network prevent macroscopic flow of the bulk polymer, resulting in a finite shear modulus. Statistical methods lead us to calculate a shear modulus, G_x: *[31]*

$$G_x = \frac{\rho RT}{M_x} \tag{2.1}$$

where M_x is molecular weight between cross-links, ρ is the density, R is the universal gas constant, and T is temperature.

A modification of Equation (2.1) is taken when entanglements in a network are considered. In networks of very long, linear polymers, entanglements impose topological constraints on each other because they cannot pass through each other[29]. The entanglements behave like temporary cross-links and the entanglement strand effectively replaces the polymer chains in the network in determining shear modulus. The shear modulus, G_e, becomes a function of average molar mass between entanglements, M_e: [39]

$$G_e = \frac{\rho RT}{M_e} \tag{2.2}$$

Since it has been shown that entanglements are not localized[40], the shear modulus of an entangled network polymer can, therefore, be thought of as the sum of the G determined from a well-developed, cross-linked network plus any contribution from entanglements in the system.[41, 42]

$$G \cong G_x + G_e \tag{2.3}$$

The importance of entanglements in the mechanical response of a polymer gel or network is evident in Equation (2.3). The limits of the above equation indicate that entanglements control plateau modulus, G_e, in networks consisting of long polymer

chains, whereas cross-links control G_x of a network for low molar mass strands. Computer simulations support the validity of Equation (2.3), indicating that entanglements will increase the modulus of the same network without entangled polymer chains[43]. Experimental evidence of this behavior is noted in end-linked poly(dimethylsiloxane) networks, where G was found to be larger than predicted value[44] and independent of chain length in very long chains[45]. Langley[42] noted this behavior when high molecular weight linear polymers were tested under dynamic conditions and the modulus remained constant. If the molecular weight increased in such experiments, it was noted that the time span of the rubbery plateau increases but the level remains constant.[46] The relevance of entanglements in systems is noted in Chapters 4 and 5.

2.3.2 Linear Viscoelasticity

Like polymer melts and solutions, polymer gels and networks may behave like rubbery solids or viscous liquids, depending on the timescale over which the properties are measured. At short times or instantaneous, small deformations, the mechanical behavior is elastic[47] and follows Hooke's law:

$$\sigma \equiv G\gamma \tag{2.4}$$

where the proportion of stress, σ, to shear strain, γ, response of a material is characterized by shear modulus, G. The material is able to recover to its original

dimensions the instant the stress applied is released. For long times and large scale deformations, the material acts like a viscous, or Newtonian, liquid [47]. Deformation of the material is irreversible, and is also delayed or time dependent. At intermediate times, polymer gels and networks exhibit mechanical behavior that is a combination of these two extremes and respond viscoelastically. In viscoelastic materials, the relaxation time, τ, is used to describe a molecule's position relative to its neighbors and relates the viscosity of the material, η, to the modulus of the material. For a Maxwell fluid with a single relaxation time:

$$\tau \equiv \frac{\eta}{G} \tag{2.5}$$

Because the materials we use in our experiments are viscoelastic in nature, we focus on two specific techniques to measure and quantify these properties.

2.3.2.1 Stress Relaxation

One method to quantify the mechanical response of gels and networks is to use stress relaxation measurements [9, 48, 49]. In stress relaxation experiments, a step strain is imposed onto the sample. If the material is perfectly elastic, the stress applied will obey Hooke's law, Equation (2.4), and will stay constant throughout the test. This response occurs in the linear regime, when the applied strain is small enough that the relaxation modulus is independent of stress applied. However, if the material behaves like a viscous liquid, the stress response will instantaneously decay to zero. A

schematic showing the difference between the stress relaxation behavior of a liquid and solid is illustrated as a dashed line and solid line, respectively, in **Figure 2.4**.

The behavior of a viscoelastic liquid or solid falls between the solid and liquid curves of **Figure 2.4** and is depicted as solid lines. Although all materials have a region of linear response at sufficiently small values of applied displacements or time scales, the stress beyond this applied strain is time dependent, $\sigma(t)$ in the case of a viscoelastic liquid or solid. The material response from the stress remaining at time t to the step strain, γ, can be characterized by a stress relaxation modulus, $G(t)$. A generalized version of Hooke's law describes this behavior:

$$G(t) \equiv \frac{\sigma(t)}{\gamma} \tag{2.6}$$

For viscoelastic solids, stress relaxation to a finite value will occur due to the elastic component of the material behavior. An equilibrium shear modulus G_{eq}, can be defined:

$$G_{eq} = \lim_{t \to \infty} G(t) \tag{2.7}$$

For viscoelastic liquids, the stress relaxes towards zero at a certain time scale. The stress relaxation modulus can be modeled as simple exponential decay. According to the Maxwell model for liquids,

$$G(t) \approx G(t) \exp(-t / \tau) \tag{2.8}$$

where τ is the relaxation time for the material. The relaxation time is the characteristic time in which a molecule's position changes when external forces alter its position relative to its neighbors. Mechanically, τ determines how easily the viscous component of a material will flow when a stress is applied. A material can therefore have multiple relaxation modes[50].

$$G(t) = \sum G_i(t) \exp(-t / \tau_i) \tag{2.9}$$

Characteristic relaxation times for a viscoelastic solid, $\tau_{(s)}$, and liquid, $\tau_{(l)}$, are noted **Figure 2.4.** These types of mechanical tests are applied throughout this dissertation.

2.3.2.2 Oscillatory Shear

Because the viscoelastic response of materials can be probed directly on different time scales, another useful method of measurement is an oscillatory shear test[51]. In this technique, a steady state sinusoidal strain, δ_{ss}, is applied with an angular frequency, ω, in simple shear:

$$\delta_{ss}(t) = \delta_{\omega} \cos(\omega t) \tag{2.10}$$

In a perfectly elastic solid, the resulting steady state oscillatory load, P_{ss}, has the following general form:

$$P_{ss}(t) = P_{\omega} \cos(\omega t) \tag{2.11}$$

The oscillatory strain and resulting stress are in-phase. A Newtonian liquid, on the other hand, behaves, according to its shear rate:

$$P_{ss}(t) = P_{\omega}\omega \sin\left(\omega t + \frac{\pi}{2}\right) \tag{2.12}$$

In this situation, the liquid responds perfectly out-of-phase to the applied stress. **Figure 2.5(a)** and **(b)** depict the difference in the resulting sine waves of a perfectly elastic solid and Newtonian liquid, respectively**.** The behavior of viscoelastic materials is between these two extreme cases and is characterized by a phase lag from the viscous component. This shift is defined as the phase angle, Δ. Since the phase angle must fall between 0^{o}C (perfectly elastic behavior) and 90^{o} (viscous behavior), Equation (2.11) can be re-written to take the phase angle, Δ, into account:

$$P_{ss}(t) = P_{\omega}\cos(\omega t + \Delta) \tag{2.13}$$

Furthermore, the phase angle can be defined as the tangent ratio of the loss modulus, G" to the storage modulus, G':

$$\tan\Delta = \frac{G''}{G'}\ , \tag{2.14}$$

where G" represent the liquid-like shear component of the material, and G' is the solid response. This property provides an indication of how much energy is lost from the elastic system and is the basis to analysis of the experiments in Chapter 3.

2.3.3 Fracture of Soft Solids

The mechanical characterization of polymers gels and networks can be further extended to include fracture. These systems often respond elastically or viscoelastically at stresses that induce failure and the crack fronts that form from fracture are usually well defined [52]. From a molecular point of view, fracture in such soft solids is interesting in that they have large spatial structural units and often have been characterized by delayed crack growth [50]. Furthermore, the classic theories of linear fracture mechanics must be extended to the bulk behavior of the material in question. For example, the large elastic deformation of rubbers [53, 54] will be characterized differently from that of a viscoelastic polymer melt [55]. In our research, we are concerned with the failure of highly elastic materials, such as elastomers.

In situations where crack propagation of elastomers can be controlled, elastic fracture mechanics principles are often applicable. Common techniques in which crack length can be measured as a function of energy required to propagate the crack include using trouser[32, 54] and edge-crack geometries[53, 54], as seen in **Figure 2.6.** In these geometries, the material is assumed to behave elastically and the energy losses confined to regions in the vicinity of the crack tip [56] . A tearing energy, based on the Griffith criterion for brittle solids, can be applied to an elastomer in these situations as[53]:

$$\frac{-\partial E}{\partial A} \geq \Im \tag{2.15}$$

where $\Im$ is the energy required to propagate a crack for each surface unit area, A. According to Equation (2.15), crack propagation occurs when the stored elastic strain energy, $\mathcal{E}$, of the system during incremental crack growth is greater than the increase in surface energy due to the creation of a new surface. The driving force for a crack to grow is to lower the total energy of the system. In Chapter 5, we allude to these fracture mechanics principles to understand elastomeric gel behavior in a compression geometry.

2.3.4 Dynamics of Entangled Polymers

Polymer gels and networks can be treated as forms of entangled polymer melts and solutions, where size and connectivity of the molecules leads to striking new properties. Unlike polymer mixtures, the behavior of polymer gels cannot be treated under mean-field conditions due to considerable variations in monomer density, and in the interactions between monomers in solution[57]. From this perspective, a polymer gel is a form of a polymer solution, and the movement of polymer chains in solvent is possible when it undergoes deformation. In this respect, the dynamics of entangled polymer chains in solvent is very relevant in understanding the mechanics and transport phenomena of polymer gels.

2.3.4.1 Gels as Semi-Dilute Polymer Solutions

From a polymer physics standpoint, a polymer gel is a semi-dilute solution. A comparison of **Figure 2.7** and **Figure 2.3** demonstrates this concept. As seen in **Figure 2.7**, a semi-dilute solution ($c>c^*$) is characterized by overlapping chains and differs from a dilute solution ($c<c^*$), where polymer chains are isolated and interact with each other only during brief times. The basis of this transition between dilute and semi-dilute solutions occurs when the random coil of monomers begins to interpenetrate at a critical concentration, c^*, a scaling law developed by de Gennes [8]. Based on this principle, the overlapping chains of a semi-dilute solution are analogous to the mesh that is created in the gel networks, as depicted in **Figure 2.3.** Furthermore, the polymer volume fraction in gels is often on the same order of magnitude as the ratio of monomer in solution to volume of solution that is required for semi-dilute solutions to form. In polymer gels, typical polymer volume fractions range from 0.05 to 0.15 [9, 58]. This value is within range of typical polymer volume fractions determined in semi-dilute solutions, which are on the order of 10^{-3} to 10^{-1} by weight [59]. Such similarities allow us to connect the principles to semi-dilute solutions to modeling gels with small polymer volume fractions.

2.3.4.2 Polymer Chain Interactions

In the semi-dilute limit, interactions between the polymer chains exist and the movement of the chains relative to the solvent can be modeled. To understand this concept clearly, we first describe the dilute behavior of the chains when there is no interaction between them, and then look at the approximations when chain overlap occurs.

When the polymer chains are non-interacting, the strands act like independent coils in hard spheres. The volume fraction of each hard sphere is approximately c/c^*, where c is the concentration of polymer in solution and c^* is the critical concentration at which polymer overlap begins[8]. Each hard sphere is a non-interacting molecule and can be described by a form of the ideal gas law. When there is no interaction between polymer chains, the behavior of the coils is denoted as:

$$\frac{\Pi M}{cRT} = 1 \tag{2.16}$$

Where Π is the osmotic pressure of the solution, M is the molecular weight of the polymer chain, R is the universal gas constant, and T is temperature.

For semi-dilute solutions, the polymer chains interpenetrate and an interaction parameter needs to be considered. Based on Equation (2.16), the behavior of the coils in a semi-dilute solution is therefore:

$$\frac{\Pi M}{cRT} = 1 + f\left(\frac{c}{c^*}\right) \tag{2.17}$$

Equation (2.17) can be further simplified by noting the scaling relation between osmotic pressure, Π, of a gel and polymer concentration, c [60]. Noda, et al. demonstrated this universal behavior for polymer gels by plotting the logarithmic form of Equation (2.17) for five poly(α-methylstyrene)s of various molecular weights in toluene [60]. The resulting plot indicated that the data produced a universal curve independent of the weight of the gels. The slope of this curve was ~1.3 for the semi-dilute regime. Based on these results, Equation (2.17) could be re-written as a power law function [60]. For c>c*:

$$\frac{\Pi M}{cRT} \propto \left(\frac{c}{c^*} \right)^{\beta} \tag{2.18}$$

where γ is an exponent that is dependent on the solution considered. For the poly(α-methylstyrene)s in toluene, β=1.3.

As chains overlap in a semi-dilute solution, two chains cannot occupy the same position in space. The chain conformation can be described as a self-avoiding walk, in which the end-to-end distance, R_0, of the polymer is related to the number of monomers, N, based on power law with a scaling exponent of 3/5[31]:

$$R_0 \sim N^{3/5} \tag{2.19}$$

The self-avoiding walk used to describe the nature of the chains in the semi-dilute solution is also applicable to the behavior of the monomers in solution at the critical concentration, c^*:

$$c^* \sim \frac{N}{R_0^3} \tag{2.20}$$

Relating Equation (2.19) to Equation (2.20), the critical concentration of solution can be approximated as:

$$c^* \sim N^{(-4/5)} \tag{2.21}$$

The behavior of the coils in a semi-dilute solution can then be approximated as:

$$\frac{\Pi M}{cRT} \sim \left(\frac{c}{c^*}\right)^{\beta} \sim N^{\beta(4/5)} \tag{2.22}$$

for c>c*. Based on the observation of Noda, et al. [60], $\beta = 5/4$, since Π is independent of concentration, c, and the molecular weight, *M,* in the semidilute regime. An approximation can be made for the osmotic pressure of a semi-dilute solution:

$$\Pi \sim c^{9/4} \sim \phi^{9/4} \tag{2.23}$$

since the polymer volume fraction scales, ϕ, in the same manner as polymer concentration. Equation (2.23) relates the effect of polymer volume fraction on the interaction between the polymer solution and solvent.

2.3.4.3 Correlation Length

To understand how a polymer network behaves in solution for a gel, a correlation length,ξ, can be defined as a reference unit within the system[8, 40, 61]. The correlation length assists us in understanding the scaling relationship in a specific

frame of reference. For a semi-dilute solution, a correlation length can be defined as the length of a monomer on an ideal, elongated polymer chain, as seen in **Figure 2.8**. At length scales greater than ξ, the monomer 'sees' other overlapping chains in solution and can therefore interact with monomers on those chains. On length scales smaller than ξ, the monomer's reference frame is limited to the other monomers on the same polymer chain and the solvent surrounding it. Monomer interaction in this case is therefore limited to those on the same chain.

If we consider the thermodynamic energy difference between each coil of polymer and solvent, the correlation length can be represented as a function of the polymer volume fraction. Since polymer chains in a semi-dilute solution can be represented as coils in hard spheres or blobs, the correlation volume of each segment is on the order of ξ^3. If the energy per correlation volume is on the order of $k_B T$, The osmotic pressure for a semidilute solution can be estimated as [62]:

$$\Pi \approx \frac{k_B T}{\xi^3} \tag{2.24}$$

which leads to the same prediction as that of the mean-field theory for semi-dilute solutions. Based on the interactions between polymer solvent and solution, the correlation length can be simplified to [8]:

$$\xi \approx \lambda \phi^{-3/4} \tag{2.25}$$

from substitution of Equation (2.23) into (2.24). λ is a constant that has been determined as 0.5 nm for most polymer systems[62]. Equation (2.25) is extremely

useful when experimentally characterizing a polymer gel because it demonstrates that the correlation length can be directly measured from osmotic pressure experiments. The ramifications of this equation from a mechanical perspective are presented in Chapter 3.

2.4 AXISYMMETRIC INDENTATION

One experimental technique used to study the mechanics of soft materials over a large range of stresses is axisymmetric indentation [63]. Axisymmetric indentation utilizes an indenter, such as a hemispherical lens or flat punch, and brings it into contact with the material of interest. Since intrinsic material properties, such as adhesion values or mechanical constants[63-67], can be extracted from this type of setup, this approach is useful in our experiments to understand polymer gel behavior under a large range of stresses.

2.4.1 Elastic Half Space and Rigid Flat Punch Geometry

Of the axisymmetric indentation geometries available, the simplest and most useful for mechanically testing soft materials over a large range of stresses is the rigid, flat punch probe[63, 66]. The principle advantage for using a rigid cylindrical punch is that the contact area remains constant at varying strains[64, 68, 69]. Furthermore, the indenter can be assumed to be perfectly rigid, since a metal punch is applied to low

modulus polymeric systems [63]. Difficulties arise in measuring mechanical properties if the punch is compliant as compared to the substrate.

A schematic of a rigid flat punch probe with radius *a* brought into contact with an isotropic, homogeneous elastic layer of thickness, *h*, is depicted in **Figure 2.9.** The elastic layer is considered to be a semi-infinite elastic solid bounded by one surface plane. The punch, with its rigid flat base of 2*a* and sharp corners, produces a line load across the surface of the elastic solid as long as there is no tilting in contact. This geometry assumes that the contact area is in plane strain.

The region close to the contact interface is important in determining the mechanical properties of the material because the contact stresses near that region, or near-field, are highly concentrated[63, 64]. At depths into the elastic layer that exceed the contact radius, the stress fields rapidly decrease to zero from the point of contact into the far field. For small strain characterization of a material, linear elasticity is applicable when the displacement of the indenter is smaller than the radius of the punch[63]. In this region, the linear relationship between load, *P*, and displacement, δ, is defined by the compliance, C:

$$C = \frac{\delta}{P} \tag{2.26}$$

Applied to an elastic half-space that is much thicker than the radius of the rigid flat punch (h>>a), an analytic expression relating the compliance to Young's modulus, *E*,

and Poisson's ratio, v, can be written when the frictionless indenter with radius a comes in contact with the elastic layer[63]:

$$C = \frac{1-v^2}{2Ea} \tag{2.27}$$

Since the elastic layer is isotropic, we substitute G for Young's modulus according to

$$E = 2G(1+v) \tag{2.28}$$

A general equation to describe the small strain response of a flat punch on an elastic layer can therefore be determined from substitution of the above equations:

$$P = \frac{4G\delta a}{(1-v)} \tag{2.29}$$

2.4.2 Modifications due to Confinement Effects

In the previous derivation, it is assumed that the thickness of the elastic half-space is much greater than the radius of a flat punch (h>>a). Modifications of Equation(2.29) are necessary when the elastic layer can no longer be approximated as an infinite half-space, since the bulk response of the material will differ from that of a thin film[70]. When the thickness of the elastic layer is approximately equal (h≈a) or much smaller than the radius of the punch (h<<a), the stress fields of the punch will be altered since the stress will be confined to regions beneath the contact area[71]. The correction factor for an incompressible layer with a Poisson's ratio of 0.5 has been determined to be[66]:

$$f(a/h) = \frac{1}{1+1.33(a/h)+1.33(a/h)^3} \tag{2.30}$$

2.4.3 Fundamental of Indentation Fracture

The approach of using axisymmetric indentation to probe the mechanical constants of an elastic layer can be utilized to understanding the fracture of a material. Traditionally, indentation fracture methods have been applied to brittle materials, such as metals and ceramics[72, 73], as a means to determine their hardness values and quantify their strength. In this section, we outline basic general fracture mechanics principles of axisymmetric indentation. This framework provides insight into applications of indentation fracture to our specific soft systems.

2.4.3.1 Contact Stress Fields

Understanding crack evolution in a material from indentation fracture requires knowledge of the contact stress field[63, 72, 74]. The nature of this contact zone is determined principally by indenter geometry and material properties. The importance of indenter shape on its crack fields is depicted in **Figure 2.10**, where the pressure distributions of these contacts vary according to their contact area. Depending on such factors, indentation induced crack patterns can be described as resulting from 'blunt' or 'sharp' contacts that are either elastic or elastic-plastic in nature, respectively[75].

Since tensile stresses near the contact region are highly concentrated, as mentioned in the elastic half-space example, crack patterns are largely dependent on the tensile component of the stress field in all indenters[74]. The effect of tensile components is most notable at indenter corners and edges, which is also illustrated in **Figure 2.10(a)**. These near-field stresses generally determine the point of crack initiation, while far-field stresses determine the propagation of the cracks[75].

In this work, our primary concern is to understand the stress fields related to the **Figure 2.10(b)**. Although our work involves utilizing a flat punch indenter, which has high stress fields at its edges, our model elastomer systems are largely elastic in nature.

2.4.3.2 Blunt Indenters

In indentation fracture, contacts that form elastic deformation zones up to the point of fracture are regarded as 'blunt.' Analysis of such contacts was first performed by Hertz in 1882 on conical fractures at elastic contacts between curved glass surfaces [72, 75]. The classic example of a blunt tip geometry is of hard spherical indenter loaded on a flat, elastic half-space, as shown in **Figure 2.10(b)**.

The evolution of crack propagation for a blunt indenter in this geometry is illustrated in steps in **Figure 2.11**[75]. As seen in **Figure 2.11(a)**, initial loading of the indenter leads to elastic deformation around the point of contact, which produces tensile stresses around the contact and compressive stresses below it. Upon further loading,

the tensile stresses and compressive stresses increase in magnitude until a surface flaw is found. A ring crack, following the maximum tensile field, is formed from the surface flaw. The surface crack is arrested until the crack extends out of the tensile region (**Figure 2.11(b)**). As the strain is increased on the elastic layer, stable crack growth follows this tensile field and deviates outwards to avoid the compressive field (**Figure 2.11(c)**). When the ring crack becomes unstable, a Hertzian cone crack is formed spontaneously (**Figure 2.11(d)**). The crack will continue to grow but may experience crack closure as the contact site consumes the surface ring crack (**Figure 2.11(e)**). Upon unloading, the crack healing occurs as the material assumes to minimize its elastic and surface energy (**Figure 2.11(f)**).

Since blunt indentation fracture concerns itself with only elastic deformation, the contact pressure for such a system can be analyzed in a similar nature as the rigid flat punch on an elastic half space in our previous example. The stress for a Hertzian contact is determined as[63]:

$$\sigma = \frac{3E_1}{4\pi k}\left(\frac{a}{r}\right) \tag{2.31}$$

and k is a constant dependent on the geometry of the system:

$$k = \frac{9}{16}\left[\frac{\left(1-v_1^{\,2}\right)}{E_1} + \frac{\left(1-v_2^{\,2}\right)}{E_2}\right] \tag{2.32}$$

where E_1 and v_1 are the respective Young's modulus and Poisson's ratio of the elastic layer and E_2 and v_2 are the material constants for the indenter. These principles, as well

as the above analysis of crack propagation, provide a background to understand the behavior of our highly elastic materials in Chapter 5.

2.5 SUMMARY

From an organizational standpoint, this chapter lays the groundwork to what will be expected in latter parts of the body of work. The fundamental theme of understanding the properties of polymer gels and networks over a range of stresses is evident. By using the indentation principles that are discussed, it is possible to measure the mechanical response for our systems of interest. This understanding of mechanical behavior is what provides us with insight into how polymer architecture is affected under deformation. Experiments and results supporting this theme are what follow in subsequent chapters.

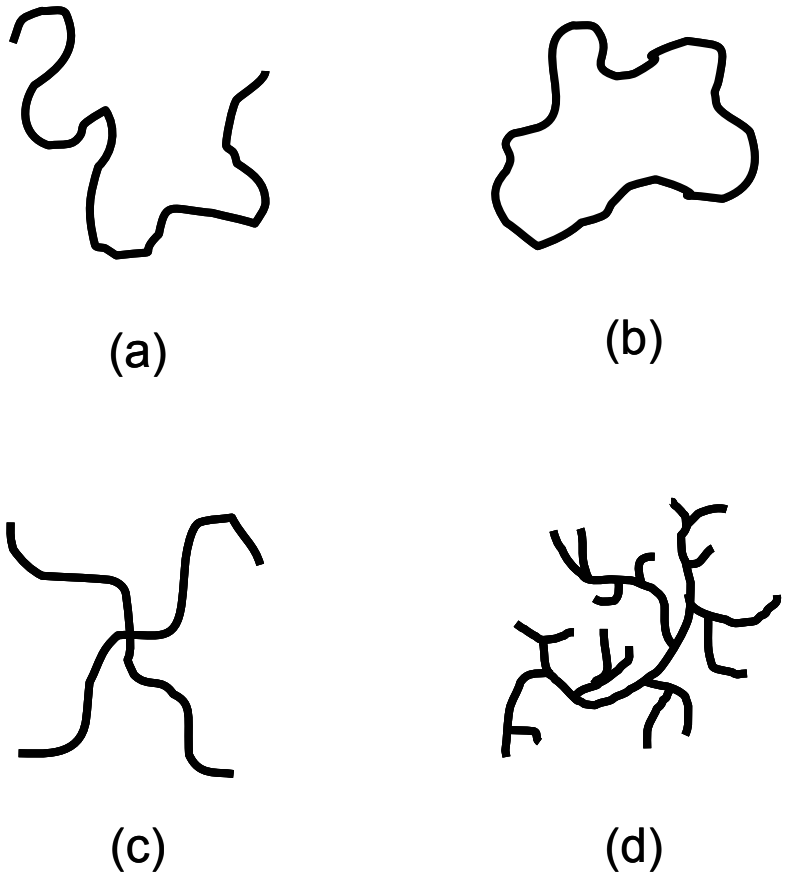

Figure 2.1. Examples of possible polymer architectures: **(a)** linear, **(b)** ring, **(c)** star, and **(d)** randomly branched.

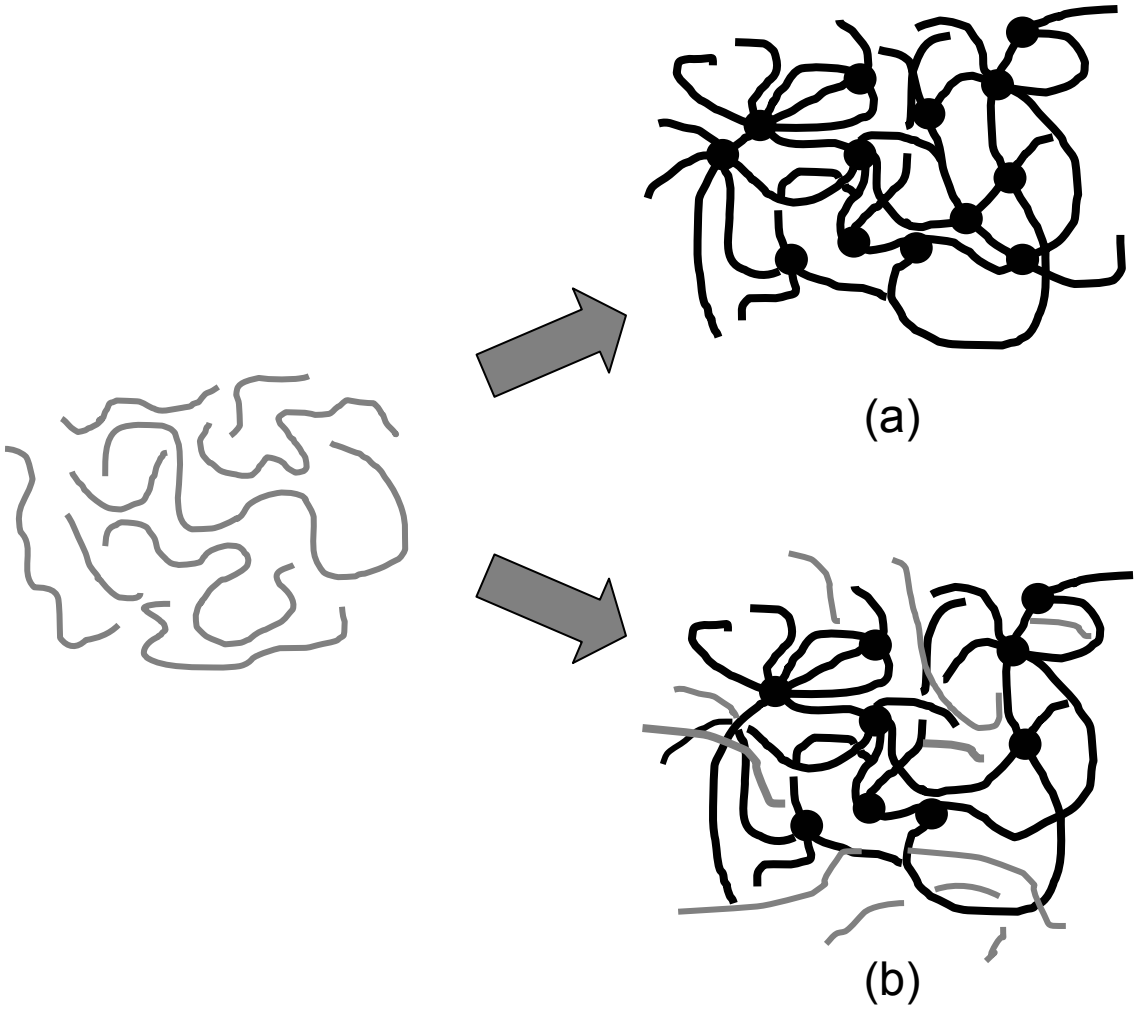

Figure 2.2. Formation of **(a)** polymer network and **(b)** gel from uncross-linked linear chains (gray lines). Polymer chains are joined at cross-links (dots) to form a network (black lines). In a gel, the unlinked chains are a continuous phase known as sol. The sol can be a solvent or another type of polymer.

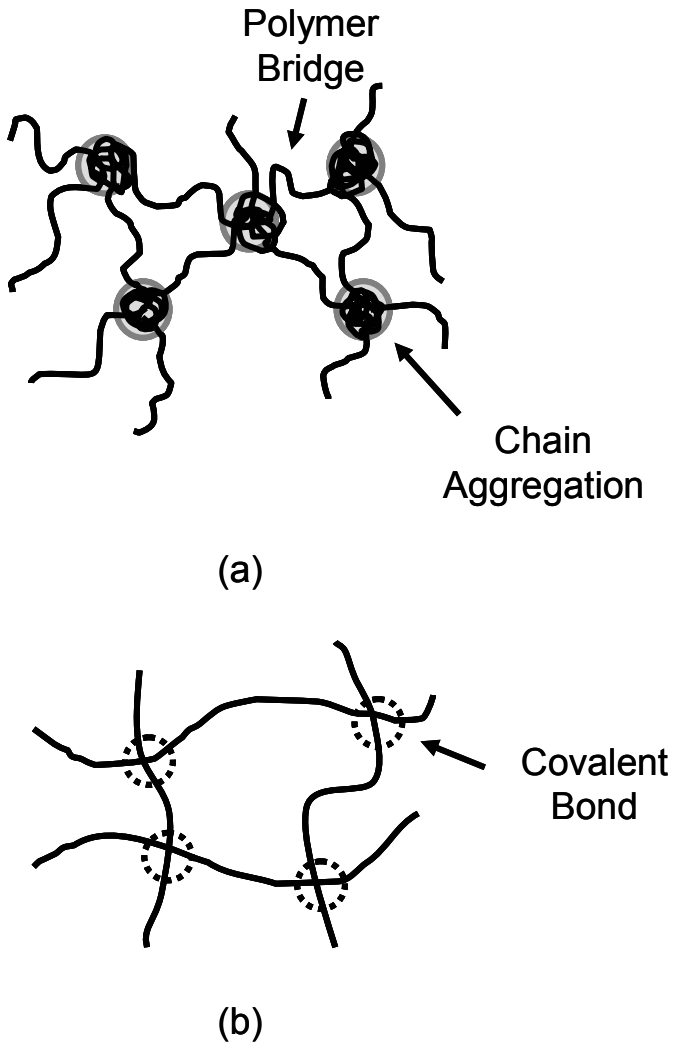

Figure 2.3. Comparison of physical and chemical gel network. The circles in the diagram represent types of cross-links in the gel. (a) A physical gel is characterized by temporary associations, such as the aggregation of endblocks in a poor solvent, known as physical bonds. (b) Chemical gels are covalently bonded.

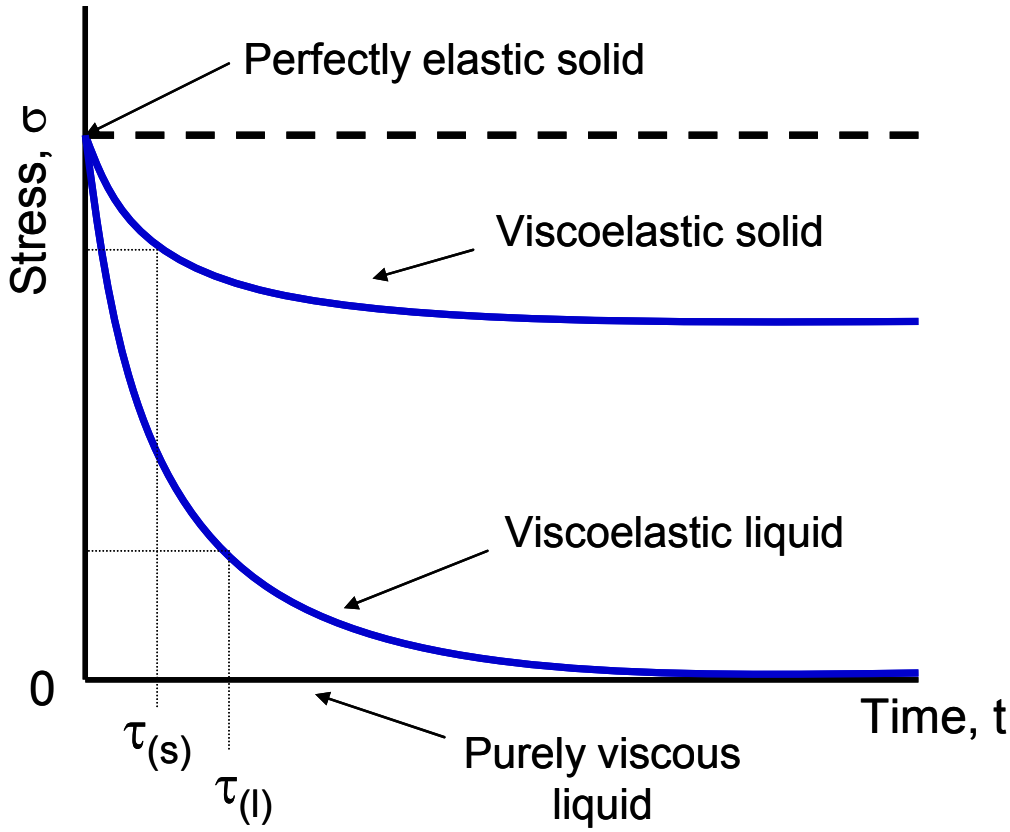

Figure 2.4. Schematic of stress relaxation response of various types of materials for infinite times. The displacement is held constant. Viscoelastic solids and liquids exhibit a characteristic relaxation time which is denoted $\tau(s)$ and $\tau(l)$, respectively. Note that the viscoelastic solid will plateau and the viscoelastic liquid will exponentially go to 0 at τ.

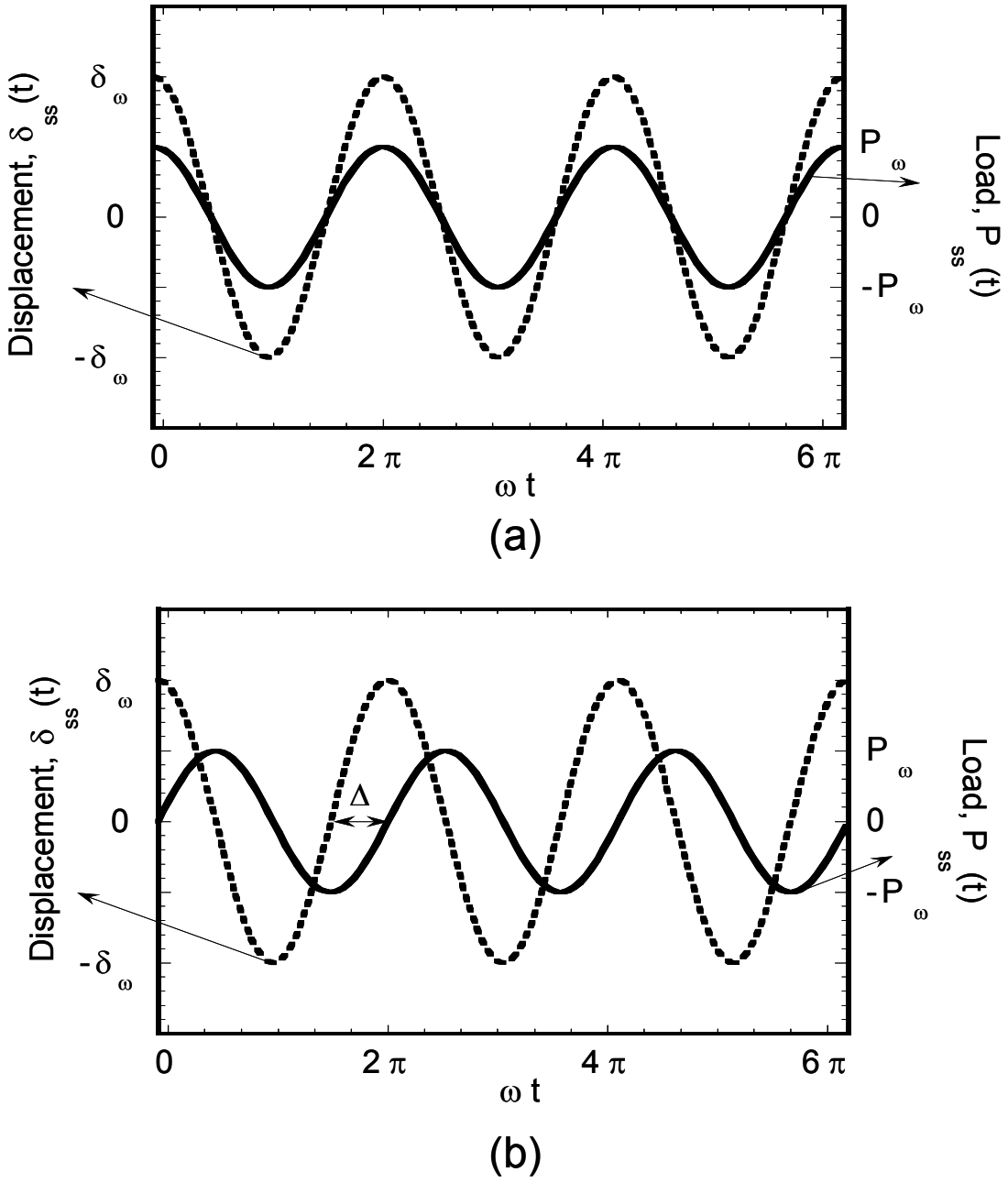

Figure 2.5. Strain response of **(a)** a perfectly elastic solid and **(b)** a Newtonian liquid during oscillatory loading and unloading. The strain response of an elastic solid is in-phase, while a liquid responds perfectly out of phase to the applied stress. The behavior of viscoelastic materials is between these two extreme cases and is characterized by a phase lag from the viscous component, which is denoted by Δ.

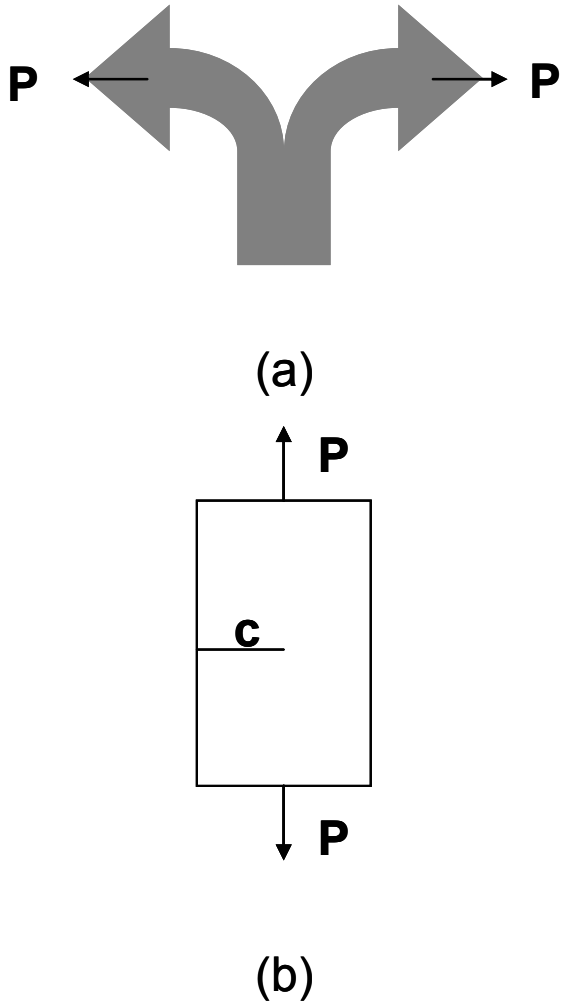

Figure 2.6. **(a)** Trouser and **(b)** edge-crack geometries.

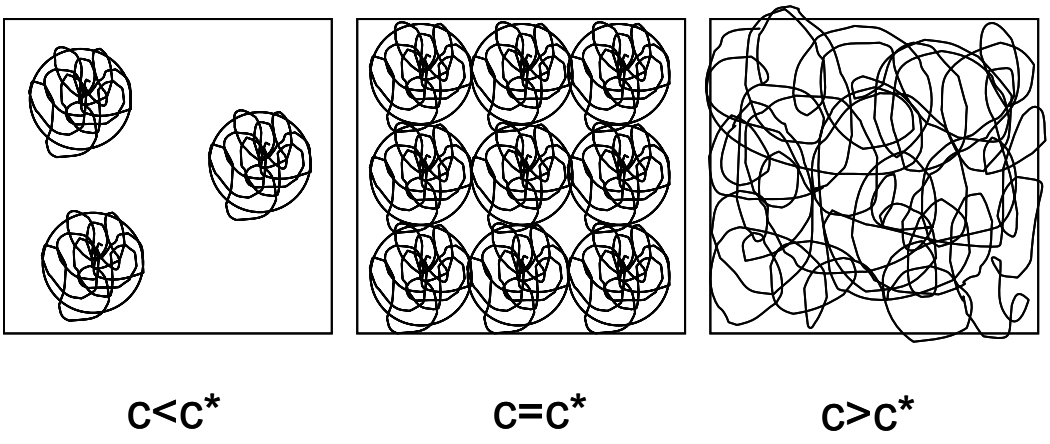

Figure 2.7. Dilute vs. semidilute solutions.
.

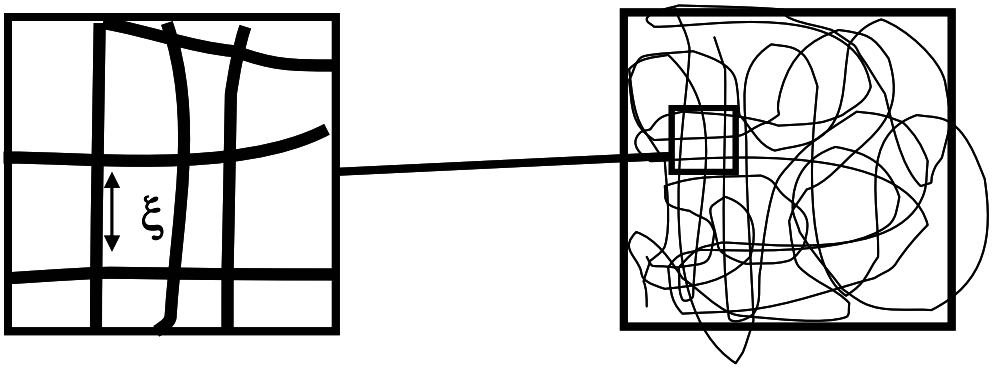

Figure 2.8. The concept of correlation length, ξ, as it relates to semi-dilute solutions

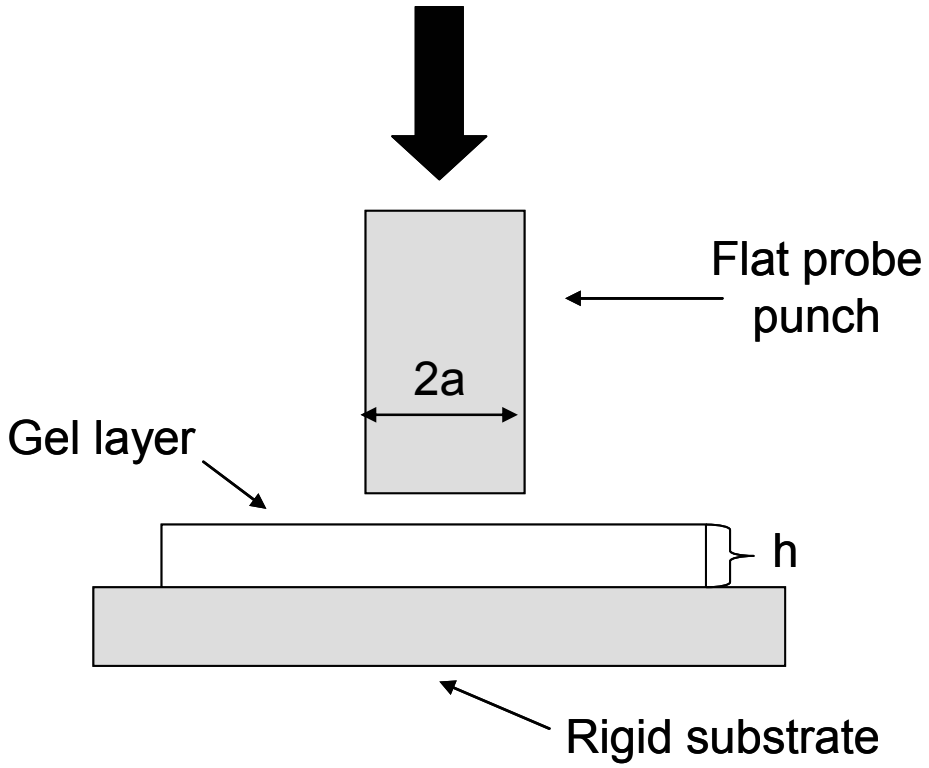

Figure 2.9. Rigid, flat punch probe geometry on an elastic half-space.

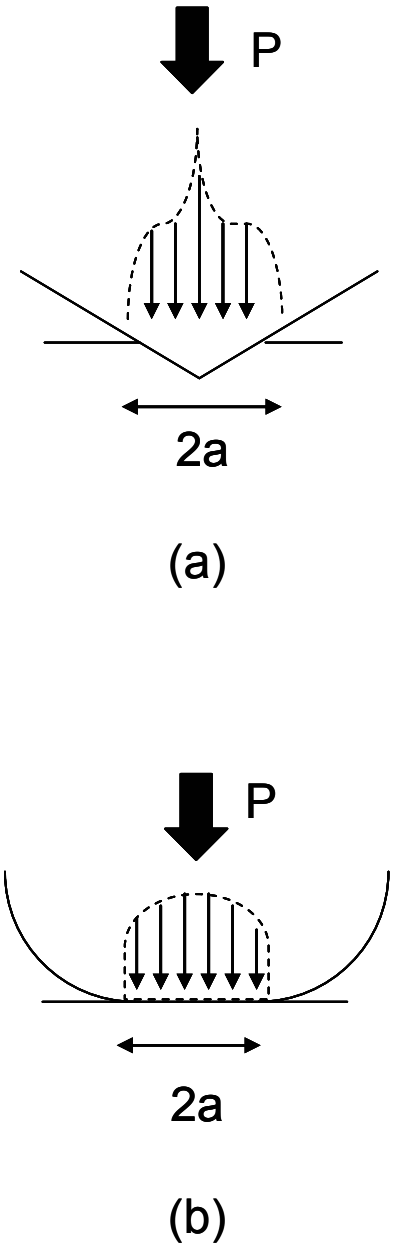

Figure 2.10. Elastic contact pressure distributions for: **(a)** sharp indenter and **(b)** sphere. *P* is the applied load and *a* is the contact radius.

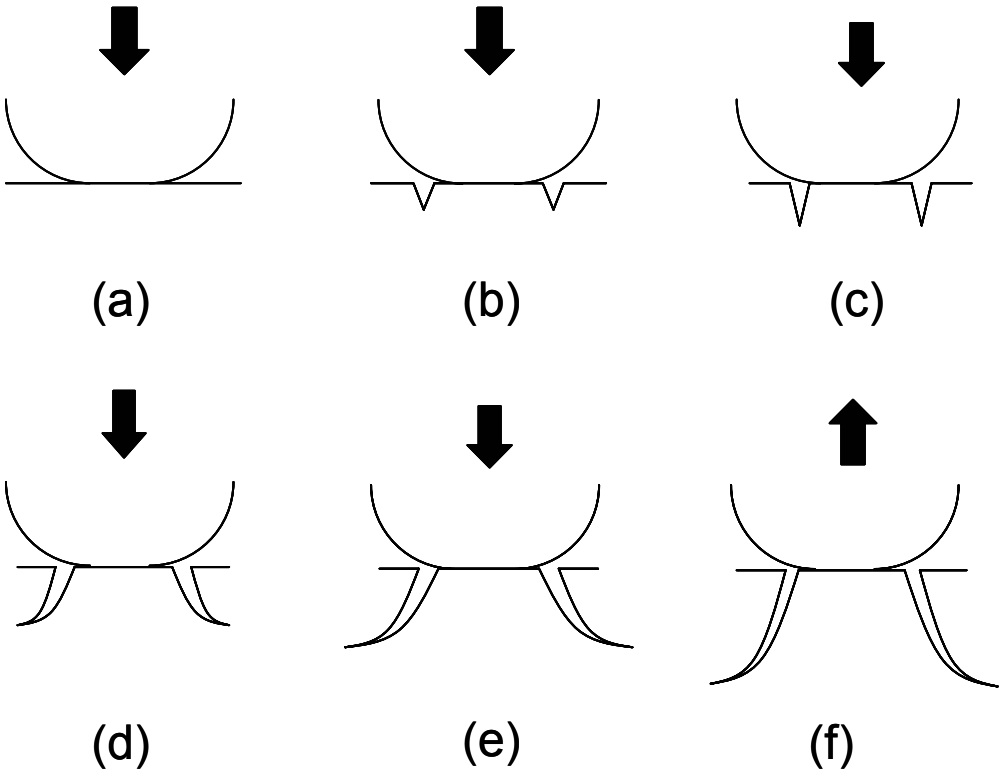

Figure 2.11. Formation of Hertzian cone crack from blunt indentation. **(a)** Initial loading of the indenter leads to elastic deformation around point of contact. Surface flaw is detected and ring crack is formed. **(b)** The surface crack is arrested until the crack extends out of its tensile region. **(c)** Stable crack growth continues to follow tensile field and avoids compressive field. **(d)** Hertzian cone crack forms when ring crack becomes unstable. **(e)** At further loading, the crack will continue to grow unless the area of contact expands beyond the surface ring crack. Crack closure will result in this case since the Hertzian cone will then be in the compressive zone. **(f)** Crack relaxes to minimize surface energy.

CHAPTER 3

CONTACT MEASUREMENT OF INTERNAL FLUID FLOW WITHIN POLYMER GELS

CHAPTER 3

CONTACT MEASUREMENT OF INTERNAL FLUID FLOW WITHIN POLYMER GELS

3.1 INTRODUCTION

Gels are porous materials composed of subunits that are able to bond with each other to form a macroscopic network. An important characteristic of gels is that their mechanical behavior depends on the time scale of the measurement used to probe the material. At sufficiently short times a gel behaves as an incompressible material, because there is no time for fluid to flow out of the network [76]. At extended times, however, the gel acts as a compressible material. This process has implications in fields ranging from soil mechanics to biomaterials development. For example, the rate at which water is expelled from the interparticle regions is a rate limiting factor in the consolidation of soil [77].

Polymer gels, consisting of a network of cross-linked polymer chains, swollen with a small molecule solvent, are another important class of gels, with widespread applications in medicine and biomedical engineering. In the eye, for example, the lens and the vitreous body, the large space behind the lens, are gels. Changes in the viscoelastic properties of the lens can lead to the loss of accommodation, or its

refractive power, while changes in its permeability can create the onset of a mature cataract [78]. Liquefaction of the vitreous body – i.e. when the gel deteriorates to a liquid phase – is believed to play an important role in retinal detachment. This process is presumably related to gel syneresis, where the vitreous body shrinks as a result of fluid escaping from its collagenous network, but additional results are needed in order to fully support this assumption [78]. Measuring the transport properties and mechanical properties of these gels could therefore have potential clinical applications. Additionally, an understanding of bulk properties in gels is applicable to the development of controlled drug delivery systems that are used in pharmaceutical [79, 80] and cosmetic [81] applications. Quantifying the bulk transport properties of gels is essential in each of these situations.

Measurement of the transport properties of polymer gels has traditionally been accomplished by light scattering or by direct mechanical measurement. For example, Hecht et al. [82] used inelastic light scattering to measure the cooperative diffusion coefficient, D_c, for a series of polyacrylamide hydrogels that were swollen in water. Values obtained for D_c ranged from 10^{-11} to 5x 10^{-11} m^2/s. Absolute scattering intensity measurements were also used to measure the longitudinal modulus, E_L [61, 83]. However, the nature of these measurements is limited to transparent samples, since light scattering is not possible for opaque gels, such as in the case of a cataract that affects the lens of the eye. These types of gels can be tested using mechanical methods, such as those utilized in rheology [58] or the techniques developed by Scherer [84].

Unfortunately, shear rheological methods that do not have a hydrostatic component are not sensitive to solvent flow, and the beam bending techniques developed by Scherrer are difficult to apply to materials with low elastic moduli such as polymer gels. Because of these limitations, we extend an established contact mechanics method, which has been shown to measure elastic constants, to include the determination of solvent flow.

Based on a contact mechanics analysis developed by Hui, *et al.* [35], a technique is presented here that is ideally suited for characterizing transport properties of polymer gels for which light scattering techniques cannot be used to quantify the effective pore size. In Hui's work it was shown that stress relaxation experiments utilizing a cylindrical punch geometry, illustrated schematically in **Figure 3.1(a)**, can be used to determine the permeability, compressibility, cooperative diffusion coefficient, Poisson's ratio and shear modulus of a gel. Although this technique proves to be very useful in theory, it is very difficult to perform experimentally. Therefore, a similar but simpler geometry has been developed. This study utilizes a flat, circular punch, in addition to flat, rectangular punch, to characterize the transport and mechanical properties of a polymer gel. These geometries are depicted in **Figures 3.1(b) and 3.1(c)**, respectively.

3.2 EXPERIMENTAL METHODS

The model system chosen for this study is a poly(n-isopropyl acrylamide) (pNIPAM) gel. pNIPAM is used because of its unique phase behavior and physical properties. These gels have generated much interest in the medical community, largely because of their phase behavior [37, 85-87]. pNIPAM gels undergo a reversible phase transition at a lower critical solution temperature (LCST) of ~33^{o}C in aqueous solutions, a temperature close to the human body [88]. Below the LCST the polymer networks swell with solvent, resulting in clear, homogeneous gels, with water molecules forming cage-like structures around hydrophobic groups of the pNIPAM macromolecules [89, 90]. The effective pore size in this situation is the average distance between intermolecular contacts, ξ, a polymer solution property often referred to as the correlation length [8, 91]. For typical polymer concentrations, ξ is of the order of 3 nm. Above the LCST, the gel dehydrates and phase separates, forming a heterogeneous, opaque structure. Phase separation occurs when the structure of the water molecules around the hydrophobic groups is disrupted, causing these hydrophobic groups to associate[90]. The collapse of the network leads to polymer-rich and solvent-rich regions throughout the gel. In these phase-separated gels, cross-links in the network, rather than polymer chain overlap, determine the pore size, *d*, which is unknown but expected to be substantially larger than 3 nm. The definition of *d* is defined more quantitatively in Section 3.1. The transition from a swollen,

homogeneous gel at T=22^{o}C to a shrunken, heterogeneous gel at T=39^{o}C is depicted in the photographs in **Figure 3.2**. Schematics in the figure show the gel with an effective pore size ξ below the LCST and a pore size of d above the LCST.

In our experiments, pNIPAM gels are formed by free-radical copolymerization of N-isopropyl acrylamide (NIPAM) monomer in aqueous media in the presence of a commercial cross-linking agent. The pNIPAM gels are prepared in small disk-shaped moulds. Gel synthesis is based upon a combination of methods as described in previous papers [92, 93]. Details of sample preparation are as follows: 0.7920g commercial N-isopropyl acrylamide (NIPAM) monomer, 0.0133g methylene bis(acrylamide) (MBA), a cross-linking agent, and 0.0040g ammonium peroxidisulfate (APS), an initiator, are dissolved in 10 mL of 0.1 M phosphate buffer saline ($Na_2B_4O_7$, ph=7.4) solution. The solution is bubbled with N_2 gas for 15 minutes to eliminate oxygen, and is brought into a N_2 rich glove bag to prevent oxygen inhibition of the polymerization reaction. In the N_2-rich environment, 4 mL of the monomer-containing solution is transferred to a vial and 9.6 μL of Tetramethylethylenediamine (TEMED) was added to it. The mixture is then micropipetted into a 3 cm polystyrene Petri dish and allowed to gel for 24 hours at 22^{o}C in the glove bag. After complete gelation, the samples are taken out of the N_2 rich environment and the gels are saturated with a 0.147 mM HCl solution to remove any unreacted reagents in each sample. The extraction fluid is exchanged 2-3 times over a period of 24 hours. The gels are stored in the PBS solution until the mechanical tests are performed.

In the indentation experiments an indenter is brought into contact with a thin layer of a pNIPAM gel, using a probe tack apparatus [48] that is shown schematically in **Figure 3.3**. The testing apparatus consists of a linear inchworm stepping motor with a velocity range of 4.0 nm/s-2.0 mm/s that controls the motion of the attached indenter. As the indenter comes into contact with a layer of gel in an environmental chamber, a load transducer monitors the normal force, while a fiber optic displacement sensor records the normal displacement. These devices are controlled and integrated from a personal computer running National Instruments LabView software.

As depicted in **Figures 3.1(b) & 3.1(c)**, two indenter geometries are used in our experiments: a rigid flat, circular punch (a = 0.39 mm or a = 3.0 mm) and a custom-designed flat, rectangular surface (a = 0.17 mm, L = 20.3 mm). These geometries provide a constant contact area during a compression test and can be used to separate sources of stress relaxation when compared with one another. These types of indenters are particularly useful in experiments where standard imaging techniques cannot be utilized to observe changes of contact area in the sample.

We subject the gel to a two-step displacement history in the linear elastic regime. **Figure 3.4** illustrates the time dependence of the load and displacement for a typical experiment. First, the rigid indenter is brought into contact with the sample until a predefined maximum compressive load is reached. The displacement is then fixed for 1000 seconds as the gel relaxes due to solvent flow and viscoelastic relaxation of the gel network. Immediately following this period of stress relaxation,

displacement oscillations with a 20 μm amplitude are applied at frequencies ranging from 1.0 Hz to 0.002 Hz. The quantitative interpretation of our results requires that we be working in the linear elastic regime, which in turn requires that the overall displacement, δ, not substantially exceed the punch dimension, *a*. Relationships between load and displacement for the same gel at 22 °C and at 39 °C are shown in **Figure 3.5**. Strain hardening effects become important for δ/a > 3 at 22 °C, and for δ/a > 1.7 at 39 °C. In addition, the elastic modulus of the gel is four times larger at 39 °C than at 22 °C. The oscillatory experiments measure an effective tangent modulus, obtained from the slopes of the load/displacement curves. The boxes in **Figure 3.5** correspond to the regimes in which the oscillatory experiments were conducted for this gel. At room temperature the oscillatory experiments were performed at the limit of the linear regime of the gel response, whereas the higher temperature oscillatory measurements were performed in a regime where some effects from strain hardening might be expected. The remainder of the experiments described here are all conducted in the linear regime.

If we ignore the effect of solvent flow for now and assume the material is incompressible with a Poisson's ratio of ν = 0.5, the relationship between load and displacement for the circular punch (Fig. 1b) can be written as follows[66]:

$$\sigma_{avg} = \frac{P}{\pi a^2} = \frac{8G}{\pi}\left(\frac{\delta}{a}\right) f_c\left(\frac{a}{h}\right), \tag{3.1}$$

where f_c is the following geometric confinement factor determined by the ratio of the indenter radius to the gel thickness, h [94]:

$$f_c = \left(1 + 1.33(a/h) + 1.33(a/h)^3\right) \tag{3.2}$$

The gel thickness, h, in our case is approximately 3 mm.

3.3 THEORETICAL TREATMENT

3.3.1 Relaxation Behavior of Gel

In order to describe the sensitivity of these experiments to solvent flow, we begin by assuming that solvent flow is the only factor responsible for the observed stress relaxation. Under conditions of pure shear, where there is no pressure gradient to drive solvent flow, there is no stress relaxation, and the material is characterized by a time-independent shear modulus, G. Under compressive loading conditions, however, the effects of solvent flow cause the gel to respond differently at short times as opposed to long times. **Figure 3.6** is a schematic illustration of the load response of a gel that is characterized by a single relaxation time, τ. In this idealized case the gel is instantaneously loaded to an initial, maximum load, P_0, at t=0. At very long times ($t \rightarrow \infty$) the load relaxes to a plateau value, P_∞. At t=0, the gel acts as an incompressible

elastic solid with a Poisson's ratio, ν, of 0.5. At $t=\infty$, the material is compressible, and behaves in a way that is qualitatively similar to a sponge from which water has been squeezed. The Poisson's ratio of this 'relaxed' gel is less than 0.5 and is defined here as ν_∞.

The ratio of the relaxed and instantaneous loads is independent of the contact dimension of the indenter, and is given by the ratio of the relevant compressive moduli for plane strain conditions. For $\nu = 0.5$ at $t = 0$ and $\nu = \nu_\infty$ at $t = \infty$ we have[35]:

$$\frac{P_\infty}{P_0} = \frac{1}{2(1-\nu_\infty)}. \tag{3.3}$$

The characteristic time, τ, required for the load to relax from P_0 to P_∞ is the diffusion time corresponding to a diffusion distance comparable to the punch dimensions:

$$\tau \approx \left(\frac{a^2}{D_c}\right) \tag{3.4}$$

where a is the width of the rectangular indenter, and the radius of the circular indenter. This equation indicates that the timescale of the experiment is dependent on the contact area of the indenter. Since viscoelastic effects characterized by a time-dependent shear modulus are independent of the contact area, Equation (3.4) provides a means for experimentally distinguishing between effects due to solvent flow and effects due to viscoelastic relaxation of the polymer network. A distinguishing feature of effects due

to solvent flow is that the time dependence of the stress relaxation depends on the characteristic punch dimension. Different punch sizes are used in our experiments for this reason.

Once D_c is obtained from the relaxation behavior of the gel, we can analyze this information to extract information about the pore size of the gel. The connection is through the following expression for D_c: [77]:

$$D_c = \frac{D_p E_L}{\eta} \tag{3.5}$$

where E_L is the longitudinal elastic modulus, D_p is the permeability of the gel, and, η is the viscosity of the solvent. The longitudinal elastic modulus determines the elastic response of a uniaxially compressed gel that maintains a constant cross-sectional area, and is related to the shear modulus and relaxed Poisson's ratio as follows[83]:

$$E_L = \frac{2G(1-v_\infty)}{1-2v_\infty}. \tag{3.6}$$

The value of D_p is determined from Darcy's Law, which governs the movement of liquid in porous media. Applied to gels , Darcy's Law states that the solvent flux, J, is proportional to the pressure gradient in the liquid, ∇p [36, 95]:

$$J = -\frac{D_p}{\eta}\nabla p \tag{3.7}$$

where η is the viscosity of the liquid. By analogy to Poiseuille's law for flow through a pipe, D_P is predicted to be proportional to the to the characteristic cross-sectional area of a pore[36]. In our case we use this proportionality to define the pore size, *d:*

$$d \equiv \sqrt{D_p} \ . \tag{3.8}$$

Rearrangement of Equations (3.4) , (3.5), and (3.8) leads to:

$$\tau \approx \frac{\eta}{E_L}\left(\frac{a}{d}\right)^2 . \tag{3.9}$$

Equation (3.9) indicates that the pore size of a gel can be predicted if the contact dimensions of the indenter are known, and the relaxation time due to solvent flow can be measured accurately.

3.3.2 Oscillatory Response

The relaxation time in our experiments is measured indirectly, by measuring the phase angle obtained during the oscillatory portion of the experiment. This approach maximizes our sensitivity to the relatively low levels of dissipation that are typically observed. We apply a steady state sinusoidal displacement, δ_{ss}, of the following form:

$$\delta_{ss}(t) = \delta_{\omega} \cos(\omega t), \tag{3.10}$$

The resulting steady state oscillatory load, P_{ss} has the following general form:

$$P_{ss}(t) = P_{\omega}\cos(\omega t + \Delta), \tag{3.11}$$

where Δ is the phase angle characterizing the response, which is equal to zero in the absence of solvent flow or viscoelastic relaxation of the gel. The data plotted in **Figure 3.7** were obtained from the same gels used to generate the data shown in **Figure 3.5**. For a given experiment, the values of Δ is related to the relative energy dissipated during each cycle:

$$\sin\Delta = \frac{\oint \mathrm{P}\mathrm{d}\delta}{\pi P_{\omega}\delta_{\omega}}. \tag{3.12}$$

The shear modulus is determined by the relative values of P_{ω} and δ_{ω}. For a flat, circular punch (**Figure 3.1(b)),** the modulus is given by the following version of Equation (3.1):

$$\frac{P_{\omega}}{\delta_{\omega}} = \frac{4aG}{(1-\nu_{eff})} f_c\left(\frac{a}{h}\right), \tag{3.13}$$

where ν_{eff} is an effective Poisson's ratio that is bounded by the limiting values of 0.5 (high frequencies) and ν_{∞} (low frequencies).

For an indenter shaped with a flat rectangular surface (where $L>>a$), the modulus is obtained from the following approximate expression [63]:

$$\frac{P_{\omega}}{\delta_{\omega}} \approx \frac{G\pi L}{(1-\nu_{eff})} \frac{1}{\ln\left((h/a)+\left((h/a)^2-1\right)^{1/2}\right)} \tag{3.14}$$

where L is the length of the rectangular punch and a is its half-width.

3.4 RESULTS AND DISCUSSION

3.4.1 Measured Elastic Moduli and Phase Angles

Elastic moduli obtained from oscillatory tests performed at 22°C and 39°C are shown in **Figure 3.8**. At room temperature, the results from different punch geometries illustrate the near-perfectly elastic character of the gels, and show that Equations (3.13) and (3.14) provide a consistent description of the elastic response of these materials. The primary advantage of the rectangular punch geometry is that measurable forces can be obtained with a very small punch dimension by working with a large aspect ratio, L/a. One disadvantage of this geometry is that great care must be used to keep the punch edge parallel to the surface of the gel, so that a uniform displacement is applied along the entire length of the indenter. Another disadvantage of the rectangular punch geometry is that the sample must be macroscopically homogeneous over the entire length of the punch. We were not able to obtain this degree of homogeneity with the gels at 39 °C. For this reason we only used the smaller circular punch at the high temperatures, from which we were able to obtain reproducible modulus data. The shear moduli plotted in **Figure 3.8** were approximated by neglecting the effects of solvent flow, i.e., by taking $\nu_{eff} = 0.5$ in Equations (3.13) and (3.14). This is a very good approximation when the phase angles are small, as is indeed the case in our

experiments. These phase angles, obtained from Equation (3.12), are plotted in **Figure 3.9**.

3.4.2 Calculation of Phase Angles

In the case where the energy dissipation is entirely due to solvent flow, a predictive model for the phase angles can be developed. We begin by defining the following response function *Y(t)*, which describes the response to a step function loading of the sample:

$$Y(t) \equiv \frac{P(t)}{\delta_0} = Y_0\left(1-\lambda\right) + \lambda Y_0 F\left(t\right). \tag{3.15}$$

where Y_0 describes the instantaneous response λ describes the fractional relaxation due to solvent flow:

$$\lambda \equiv \frac{P_0 - P_\infty}{P_0}. \tag{3.16}$$

The generalized treatment presented here is valid for any value of λ. However, for an elastic half space (a/h <<1) we note that λ can be obtained from Equation (3.3):

$$\lambda = \frac{1-2\nu_\infty}{2(1-\nu_\infty)} = \frac{G}{E_L} \tag{3.17}$$

F(t) is a general function that defines the time dependence of the relaxation, and is defined so that *F(0)* = 1 and *F(∞)* = 0. The value of *Y(∞)*, which we refer to as Y_∞, is equal to $Y_0(1-\lambda)$.

The time-independent term on the right hand side of Equation (3.15) gives an elastic contribution to the stress that is in phase with the applied displacement. Linear superposition is used to obtain the contribution of the time-dependent term in Equation (3.15) to the steady state oscillatory response. If we consider the following steady-state oscillatory displacement function:

$$\delta_{ss}(t) = \delta_\omega e^{i\omega t}, \tag{3.18}$$

the resulting steady state force is:

$$P_{ss}(t) = \left[i\omega \int_0^\infty \left[Y(\beta) - Y_\infty \right] e^{-i\omega\beta} d\beta + Y_\infty \right] \delta_\omega e^{-i\omega t}(t). \tag{3.19}$$

The phase angle is given by:

$$\tan\Delta \equiv \frac{\mathrm{Im}\, P_{ss}}{\mathrm{Re}\, P_{ss}}. \tag{3.20}$$

To access the phase angle from the relaxation curve, Equation (3.19) can be written in the form of a Fourier transform. Recall that for a function $\phi(\omega)$, the Fourier transform is defined

$$\tilde{\phi}(\omega) \equiv \int_{-\infty}^{\infty} \phi(\beta) e^{-i\omega\beta} d\beta. \tag{3.21}$$

If we define

$$\phi(\omega) \equiv \begin{cases} Y(t) - Y_\infty & t > 0 \\ 0 & t < 0 \end{cases}, \tag{3.22}$$

then Equation (3.19) becomes:

$$P_{ss}(t) = \left[i\omega\tilde{\phi}(\omega) + Y_\infty \right] \delta_\omega e^{i\omega t}(t). \tag{3.23}$$

From Equation (3.20), the phase angle can be written as:

$$\tan\Delta \equiv \frac{\omega \,\mathrm{Re}\left[\tilde{\phi}(\omega)\right]}{Y_\infty - \omega \,\mathrm{Im}\left[\tilde{\phi}(\omega)\right]} \tag{3.24}$$

The specific functional form of the unit force response, Y*(t)*, depends on the loading geometry, and is not generally available. However, for an indenter with circular cross section against a thick elastic layer (*a/h* << 1), Lin et al. have obtained the following expression for Y*(t)* [64]:

$$Y(t) \cong 8Ga\left[1 - \frac{1-2\nu}{2(1-\nu)} erf\left(f(\kappa)\right)\right]. \tag{3.25}$$

where

$$f(\kappa) = \left(\sqrt{\kappa} - 0.23\kappa + 0.02\kappa^{3/2}\right) \tag{3.26}$$

and κ is the normalized time:

$$\kappa \equiv \frac{D_c t}{a^2}. \tag{3.27}$$

Applying Equation (3.24) to the parameters in Equation (3.15) that specify the load relaxation function, the phase angle is:

$$\tan\Delta = \frac{\lambda \,\mathrm{Im}\, I(\omega)}{(1-\lambda) + \lambda \,\mathrm{Re}\, I(\omega)} \tag{3.28}$$

where *I(ω)* for our geometry is:

$$I(\omega) \equiv i\omega \int_0^\infty \left[1 - erf\left(f(\kappa)\right)\right] e^{-i\Omega t} dt\,. \tag{3.29}$$

And Ω as the normalized angular frequency:

$$\Omega \equiv \frac{a^2 \omega}{D_c} = \left(\frac{a}{d}\right)^2 \frac{\lambda \eta \omega}{G} \tag{3.30}$$

Combination of the above equations leads to the following approximate expression for the phase angle for a flat circular punch, with details of the derivation given in the appendix:

$$\tan\Delta \approx \frac{\lambda\sqrt{\sqrt{1+\Omega^2}-1}}{\sqrt{2}\sqrt{1+\Omega^2} - \lambda\sqrt{\sqrt{1+\Omega^2}+1}} \tag{3.31}$$

Equation (3.31) is a central theoretical result of this paper, which relates a measurable phase angle to the relaxed Poisson ratio (through λ) and the pore size (through Ω).

Values of the phase angle obtained from Equation (3.31) are plotted as a function of Ω in **Figure 3.10**, for different values of the relaxed Poisson's ratio, ν_∞. Equation (3.17) was used to obtain values of λ from ν_∞. In order to estimate the values of Ω that are expected to correspond to our room temperature experiments, we use previously measured values of D_c (10^{-11} to 5x 10^{-11} m^2/s) for gels in good solvent conditions[82] and the values of a (0.17 – 3.0 mm), and ω (0.01 - 8 s^{-1}) used in our experiments. In this way we estimate values for Ω in our room temperature experiments that range from 6 to 7x10^6. The predicted value of ν_∞ for a polymer gel swollen to equilibrium in its own solvent is 0.25, although higher values are generally obtained experimentally[61, 83]. It is not surprising, therefore, to obtain phase angles from our experiments at room temperature that are very low in all cases as estimated from Equation (3.31). The values of Ω for the smallest punch dimensions that we are able to utilize experimentally are still too large for these room temperature experiments, where the effective pore size is only a few nanometers. The situation at the higher temperatures is more favorable. Here, the increase observed at the lowest phase angles is a potential consequence of solvent flow. To quantify this effect in more detail we use the following approximation of Equation (3.31) that is valid for $\Omega >> 1$:

$$\tan\Delta \approx \frac{\lambda}{\sqrt{2\Omega}} = \frac{1}{\sqrt{\omega}}\left(\frac{d}{a}\right)\sqrt{\frac{2G\lambda}{\eta}}\,. \qquad (3.32)$$

The solid line in **Figure 3.9** represents $\left(\frac{d}{a}\right)\sqrt{\frac{2G\lambda}{\eta}} = 5.6x10^{-3}$. With G = 1.2x10^4 Pa, a = 390 μm, η = 10^{-3} Pa-s, the corresponding value of $d\sqrt{\lambda}$ is 0.44 nm. Because viscoelastic contributions (*i.e*, a time dependence of the shear modulus, G) will increase the measured phase angle, this value of $d\sqrt{\lambda}$ is an upper bound. The magnitude of this upper bound is sufficient to make some statements about the transport properties of the gel above the LCST. Specifically, the picture of an interconnected network of pores with a characteristic size larger than the correlation length, ξ of the homogeneous gel is not consistent with our data. Suppose, for example, that the pore size were equal to the correlation length of 3 nm obtained from direct measurements of the collective diffusion coefficient for polymer solutions of concentrations comparable to the ones studied here[96]. From this we obtain an upper bound of 0.02 for λ, which in turn corresponds to a lower bound of 0.49 for the relaxed Poisson ratio, ν_∞.. This calculated value of ν_∞. is greater than the values measured for actual polymer gels, which range from a theoretical value of ν_∞.=0.25 for good solvent conditions, up to a maximum of about 0.4[61, 83], and indicates that the gel above the LCST behaves more like an incompressible solid, in which water does not have time to escape from the network. However, the thermodynamic penalty for expulsion of water from the gel decreases above the transition temperature, and ν_∞ is determined by the ability to expel solvent from the solvent rich regions of the gel. One expects that ν_∞ must decrease even

further under these conditions, which is inconsistent with the lower limit of 0.49 that we obtain from our data. On the contrary, our result is consistent with the formation of a closed cell network, where the solvent rich regions are not interconnected. This result has important implications for the formation of these gels, and explains why the gels do not shrink by continuous expulsion of solvent from the solvent rich domains when the temperature is increased above the transition temperature.

3.5 CONCLUSIONS

A theoretical framework for studying the transport properties and mechanical behavior of gels at small strains has been developed, and used to interpret model experiments performed with poly(n-isopropyl acrylamide) gels. Energy dissipation from solvent flow can be differentiated from network viscoelasticity when various indenter sizes are used to probe a gel under compression. At small strains, the elastic constants for the gel below the lower critical solution temperature were shown to be independent of punch size and frequency. Because our experimental testing apparatus is sensitive to very small phase angles, we were able to show that solvent transport through the gels above the critical solution temperature is inhibited in comparison to the transport rate at low temperatures, where local phase separation is not observed.

3.6 ACKNOWLEDGMENTS

Support to W. Lin in the form of a National Physical Science Consortium Fellowship and to K. Shull from the National Science Foundation (DMR-021416) is gratefully acknowledged. Y.Y. Lin is supported by National Science Council in Taiwan (NCSC93-2211-E006-069).

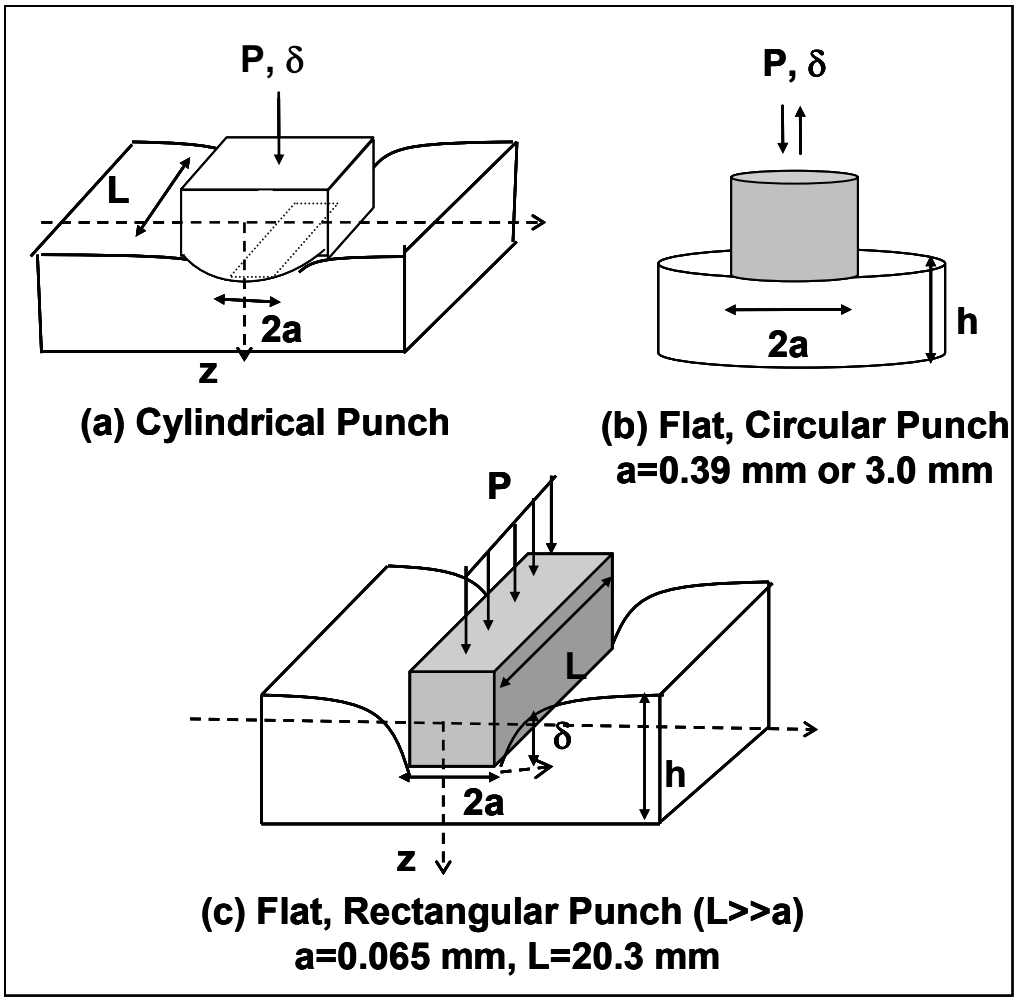

Figure 3.1. Indenter geometries used in the experiments.

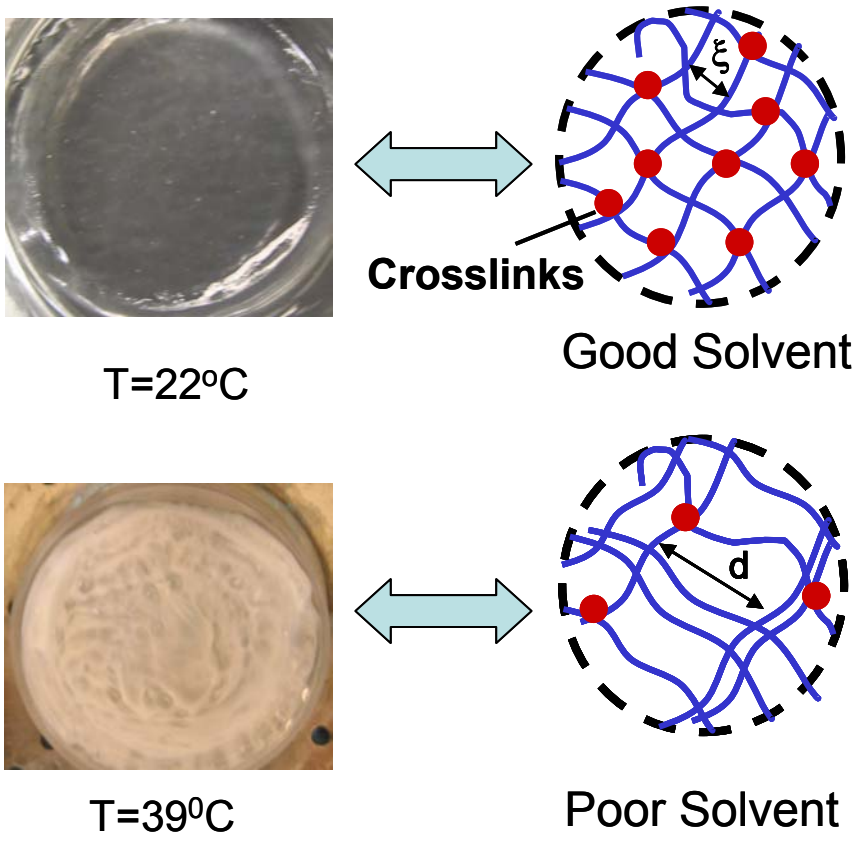

Figure 3.2. Photographs and schematic illustrations of the gel structure for pNIPAM above and below the critical temperature.

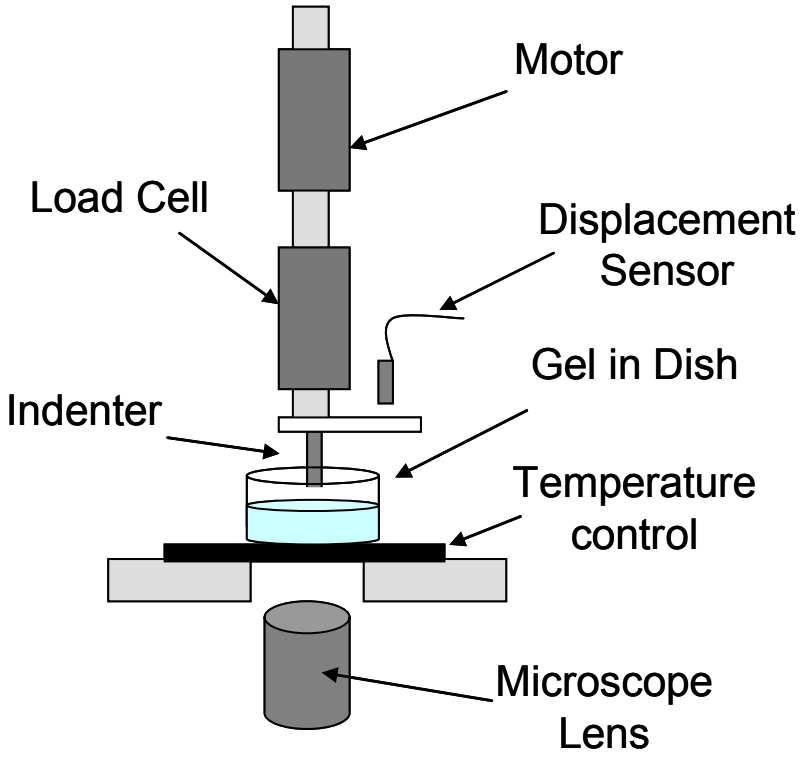

Figure 3.3. The probe tack apparatus.

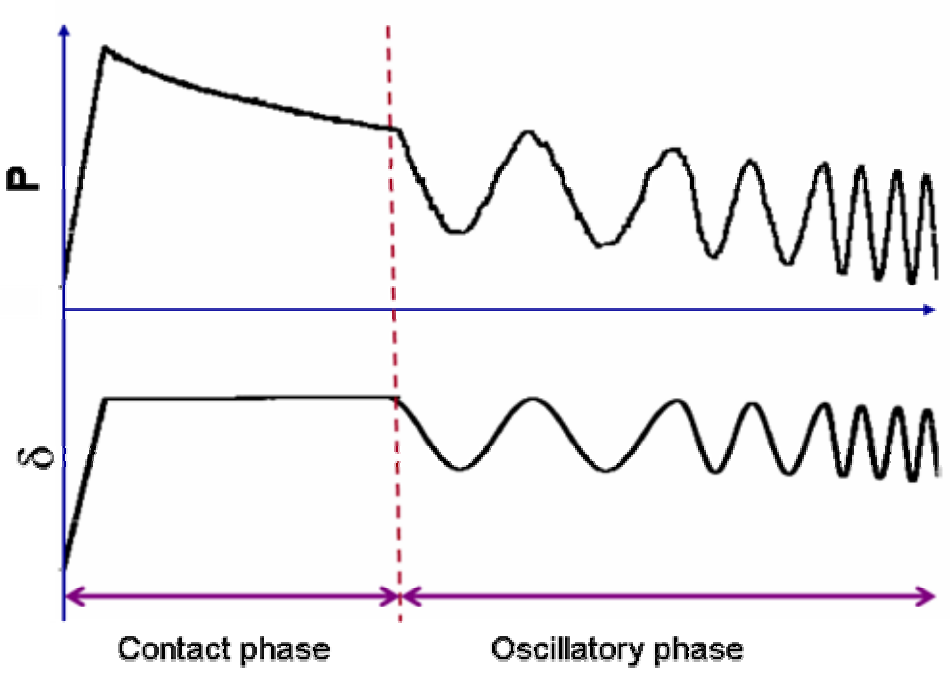

Figure 3.4. Load (P) vs. displacement (δ) histories for a typical experiment.

.

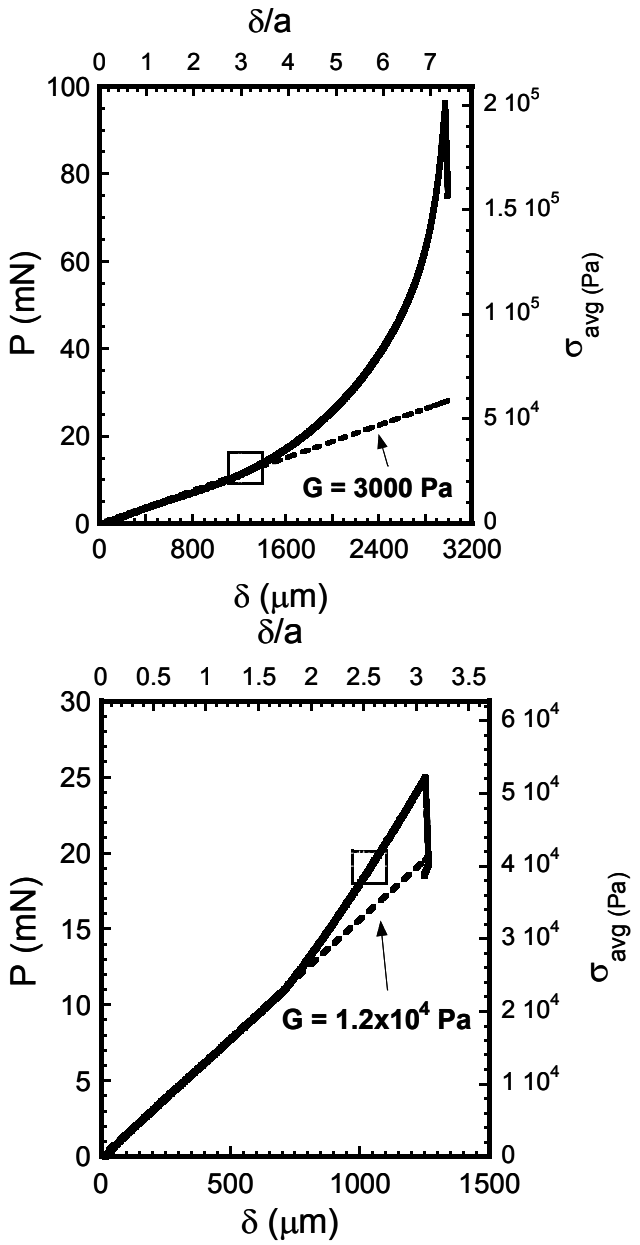

Figure 3.5. Load-displacement relationship illustrating the onset of nonlinear response for large δ/a using a 0.39 mm radius circular punch and a pNIPAM gel: **(a)** 22°C, a/h = 0.137; **(b)** 39°C, a/h = 0.179. The boxes on the graph indicate the regimes in which the oscillatory experiments were conducted (**Figure 3.6**). The dashed lines represent the linear response given by Equations (3.1) and (3.2).

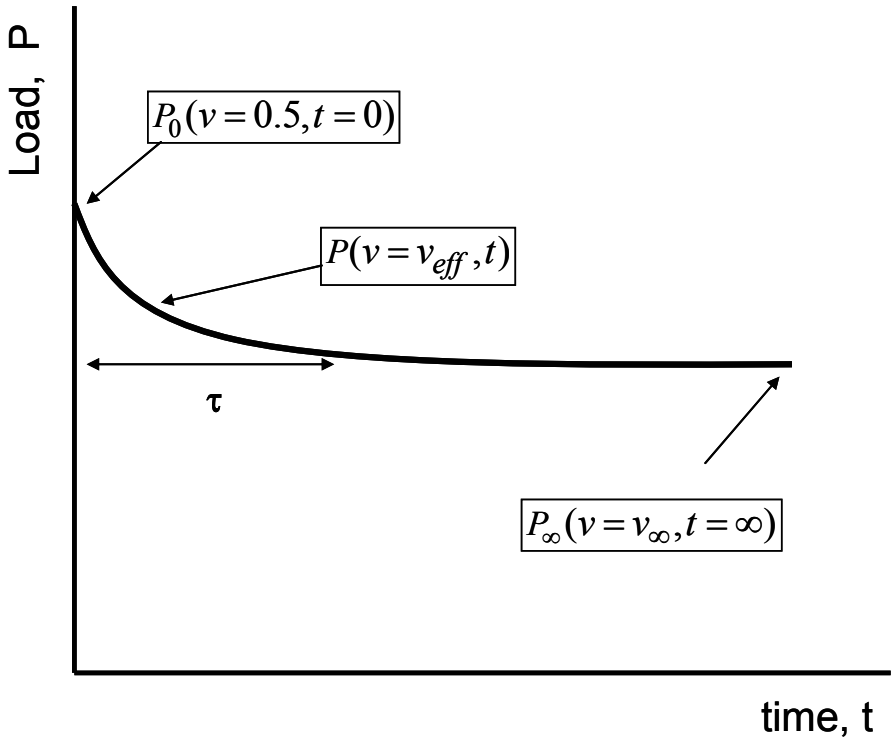

Figure 3.6. Idealized relaxation behavior of an elastic gel under compression.

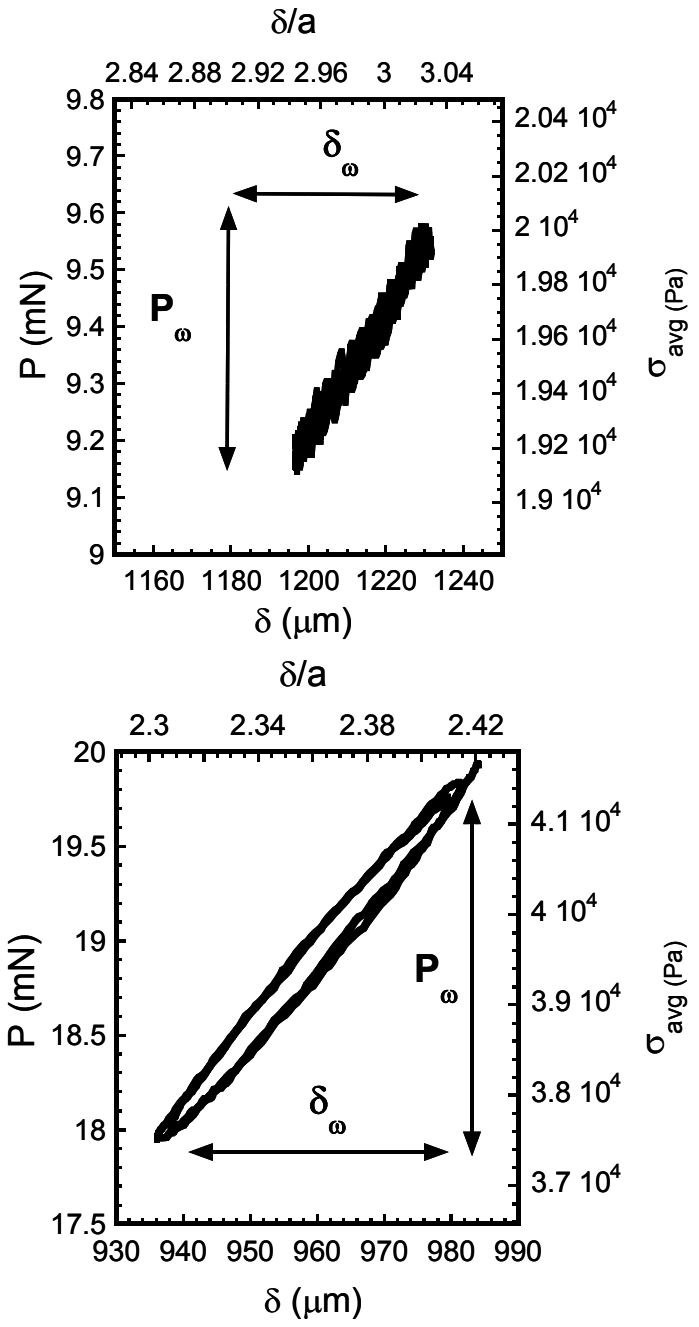

.

Figure 3.7. Oscillatory load-displacement behavior at $\omega = 0.50\ s^{-1}$ for a pNIPAM gel, using a circular punch with a = 390 μm: **(a)** 22°C ; **(b)** 39°C.

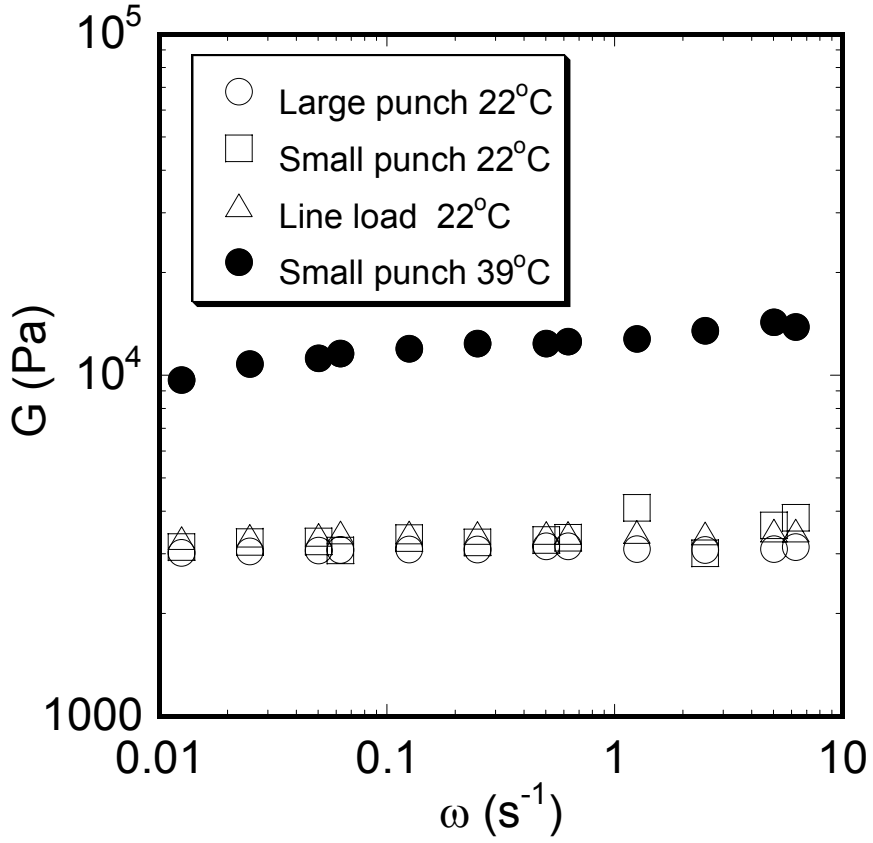

Figure 3.8. Values of the shear modulus obtained from application of Equation (3.13) to data obtained from the oscillatory experiments.

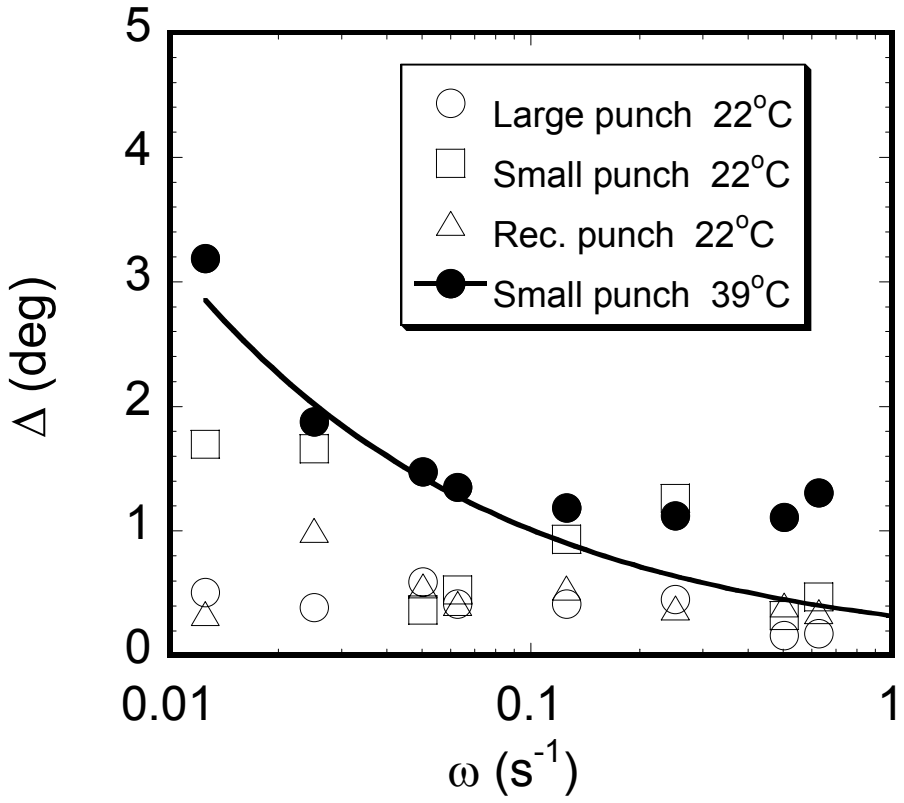

Figure 3.9. Phase angles obtained from application of Equation (12) to the oscillatory data. The solid line is the prediction of Equation 32, with $d/\lambda^{1/2} = 0.44$ nm.

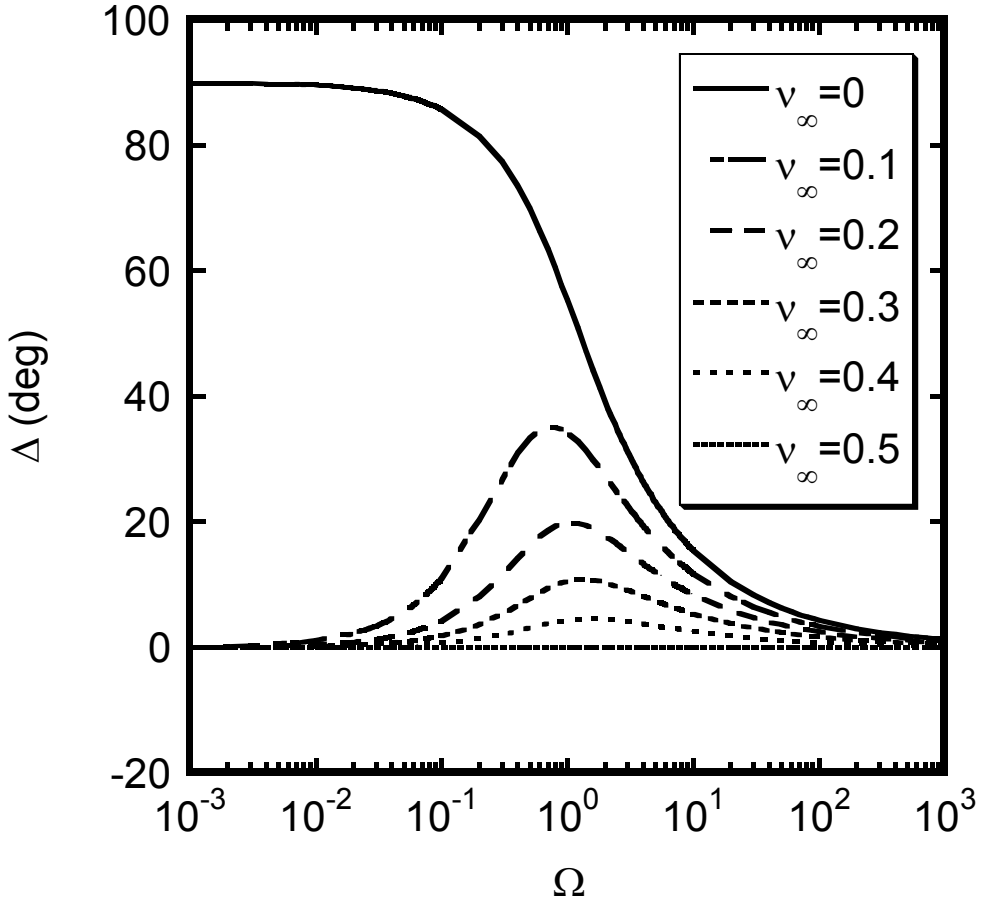

Figure 3.10. Calculated phase angles as a function of the normalized angular frequency from Equation (3.31), for different values of the relaxed Poisson's ratio.

CHAPTER 4

MECHANICAL CHARACTERIZATION OF SILICONE GEL LAYERS

CHAPTER 4

MECHANICAL CHARACTERIZATION OF SILICONE GEL LAYERS

4.1 INTRODUCTION

Understanding the properties of highly deformable materials, such as elastomers and polymer gels, at large strains is an important avenue to explore in materials science. From a mechanical perspective, the deformation of these materials can no longer be explained by the theories of linear elasticity. The stress concentration at the point of deformation is largely dependent on intrinsic material parameters. The structure of a material, for example, plays a role in this type of behavior.

Consider the difference in mechanical response of two samples: a physically cross-linked polymer gel versus a chemically cross-linked rubber elastomer at small and large strains. In a low strain experiment, the deformations are often small enough that the structure of either material is not affected by the deformation time scale. This response is expected when the materials are tested in the linear elastic regime. Upon extended deformation, the response of the materials will vary. At high strains, the chains in the polymer gel will separate, resulting in flow and permanent deformation. The rubbery polymer chains, on the other hand, will be restricted by the physical cross-

links in the system and will rapidly recover upon removal of the stress applied[54] In each case, the strength of the bond plays an important role in the behavior of the material at extended strains. Such a response is difficult to predict and is very important in applications where appreciable stresses are used.

Standard methods to measure large deformations of soft materials often are in tension[97, 98]. Devices, such as tensile testers, are often employed. In tensile testing, experimental difficulties are present for weaker gels due to the geometries of the samples. Common geometries for tension tests include gel strips, dumbbells or cylinders [99, 100]. Clamping a weak gel to the testing apparatus leads to preferential failure at the point that it is attached [100], whereas adhesion to the surface of the tensile tester becomes an issue when attaching cylindrical samples of gel to the plates of an Instron apparatus. To overcome these difficulties, biaxial tensile experiments can be performed but boundary effects limit the test region to a small portion of the sample [101]. Another approach is to utilize ring-shaped geometries of gel samples [100]; however, deflection due to viscoelastic flow or gel syneresis in very soft materials is still of concern. In this respect, compression experiments pose less experimental difficulties.

Although it is much easier to compress a cylindrical sample of gel, there are still difficulties in practicality to obtain meaningful data over a large range of strains. If a cylindrical sample of gel with a Poisson's ratio of 0.5 is placed between two parallel plates and undergoes uniaxial compression in the z-direction, the gel will act

incompressibly. The biaxial extension in the x- and y- directions will be related to the uniaxial extension in the z-direction. However, this extension will only occur if there is no friction between the interface of the gel surface and the plates. If there is a component of friction, the response of the sample will be dominated by this force. The gel will bulge and a barrel-shaped sample will result [102]. Furthermore, the limitation of these classic compressive tests is that a localized area of the sample cannot be probed, especially when a gel is not homogeneous in nature. This drawback can also be limiting to applications in medicine [103] and food [104], where the local strength of a material is important for safety or texture, respectively.

One solution to these issues is to utilize a compression experiment with a flat punch probe, as seen in **Figure 2.5**. In our work, we conduct experiments in this geometry because they can be performed very easily when the radius of the indenter is small compared to the dimensions of the sample. Although a consequence of this indentation technique is that the strain field is not uniform, material properties can be probed locally and transparency of the material is not necessary for contact area measurements. By applying this geometry, a single sample and instrument can be utilized to measure small and large scale deformation of a material; however, caution must be exercised beyond the non-linear regime, since strain fields are difficult to quantify. For this reason, we utilize elastomeric gels as model systems because their response will remain elastic until fracture. By utilizing these materials and the flat punch probe technique, our aim is to characterize the mechanical properties of soft

materials over a large range of stresses prior to fracture. Our intention is to gain a better understanding of how these responses change as a result of material structure and geometry.

4.2 METHODS

4.2.1 Model Systems

The materials chosen to model deformation at over a range of stresses prior to fracture are a series of chemically cross-linked poly(dimethylsiloxanes) (PDMS) gels, commonly referred to as silicone gels. We utilize silicone gels because they are frequently used in experiments as a simple model network to understand much more complicated systems [105] and are widely used due to their physical and mechanical properties. In the microelectronics industry, for example, PDMS is a superior choice as an encapsulant in packaging due to its high resistivity and thermal stability [106]. PDMS is also chemically inert and serves as an excellent barrier to water, making it well suited for applications such as adhesives, coatings, sealants [105], and potentially, cosmetics [107]. Because the materials in these applications often undergo appreciable stresses, we utilize silicones as a simple model elastic system to investigate the role of the network in relation to an added sol fraction under large scale deformation. Understanding this behavior provides insight into failure phenomena and the network properties for highly, elastic gels.

4.2.2 Chemistry

Silicone gels were prepared by a hydrosilation reaction [28], as shown in **Figure 4.1.** The reaction first begins by combining various fractions of vinyl-terminated poly(dimethylsiloxane) (PDMS) and end capped tri-methyl poly(dimethylsiloxanes). A tetrafunctional silane is added to the solution as a cross-linker and the vinyl-terminated poly(dimethylsiloxane) (PDMS) reacts with it to form a siloxane network. Because the end capped tri-methyl poly(dimethylsiloxanes) contains no functional groups to create cross-links for a network, it becomes the sol fraction of the newly formed gel [24]. The chosen catalyst for the reaction is a platinum(II) complex, which has been reported to have a 90% rate of conversion [22]. The above reagents were all obtained from Gelest, Inc.

4.2.3 Sample Preparation

Two sets of samples were prepared. For the first group, six different molecular weights of vinyl-terminated PDMS were chosen to represent samples without added sol fraction. The molecular weights of vinyl-terminated PDMS ranged from 500 g/mol to 117000 g/mol and are listed in **Table 4.1**. For the second set of samples, a series of twelve silicones with various amounts of added sol fraction were prepared. These

samples are listed in **Table 4.2.** Preparation for these silicones with added sol fraction is detailed below, since the samples of **Table 4.1** are made in a similar manner.

From **Table 4.2,** duplicates of twelve samples the size of sterile Nalgene Petri dish were prepared, using a method similar to the technique described by Larsen et al[24]. Standard vinyl-terminated PDMS solutions were initially made for the base network, and the weight percentage of sol was added accordingly. For our systems, three vinyl-terminated PDMS prepolymers with molecular weights of 500g/mol (V05), 28,000 g/mol (V31), and 117,000 g/mol (V46) and three tri-methyl PDMS prepolymers with molecular weights of 1250 g/mol (T11), 28000 g/mol (T31), and 139,000 g/mol (T51) were chosen. The tri-methyl PDMS prepolymers were added in weight fractions of 0.20, 0.40, and 0.50 of the total solution. In vinyl-terminated PDMS solutions where no tri-methyl PDMS prepolymers were added, the gel formed will be referred to as 'neat.'

To standardize the base network for each series of samples, 500 mL of a selected vinyl-terminated PDMS was poured into a clean glass beaker and 200 ppm of tetrakis(dimethylsiloxy)silane (hardener) was added to it. This solution was thoroughly mixed for about 3-5 minutes and 60 mL quantities of this solution were divided into 12 Al dishes.

A pre-measured amount of tri-methyl PDMS was then added to the vinyl-terminated PDMS and mixed with an Al spatula. Mixing time varied from 3-5 minutes. When the prepolymers and hardener were thoroughly mixed, catalyst was added into

solution and mixed for another 3-5 minutes. After mixing, 30 mL of solution was poured into a mould and immediately placed under vacuum for times ranging from 10 seconds to 15 minutes, depending on the viscosity of the solution. The samples were placed in an oven at 82^{o}C for 24 hours to ensure complete curing.

Because of the sensitivity of the reaction, issues with premature and incomplete curing were encountered. Premature curing was a problem due to the working time required. Preparation for one set of samples often took approximately 10-20 minutes, depending on the viscosity and molecular weight of the PDMS involved. When no additional sol was added to a sample solution, cure times were faster for the lower molecular weight samples compared to high molecular weight samples. Occasionally, a solution would completely cure before it could be poured into the mold. When sol was added to vinyl-terminated PDMS, cure times were comparable to the neat gels; however, mix times increased due to the differences in viscosity between the two materials. Minimizing the amount of working time and delaying the addition of catalyst is suggested to avoid premature curing.

One method to deal with the problem of incomplete curing was to mix the solutions by hand. Manual mixing of the solutions prevented the reaction from being accelerated, as this problem was especially prevalent in synthesizing the silicone networks with low molecular weight strands. In these cases, use of a blade mixer caused the mixture to cure before it could be poured into a mould. For silicones with high molecular weight chains, hand mixing was a better alternative to using the blade

mixer because the total quantity of hardener and catalyst required for these reactions was only a small fraction of the total solution. High molecular weight silicones made with the blade mixer would not cure because it was difficult to tell if even dispersion of hardener or catalyst occurred throughout the mixture.

Furthermore, the issue of incomplete curing could be resolved if the contamination of the catalyst was minimized. Because the catalyst mechanism requires that a metal ion both coordinate the olefin and cleave the Si-H bond[22], the catalyst is easily contaminated when it is in contact with trace elements of sulfur, tin, or nitrogen. Use of latex gloves and wooden spoons, as well as some plastic cups, where tin is used as a catalyst, can prevent the silicone from curing. To minimize contamination, Al trays and beakers were used in sample preparation and Al spatulas were used for mixing. Sterile Nalgene brand Petri dishes were also used as molds and did not pose a problem with curing. Between each batch of samples, the spatulas and beaker were cleaned in a solution of methyl-ethylketone and sonicated for 10 minutes at a solution temperature of 30^{o}C to prevent contamination.

Incomplete curing, however, could not be resolved for several of the samples containing 50% sol fraction. Curing, for example, was difficult for mixtures containing a tri-methyl prepolymer solution with very short chain lengths (e.g. T11) and a vinyl-terminated prepolymer solution with very long polymer chains (e.g. V46). The problem of curing in this situation is likely to be attributed to the high fraction of tri-

methyl PDMS present, which inhibits cross-linking and entanglement formation in the network, and the low cross-link density of vinyl-terminated PDMS.

4.2.4 Methods

Compression tests of the prepared silicone gels were performed on a flat punch probe apparatus and Test Resources 200R Research Universal Test System, as seen in **Figure 4.2** and **Figure 4.3.** As described in previous chapters and seen in **Figure 4.3**, the flat punch indenter consists of Burleigh inchworm motor attached to a Lucas Schaevitz 50 gm load cell. An indenter is attached below the load cell and a Philtec optical displacement sensor determines the amount of distance the motor travels. To replicate the experiments performed on the flat punch probe apparatus at Northwestern University, a Test Resources 200R System was modified to expand the capabilities of the instrument. A 250 gm load cell (Test Resources 200R) was used to measure the silicone gels and an indenter adapter, as seen in **Figure 4.2**, was custom built and fitted to the instrument for compression tests. The displacement resolution of the Test Resources 200R Test System is 0.1 μm, whereas the optical displacement sensor on the probe tack apparatus has a resolution of 0.38 μm.

Utilizing these instruments, the mechanical response of the samples was determined by performing a series of stress relaxation tests using an indenter with a radius of 0.39 mm. In one type of stress relaxation test, the indenter was brought into

contact with the gel, loaded to a maximum compressive force, held for 1000s, and then retracted from the gel. The maximum compressive loads set for these experiments were 100 mN and 2000 mN. In another experiment, the maximum load was set to 2000 mN and a series of stress relaxation tests were performed at 500 s intervals in the same spot. Experiments on both these devices were performed at a loading and unloading rate of 25 microns/s.

Shear moduli of the samples were measured with a Rheometrics ARES rheometer in a torsion geometry. A strain sweep for temperatures of -60^{o}C, -40^{o}C, and 20^{o}C was initially performed on rectangular samples cut from the moulds. Frequency sweeps from 0.1 Hz to 1 Hz were performed at 20^{o}C. The storage modulus (G'), loss modulus (G"), and the loss tangent (tan δ) were determined from the data collected.

After compression and rheological testing, Soxhlet extractions of the silicones were performed for 48 hours in toluene. A Büchi heating bath and vacuum controller was used to extract solvent out of the samples. The samples were then air dried for 24 hours and placed in a vacuum oven for 24 hours at 120^{o}C. The weight loss of the bar and the amount of solvent extracted was recorded. A compression test using the Test Resources 200R system was performed on the extracted samples.

4.3 RESULTS AND DISCUSSION

A typical loading-unloading graph of a silicone sample is illustrated in **Figure 4.4.** The regions in which our gels were measured are highlighted in the figure. Region **(a)** represents the small strain response of the gel, whereas region **(b)** marks a large deformation region of the sample. The dashed line in this figure acts as a guide for the eye and demonstrates where linear elastic behavior of the sample is expected, as well as where it begins to deviate. From these types of measurements, the mechanical properties obtained from **(a)** allowed us to probe the linear elastic behavior of our samples, while the response at **(b)** gave us an indication of how the gels behaved beyond the Hookean regime. Based on such measurements**,** we were able to characterize each individual gel from a mechanical standpoint over a range of stresses prior to fracture and determine how its structure and geometry affected its response. In particular, the effect of molecular weight, the addition of sol fraction, the role of entanglements, and the geometry of the sample were determined for our samples and are detailed below.

4.3.1 Molecular Weight and Structure

Characterization of the neat gels over a range of stresses was first performed to understand how molecular weight and structure affects their mechanical properties.

Additionally, the results of these experiments were used to calibrate our measurements on the different instruments.

The value of shear modulus, G*, was first determined for each of the neat gels. These values were calculated from data obtained in the flat punch compression tests with the assumption that the material is incompressible (Poisson's ratio, ν, is 0.5) and that each sample is perfect end-linked. From the corresponding load, *P*, and displacement, δ, G* is [71] could be calculated as:

$$G^* = \frac{P}{8a\delta} f_c\left(\frac{a}{h}\right), \tag{4.1}$$

when the punch radius, *a* ,is 0.39 mm. f_c in the above equation is the geometric confinement factor determined by the ratio of the indenter radius to the gel thickness, *h [66]*:

$$f_c = \left(1 + 1.33(a/h) + 1.33(a/h)^3\right). \tag{4.2}$$

Results of these measured shear moduli are plotted in **Figure 4.5**. The moduli data from **Figure 4.5** assume that our samples are perfectly end-linked and that the existence of impurities in our neat gels are insignificant, two assumptions that are consistent to similar previous studies[26-28, 108, 109]. As a comparison for the methods and instruments used, the G* values of these gels are plotted against literature values for tetrafunctional end-linked PDMS networks [26, 44]**.** One result that can be

concluded from **Figure 4.5** is that the measured values of G* from the compression tests agree with literature and rheology.

Additionally, **Figure 4.6** further supports that the existence of impurities in our neat gels are insignificant and that our gels are nearly ideal. **Figure 4.6** shows the corresponding average percent of extracted material for each sample and indicates that the measured reaction conversion in our samples is noted to be greater than 90%. Impurities in the reactants are attributed to the unreacted, extracted material, since several studies have shown that commercially available oligomeric PDMS reactants have 2-5% of 300-1500 molecular weight impurities[26-28]. Because it has been shown that such impurities do not have a significant impact on the properties of the higher molecular weight samples [26], these results allow us to assume that the presence of defects will not affect our measurements from a mechanical standpoint. Our results can therefore be interpreted based on the theory of rubber elasticity to our measurements

Based on these results, **Figure 4.5** also demonstrates the presence of entanglements in the network. Interpenetrating entanglements become more prominent than covalent cross-links in controlling the modulus of polymer networks with network strands that exceed 28,000 gm/mol. An entanglement plateau, G_e, of approximately 1.0×10^5 Pa is determined from **Figure 4.5**, which is consistent to the value of $G_e = 2.0 \times 10^5$ Pa reported by Patel, et al. for linear PDMS melts of molecular weights above 20,000 g/mol [44].

The modulus in our gels becomes nearly independent of molecular weight of the network strands between cross-links in the limit of very long network strands. As noted in Chapter 2, this behavior is consistent with the expected modulus of an entangled polymer network, whose sum can be approximated as (1) the affine, or small scale, deformation of the cross-links, G_x, and (2) an additional contribution to the modulus due to topolographic entanglements, G_x [28, 110, 111]:

$$G \approx G_x + G_e = \frac{\rho RT}{M_x} + \frac{\rho RT}{M_e} \tag{4.3}$$

For polymer networks with low molecular weight between cross-links, ($M_x > M_e$), the modulus is controlled by cross-links and $G \cong G_x$. For networks with high molecular weight between cross-links, ($M_x < M_e$), entanglements dominate and $G \cong G_e$. This behavior also is consistent with the expected response of polymer melt experiments at short time scales, where a temporary entanglement network is said to be formed due to the topological constraints that each polymer chain imposes on each other [112].

Such an effect of molecular weight and structure on mechanical properties is not limited only to the small strain regime. At a stress of 4.2×10^6 Pa, which is greater than the moduli value of the samples found in **Figure 4.5**, the response of the silicones is correlated to their molecular weights. As plotted in **Figure 4.7**, a greater percentage of relaxation is observed as the molecular weight of the sample increases. The exception to this behavior is noted for the 28,000 g/mol sample, which relaxes to a lower value of stress than the 49,000 g/mol or 72,000 g/mol sample during the duration of the

experiment. Although the 28,000 g/mol sample has a molecular weight lower than the 72,000 g/mol sample, the average percent of extracted material for the 28,000 g/mol sample is the largest by comparison in the samples tested, as indicated in **Figure 4.6**. This value indicates a weaker network possibly due to contamination of the sample during preparation.

The results of the neat gel indentation experiments indicate that the techniques and instruments applied to small strain measurements can be extended to characterizing silicone samples at higher stresses. The influence of molecular weight on the mechanical properties of silicones has also been shown. Furthermore, the results serve as a basis for comparison for probing the behavior of the elastomers when a sol fraction is added to them.

4.3.2 The Addition of Sol Fraction

As a comparison to three selected neat gels, the shear moduli of the gels with added sol fraction were measured. The small strain response of the 800g/mol (V05), 28,000 g/mol (V31) and 117,000 g/mol (V46) based vinyl silicones with added trimethyl-terminated PDMS are plotted in **Figure 4.8(a), (b),** and **(c)**, respectively**.**

From these results, the difficulty in synthesizing silicones with low molecular weight network chains is illustrated in **Figure 4.8(a).** The measured shear modulus of the V05 samples range from $4x10^5$ Pa to $3.3x10^4$ Pa and are quite scattered. Because

the working time in preparing these samples is on the order of 15 minutes before gelation occurs, there is little time to thoroughly mix the sample before the reaction begins. Use of a blade mixer is not possible because the mechanical energy from a blade mixer accelerates the reaction. The samples often gelled before even distribution of the catalyst could occur. These results indicate that poor mixing leads to incomplete cross-linking in the samples.

In contrast, the moduli measurements of the V31 and V46 gels are more reproducible and consistent, as shown in **Figure 4.8(b)** and **Figure 4.8(c)**. In these gels, shear modulus values decrease as sol fraction increases. However, the reported behavior is independent of the chain length of the added tri-methyl PDMS. For V31, the measurements decrease linearly from $7.5x10^4$ Pa for a sample with no added sol fraction to $1.3\ x10^4$ Pa for a sample with 50% capped PDMS added to it. Likewise, a sample with 100% V46 has an approximate value of $6.7x10^4$ Pa, whereas a sample with 50%V46-50% TXX has an estimated measured value of $1x10^4$ Pa.

One explanation for the behavior depicted in **Figure 4.8(b)** and **Figure 4.8(c)** is that the effect of added sol to the base vinyl-terminated PDMS network is comparable to the response of large quantities of unreacted material in the sample. A comparison of results from previous work [26-28, 113]on tetrafunctional end-linked PDMS networks demonstrates that an increase in the unreacted material within a sample will decrease the modulus of a sample. A study of imperfect networks formed by end-linking various concentrations of mixtures of a difunctional PDMS with

monofunctional PDMS also follows a similar trend [44]. As networks become more imperfect, the shear modulus drops linearly due to the addition of pendant chains in the system [44].

Another way to describe this system is to consider it as a covalently cross-linked vinyl-terminated PDMS base network interpenetrated by a tri-methyl PDMS network of entangled chains. Like an interpenetrating network, the effective load transfer occurs between the two networks [34, 114] and the effective modulus will have a linear relationship of the moduli of the two networks weighted by their volume fraction. Because the tri-methyl PDMS is not chemically cross-linked, the addition of tri-methyl PDMS decreases the effective modulus of the base network. At high stresses, the effect is magnified, as shown in **Figure 4.9(a)** and **Figure 4.9(b**). The stress relaxation experiments of **Figure 4.9(a)** and **Figure 4.9(b)** show that a gel with increasing sol fraction with a very long chain length (>28,000 gm/mol) causes greater relaxation of the gel.

4.3.3 Entanglements and Polymer Chains At High Stresses

Further characterization of two silicone gels was performed using repeated stress relaxation experiments to probe the effect of entanglements and polymer chains at stresses beyond their moduli values**.** Results of these experiments are illustrated in **Figure 4.10(a)** for the V31 base network with no added sol fraction and **Figure 4.10(b)**

for the corresponding gel with 20% added T31. In each sample, there is an increasing plateau stress with repeated loading of the indenter, indicating accumulated damage in the gel network. In the first two cycles, the irreversible behavior may be due to the movement of entanglements and the uncoiling of the polymer chains. Upon further re-loading to the same maximum load, polymer chains are stretched taut. This behavior has been suggested for fracture experiments in gelatin gels [115] and can be further demonstrated by **Figure 4.11,** where failure of the sample occurs after loading it for a 500 s cycle and waiting 24 hours before repeating the experiment in the same spot. From these experiments, it is evident that entanglements and polymer chain stretching play an important role in the elastic response of the material.

4.3.4 Geometric Confinement

Because our gels are highly deformable, one consequence of mechanically characterizing our samples is to consider the geometric confinement of the elastic layer under compression. As noted in Equation (4.2) and in Chapter 2, modifications are necessary in calculating mechanical constants when an elastic layer of gel can no longer be approximated as an infinite half-space. This aspect is especially important in our experiments, since our gels are deformed at stresses beyond the linear elastic regime. At such large stresses, the length scale of the contact area will surpass the dimensions of elastic layer of the gel, which will result in an increase in the stiffness of the gel[70].

Because the effect of the substrate on the elastic layer must be taken in account in our experiments, the degree of confinement of the gel can be determined with respect to the contact radius, a. We utilize this value because of its effect in the Hertz elasticity analysis, found in Equation (2.31). In this Equation, an indenter becomes 'sharp' when its indenter radius, r, approaches 0 at a fixed contact, a. Note that the indenter radius is for a spherical indenter in this situation. At this limit, the higher contact pressures result in stress singularities and an alteration of the stress fields at the point of contact. The material therefore 'sees' a different stress field than that is predicted from the Hertzian analysis. The contact radius, a, which in our case is also the punch size, can therefore be scaled by the thickness, h, of the elastic layer to form a dimensionless ratio of a/h. This ratio gives us an indication of how stiff the material will become when the samples are of finite size, since the stress fields will be altered. The a/h parameter was first proposed by Gent and Shultz [116]to describe the effective modulus of confined rubber blocks.

To understand the effect of confinement, the elastic layer is modeled over small and large deformations. Our focus in these models is on the actual displacement of the punch relative to the thickness of the sample, or δ/h, since, a larger displacement of the punch will lead to a more confined gel. Utilizing this dimension, the a/h parameter can be applied to determine the effective strain the material 'sees' at these displacements. A schematic of these dimensions is illustrated in **Figure 4.12(a).**

In our models, we assume that there are no frictional forces between the substrate and gel, as well between the punch and gel. Although it is likely that the substrate will not be frictionless, this assumption is likely valid for the punch. At small strains, the thickness of the sample is very large compared to the punch radius (*h>>a)* and the punch displacement (*h>>δ)*. Ignoring the *a/h* correction, the resulting load can be modeled as the elastic half-space result [66]

$$P = 8Ga\delta \tag{4.4}$$

The stress is then:

$$\frac{P}{\pi a^2} = \frac{8G}{\pi}\left(\frac{\delta}{a}\right) \tag{4.5}$$

At large deformations, the stress can be assumed to be dominated by biaxial extension of the material under the punch itself. Using the Neohookean model, the equation for the stress

$$\frac{P}{\pi a^2} = G\left(\mu - 1/\mu^2\right) \tag{4.6}$$

where μ is the extension ratio. Based on the **Figure 4.12(a)**,

$$\mu = \left(h - \delta\right)/h = 1 - \delta/h \tag{4.7}$$

Upon substitution of (4.7) into (4.6),. the load becomes

$$\frac{P}{\pi a^2} = G\left(\frac{\left(h-\delta\right)}{h} - \frac{h^2}{\left(h-\delta\right)^2}\right) \tag{4.8}$$

A sensible approximation of the load at large strain is to add both contributions:

$$\frac{P}{\pi a^2} = G\left(\frac{8}{\pi}\left(\frac{\delta}{a}\right) + \frac{(h-\delta)}{h} - \frac{h^2}{(h-\delta)^2}\right) \tag{4.9}$$

In terms of the *a/h* parameter and the displacement of the indenter relative to its thickness (δ/h),

$$\frac{P}{\pi a^2 G} = 1 + \frac{\delta}{h}\left[\frac{8}{\pi}\frac{1}{(a/h)} - 1\right] - \frac{1}{(1-\delta/h)^2} \tag{4.10}$$

A plot of $P/\pi a^2 G$ vs. δ/h, from Equation (4.10) for the *a/h* ratios of 0.1, 0.2, and 0.5 is shown in **Figure 4.12(b)**. As seen from this graph, the degree of confinement is greatest when a small indenter is displaced close to the substrate at high loads (i.e. when $a/h \rightarrow 0$ and $\delta/h \approx 1$). In contrast, geometric confinement is negligible when the elastic layer can be considered a half-space and the Hertzian analysis is valid. As noted above, this approximation occurs when *a* is large ($a/h \rightarrow 1$) and the strains applied are small ($\delta/h \approx 0$). For our studies, *a/h* can be approximated by the solid line, representing a/h=0.1. At very large deformations, the confinement effect would be magnified, since the *a/h* curves converge asymptotically. The results of this analysis indicate that stress distributions in these situations are altered when the material is confined to a thin layer and the substrate needs to be taken into account.

4.4 CONCLUSIONS

By utilizing a flat punch probe indentation technique, silicone based gels were characterized over a range of stresses prior to fracture. In particular, the effect of molecular weight, the addition of sol fraction, the role of entanglements, and the effect of geometric confinement on their mechanical properties was determined for our samples.

The effect of molecular weight and structure was determined by probing the small strain response and large scale deformation behavior of tetrafunctional end-linked silicones with molecular weights ranging from 800 g/mol to 117,000 g/mol. An entanglement plateau of approximately $1.0x10^5$ Pa is found to dominate in samples with high molecular weights (>28,000 g/mol). High stress tests of these neat gels indicate that greater relaxation will occur with longer chain lengths. Extractions of the samples indicate that there is greater than 90% reaction conversion for our samples and that impurities in our samples can be neglected.

The addition of sol to three base networks with molecular weights of 500 g/mol, 28,000 g/mol and 117,000 g/mol altered the mechanical properties of the silicones when compared to the corresponding neat gel. At small strains, increasing the amount of added sol fraction in a gel weakened the network and caused the modulus to drop. The value of the modulus measured was found to be independent of the weight of the sol fraction added. Similar behavior was noted for stress relaxation tests at high stresses.

A comparison of repeated stress-relaxation experiments between a neat gel and a corresponding sample with 20% added solvent suggests that a form of irreversible damage accumulation occurs. One possibility that this behavior may occur is due to the role of entanglement motion and polymer chain extension at high stresses. The behavior of these samples suggests that the gel network plays a relatively significant role in the elastic response of the sample at large stresses.

A model for geometric confinement of the elastic layer under large scale deformation was also determined. Utilizing a Neohookean model for large strains, the degree of confinement could be described by the punch size and is dependent on the displacement of the indenter relative to the thickness of the sample. At very large deformations, the confinement effect is magnified and the stress distributions in these situations would be affected by the substrate. These results of these experiments and model are of potential importance when understanding the fracture behavior of gels.

4.5 ACKNOWLEDGEMENTS

The author acknowledges Drs. Joseph L. Lenhart, Philip J. Cole, and Michael Kelly for funding support and the opportunity to work at Sandia National Laboratories in Albuquerque, NM. Sandia is a multiprogram laboratory operated by Sandia Corporation, a Lockheed Martin Company, for the United States Department of

Energy's National Nuclear Security Administration under contract DE-AC04-94AL85000.

The author would also like to acknowledge the following people for their contributions: Scott Spanglar for acquisition of rheology data; Kevin Austin for assistance in setting up the R200; Duane Schneider and Jennifer Corona for the extraction data; John Schroeder for material inventory; and G. Craig Clark, Bob Winters, and Nina Baum for assistance in sample preparation.

Molecular Weight (g/mol)	Sample Name
500	V05
6000	V21
28000	V31
49000	V35
72000	V42
117000	V46

Table 4.1. Vinyl-terminated PDMS samples with no added sol fraction.

Sample	Sol Fraction	Type of Sol	Fraction of Base Network	Base Network
1	0		1	V05
2	.20	T11	0.8	V05
3	.40	T11	0.6	V05
4	.50	T11	0.5	V05
5	0		1	V31
6	.20	T31	0.8	V31
7	.40	T31	0.6	V31
8	.50	T31	0.5	V31
9	0		1	V46
10	.20	T51	0.8	V46
11	.40	T51	0.6	V46
12	.50	T51	0.5	V46

Table 4.2. Silicone samples with added sol fraction.

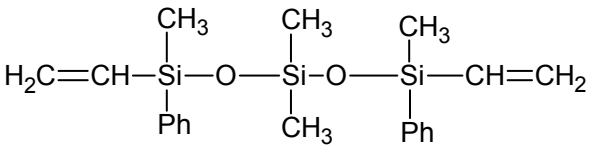

Vinyl terminated PDMS (VXX)

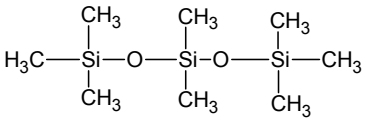

Tri-methylsiloxy terminated PDMS (TXX)
0%, 20%, 40%, 50% sol fraction

+

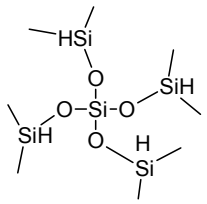

Tetrakis(dimethylsiloxy)silane
(cross-linker)

Pt
Hydrosilation

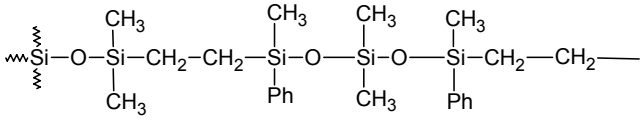

PDMS network with sol fraction

Figure 4.1. Silicone chemistry. Vinyl-terminated PDMS is hydrosilated with a cross-linker, tetrakis(dimethylsiloxy)silane to form a branched PDMS network. A silicone gel is formed when tri-methylsiloxy terminated PDMS (TXX) is added in increments of 0%, 20%, 40%, 50% by weight to form a sol fraction.

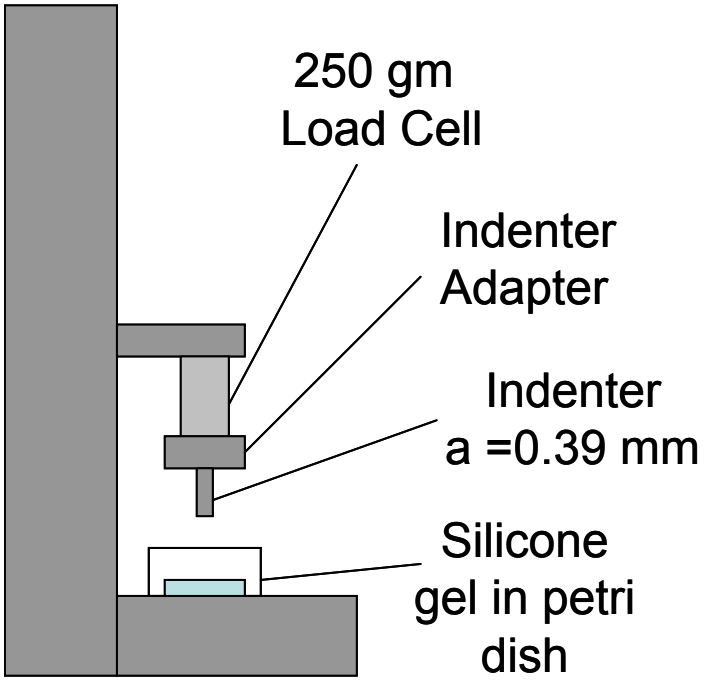

Figure 4.2. Test Resource 200R System with 250 gm load cell.

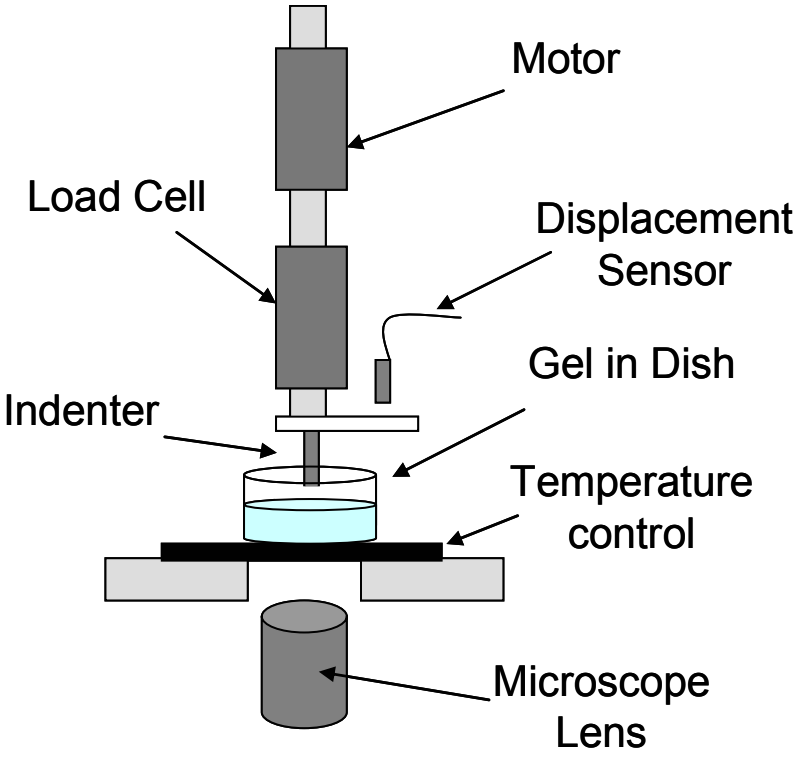

Figure 4.3. The probe tack apparatus.

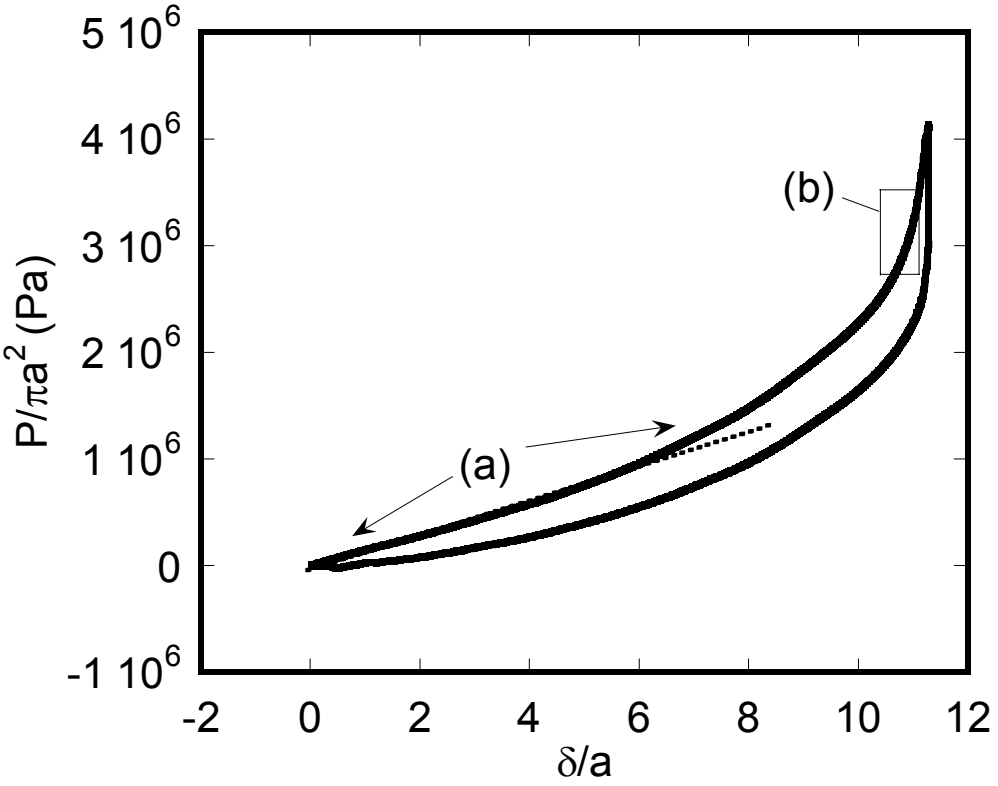

Figure 4.4. Elastic and large scale deformation regions of silicone. **(a)** The dashed line indicates where behavior of the sample deviates from elastic behavior to plastic deformation. **(b)** Large deformation region of the sample.

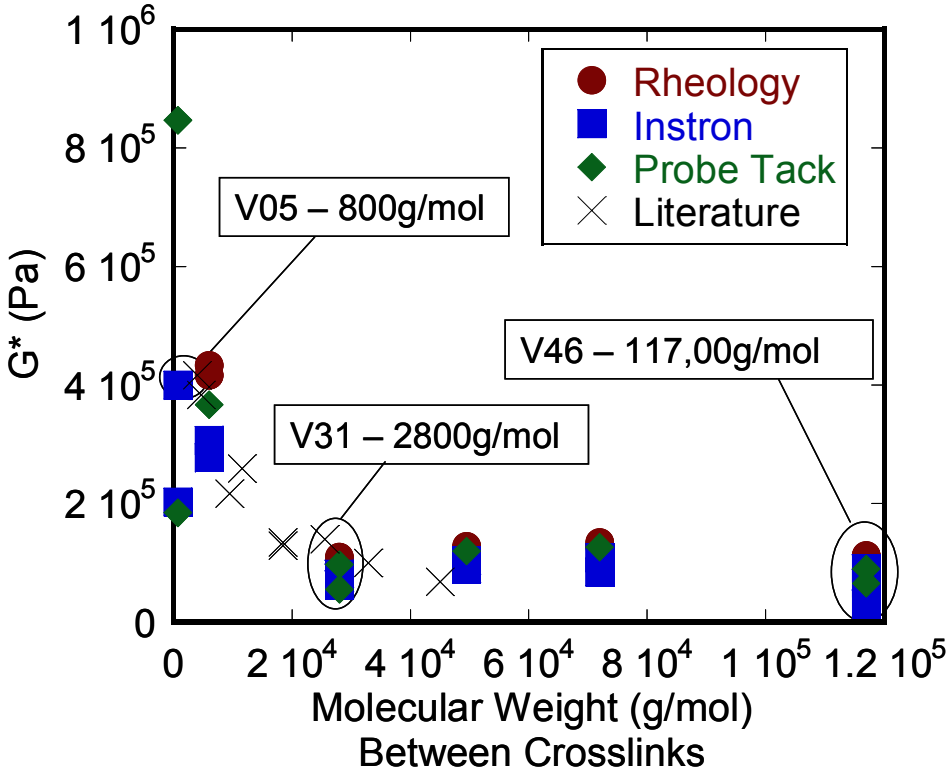

Figure 4.5. The modulus of varying molecular weights of silicone with no added sol component. Crosses (X) indicate values found in the literature. The base networks highlighted in the figure indicate the chosen weights in which 20%, 40%, and 50% by weight of tri-methyl terminated PDMS were added in later experiments.

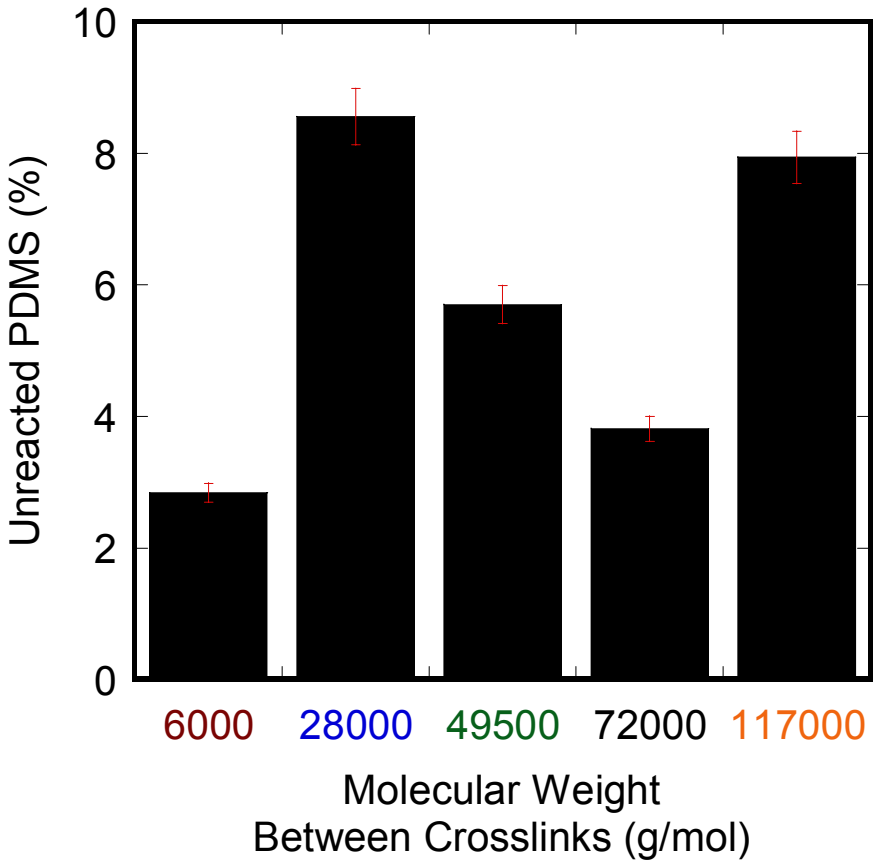

Figure 4.6. Extraction data for silicones with no added sol fraction.

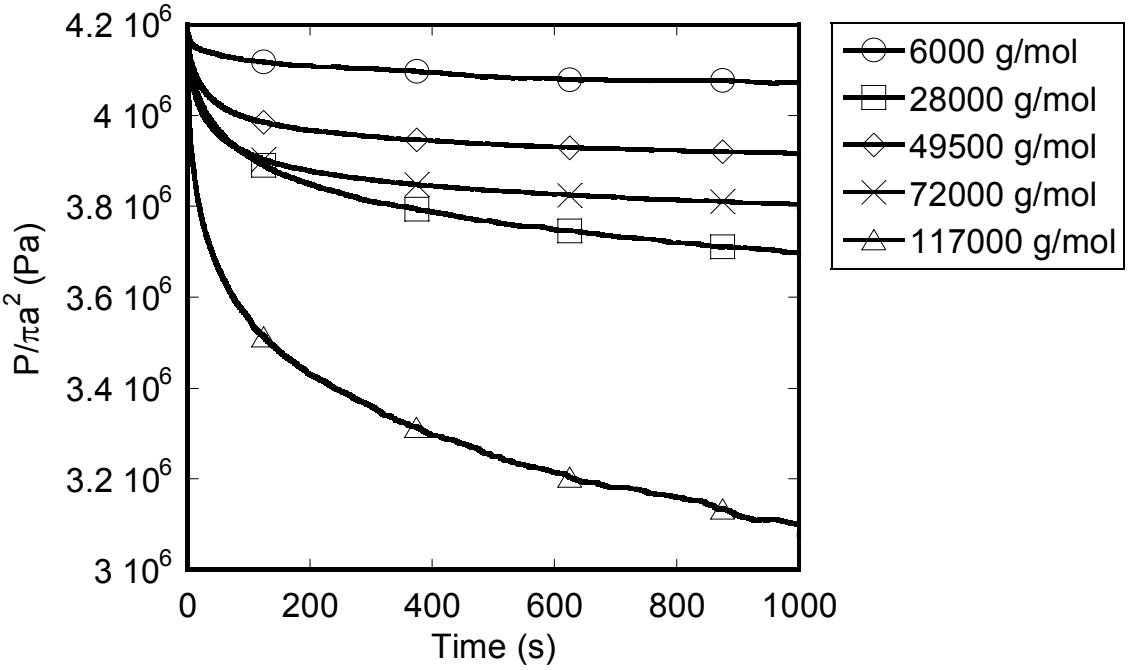

Figure 4.7. High stress response of the gels. The longer the chain length between cross-links, the greater the relaxation. The effect of unreacted material in the 28,000 g/mol sample is apparent under large deformations.

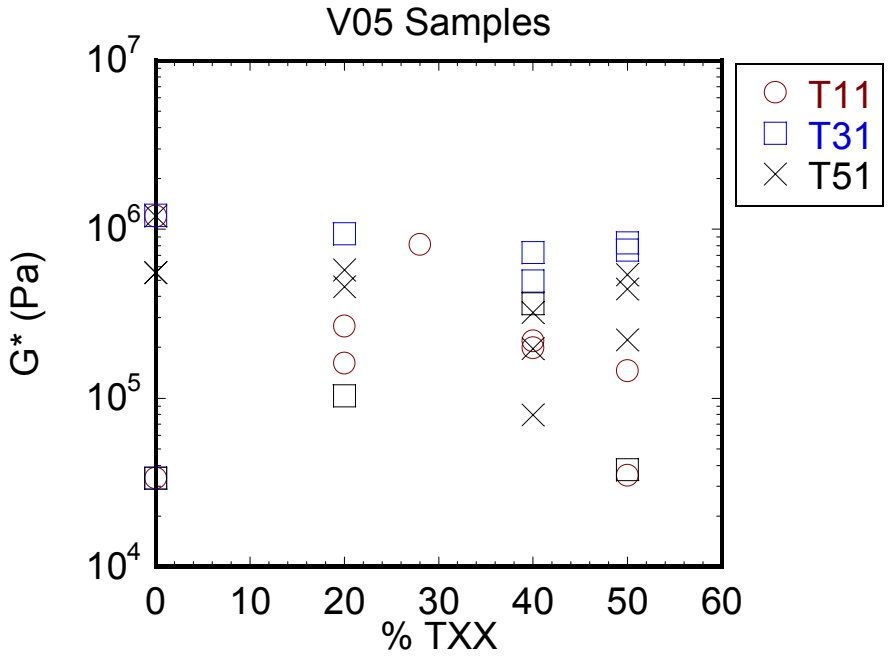
V05 Samples
10^7
10^6
10^5
10^4
G* (Pa)
0
10
20
30
40
50
60
% TXX
T11
T31
T51

(a)

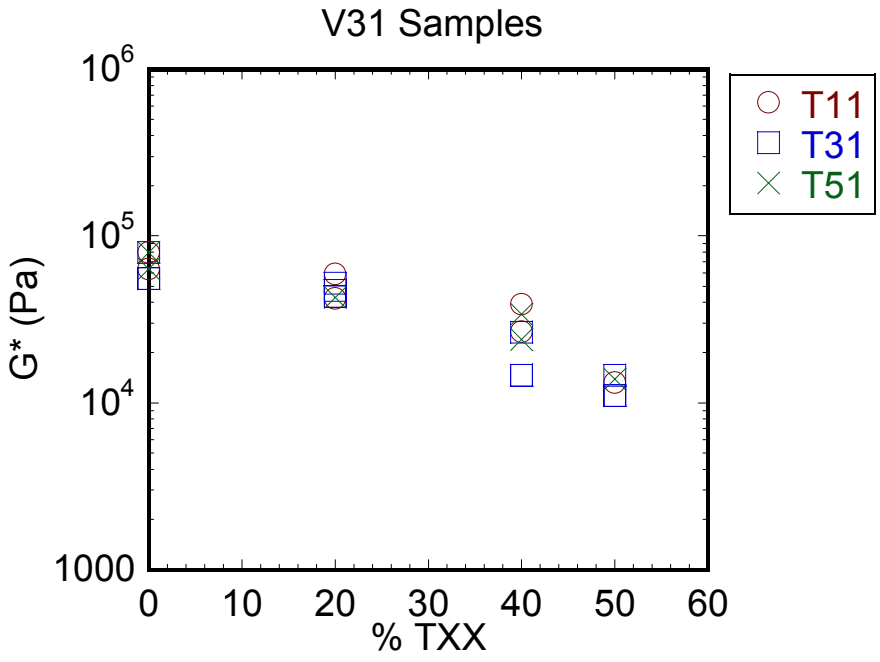
V31 Samples
10^6
10^5
10^4
1000
G* (Pa)
0
10
20
30
40
50
60
% TXX
T11
T31
T51

(b)

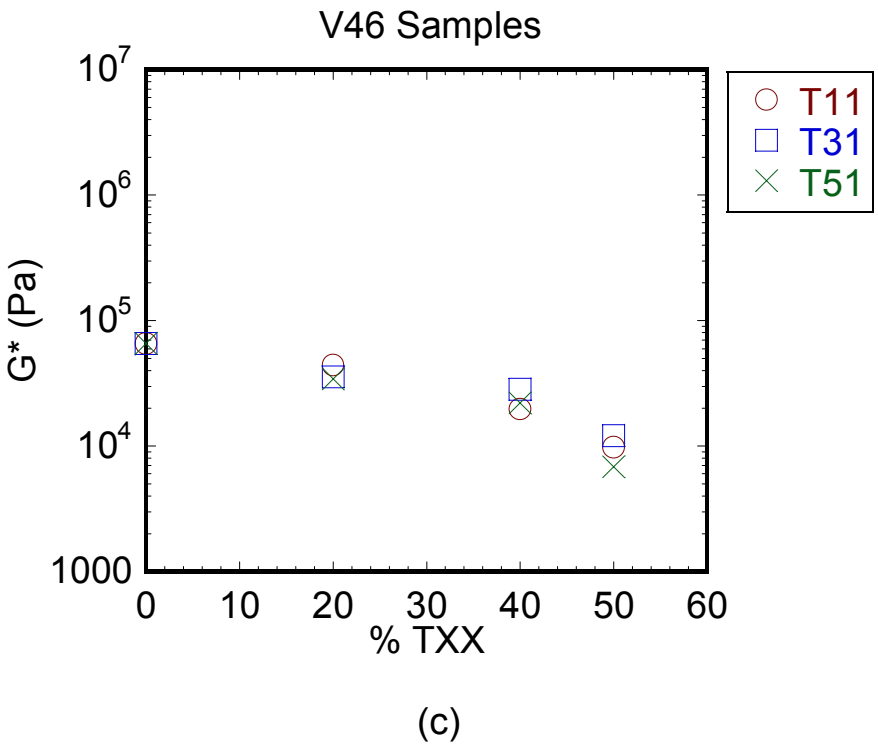

Figure 4.8. Modulus measurements when tri-methyl PDMS is added vinyl-terminated PDMS base networks of **(a)** 800 g/mol (V05) **(b)** 28,000 g/mol (V31), and **(c)** 117,000 g/mol (V46).

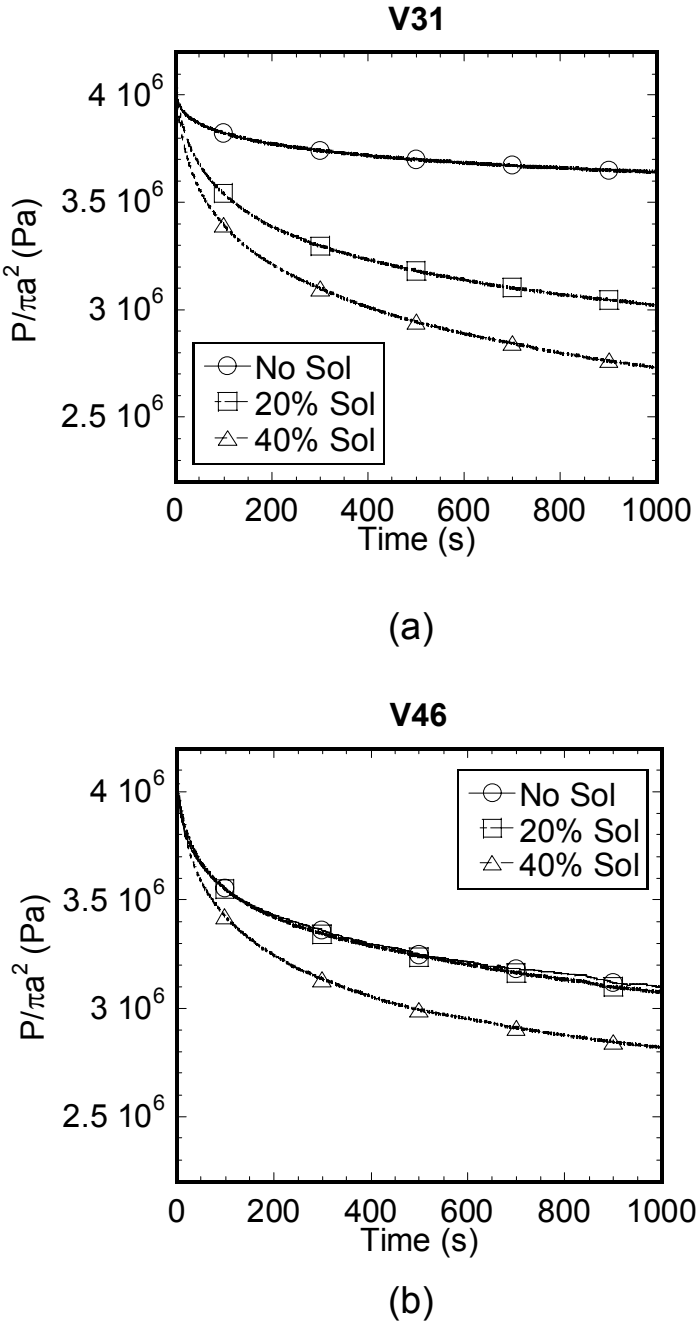

Figure 4.9. A comparison of large stress measurements for **(a)** 28,000 g/mol (V31) and **(b)** 117,000 g/mol (V46) when sol fractions of 20% and 40% are added.

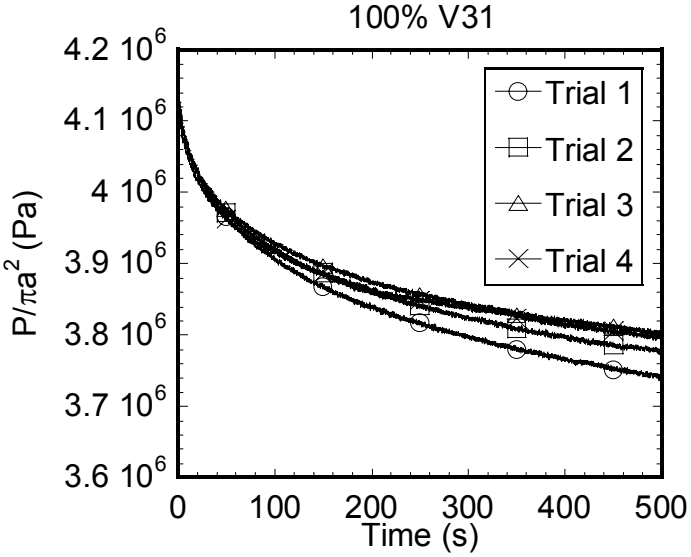

(a)

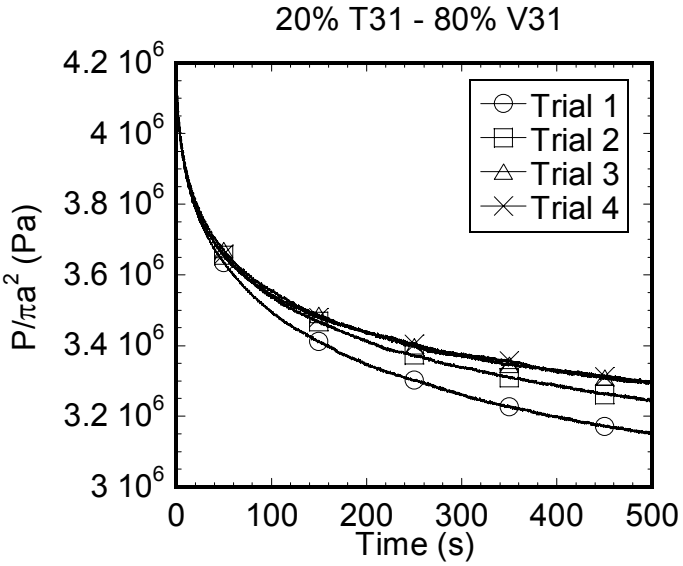

(b)

Figure 4.10. Evidence of polymer chain elongation from repeated stress-relaxation measurements focused on one point on a sample. For a V31 base network with **(a)** no sol fraction added and **(b)** 20% T31 added.

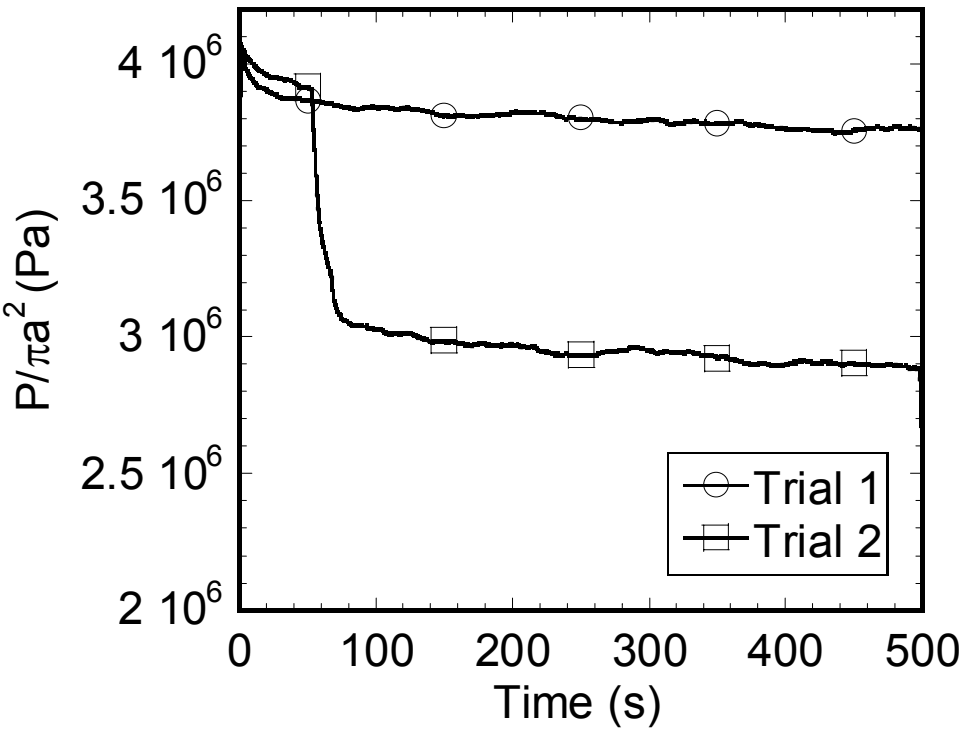

Figure 4.11. Failure of silicone with no sol added after repeated loading on same point. There is a 24 hour period of time between Trial 1 and Trial 2.

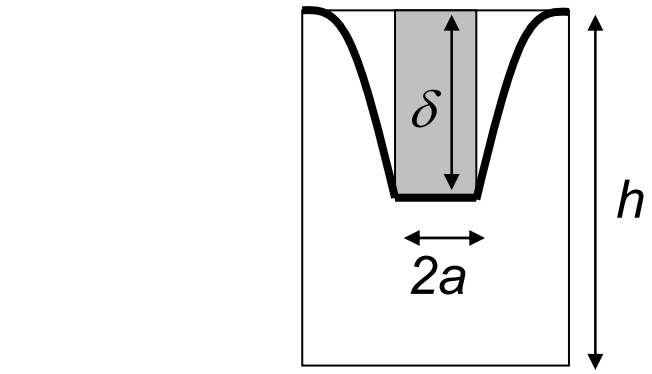

(a)

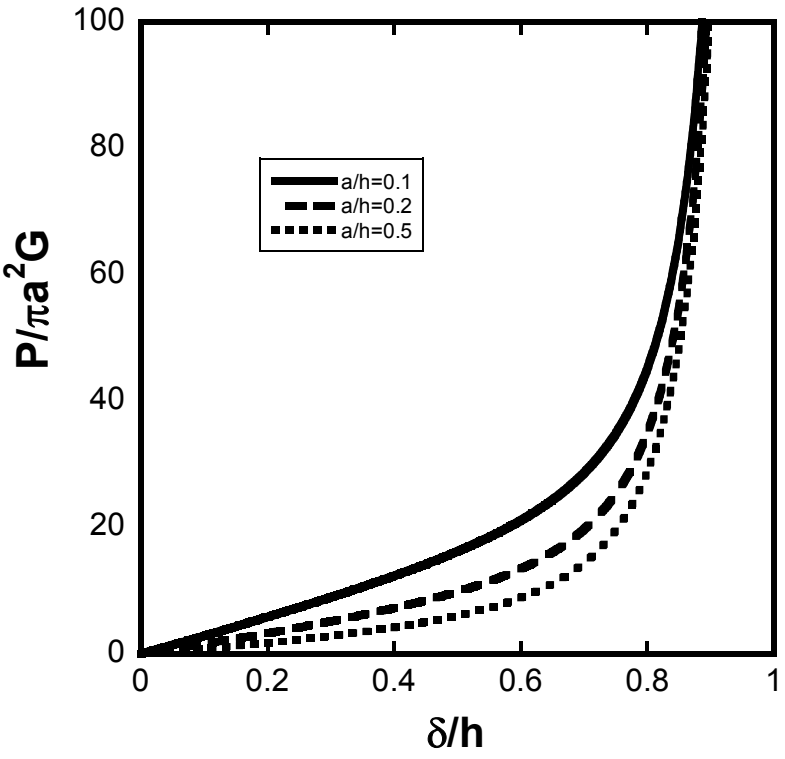

(b)

Figure 4.12. The effect of geometric confinement.

CHAPTER 5

DEFORMATION AND FAILURE MODES OF SILICONE GEL LAYERS

CHAPTER 5

DEFORMATION AND FAILURE MODES OF SILICONE GEL LAYERS

5.1 INTRODUCTION

Historically, research on the fracture of soft solids, particularly polymer gels, has often been neglected. Studies on fracture in the past primarily focused on brittle solid materials, such as metals and ceramics [72]. The slow growth of interest in this field can be attributed to the view that polymers are mechanically weak and therefore, not useful in areas where the fracture properties are relevant. The moduli of these soft materials ranges from ~ 10^3 to 10^6 Pa as compared to metals, which have moduli on the order of 10^{12} [66]. However, as the need for lightweight, cost-effective, mechanically robust soft materials increases due to the demands of technology, polymer gels are becoming more popular in industrial applications. As a result, there is increased interest in the topic of fracture in these highly, deformable materials [52].

In the past, studies were primarily focused on cohesive failure within a polymeric system, such as vulcanized rubber and polyurethanes. For example, extensive research on the fracture energies and strength of elastomers has been performed by Gent, et al. [30, 32, 117], whereas the processes of fracture on such highly elastic materials has been noted in the classic paper by Lake and Thomas [54].

Such studies often required an incision to be made in the sample to form notch-type tests [118] and include typical geometries such as trouser [119] or edge-crack test pieces [12] to study tearing. Current studies of a similar nature have shifted to understanding the failure mechanisms of biopolymers [115] and the effect of solvent in crack tips [120].

More recently, fracture research on polymeric materials has been driven by the aspect of adhesion [65, 121]. Failure mechanisms and processes of soft solids have been studied for geometries that include peel tests[65, 122], dual cantilever beams [123, 124], adhering spheres[65], and indenters [65] on viscoelastic bodies. Polymer gel research in this area has been applied to understanding debonding mechanisms in pressure sensitive adhesives[125] and the adhesion of thin polymer films [126]. Most of the experimental research on such soft systems has primarily focused their physical properties [58, 127].

Despite this growing interest in the failure of soft materials, there have been very few studies on the indentation fracture of soft solid elastic layers in compression[128]. When polymeric materials are tested in this geometry, they usually act as a soft substrate and are coated with a thin brittle layer to simulate dental coatings[129, 130], so little is known about the failure of these materials independent of the coating. The closest fracture studies of polymer gels which apply indentation techniques have focused on the puncture of biological tissues and silicone rubbers to understand the wounding of skin and the breaking of latex gloves [101, 131-133].

These experiments are often performed in geometries in which the material is not fully supported by a rigid substrate [101, 131, 132]. **Figure 5.1** depicts this geometry, which has been adapted from the work of Shergold and Fleck, as well as Nyguen and Vu-Khanh [132, 133]. Simulations have been performed to understand the failure of materials in this geometry [133].

Such experiments are useful in providing insight into the fracture processes of soft solids, however their geometries limit the types of materials that can be tested. One drawback to the puncture experiments is that a material used cannot sag under its own weight for the duration of the experiment. Highly, deformable soft solids would be difficult to use, as well as gels with a high sol fraction or those that may dry out during testing. Furthermore the samples would have to be large enough so that the chosen indenter is much smaller than the sample size to avoid edge effects. Another disadvantage in using the particular setup performed by Shergold and Fleck is that the velocity of the punch cannot be controlled[132]. In situations where these conditions cannot be met, a more controlled geometry is necessary. Minimization of these issues is possible if we apply indentation fracture to an elastic layer on a substrate.

In this work, we utilize this indentation geometry on thick polymer gel layers on a rigid substrate and apply compressive stresses on our gels to induce failure. In doing so, we explore the mechanisms of fracture in highly, deformable solids and understand how the addition of sol fraction affects failure. Although computational feasibility studies have been performed on biological tissues utilizing a similar approach[101],

there is still little experimental work that has been done for this particular geometry. Since most current studies in this area apply spherical indenters to determine the nonlinear properties of such materials[101], our approach complements these studies and provides another perspective in understanding the bulking behavior of soft matter. Furthermore, our interest in this geometry stems from its potential avenues for applications. For example, this geometry can be used to model the behavior of bulk tissue in biological systems. The results of our experiments may help develop improved prosthodontic treatment procedures, and allow better management of soft-tissue recovery following trauma[134]. Additionally, the indentation fracture of a highly compliant solid in this geometry can be used to simulate chewing and understand food texture in soft solids [135].

5.2 EXPERIMENTAL

5.2.1 Systems of Interest

Silicone based gels were chosen as model systems for these experiments due to their highly elastic network and their ubiquity in the medical and dental community. In particular, the gels labeled Samples 5 and 6 in **Table 4.2** were selected for indentation fracture experiments, since they had been well-characterized. As noted before, the network of the gels was formed from vinyl-terminated PDMS prepolymers with a molecular weight of 28,000 g/mol (V31). Tri-methyl PDMS prepolymers with a

molecular weight of 28,000 g/mol (T31) were added at a fraction of 20% by weight during sample preparation to form silicone gel systems. The sample without this sol fraction is referred to as the neat gel, and the one with 20% added sol fraction as the modified gel.

5.2.2 Methods

Fracture experiments were performed on the flat punch probe apparatus that is described in Chapters 3 and 4. Modifications of this apparatus were taken to account for the large range of stresses necessary for fracture. For example, a 1 kg load cell (Sensotec) was used to measure the force applied to the system, instead of a 50 gm device (Lucas Schaevitz). The use of smaller stainless steel indenters with radii of 0.17 mm and 0.21 mm were tested to induce larger stresses at lower loads; however, bowing of these indenter shafts at such high loads resulted. An indenter with a radius of 0.39 mm was chosen to avoid this issue. Additionally, a side camera was attached to the device to take photographic images of these experiments. A schematic of the sample geometry is depicted in **Figure 4.3**.

Compressive loads that induced indentation fracture were applied to the silicone gels. The method consisted of compressing the gels at a rate of 25 μm/s with a flat punch probe indenter to a maximum load and then holding it in place for 1000s at a constant displacement. At the end of 1000s, the gel was unloaded at the rate of 25

μm/s. To determine the range of stresses required to test each sample, a maximum force of 8.0 N, which corresponds to the upper range of our load cell, was first applied to the gel. If fracture could be induced, the maximum stress applied was decreased in a stepwise manner until failure did not occur in the sample. When a range of stresses was determined at which failure would occur, an array of loads was selected for our experiments. For each load chosen, the value was programmed into LabView and the test was repeated five times on different points of the sample due to the statistical nature of fracture.

5.3 RESULTS AND DISCUSSION

5.3.1 Delayed Fracture Behavior

From our data, a generalized delayed fracture event was noted for both the neat and modified gels. The typical stress, σ, versus time, t, response of a silicone sample that has undergone fracture in our strain–controlled experiments is illustrated in **Figure 5.2.** From this graph, a number of features can be defined as the gel is held at a constant displacement, δ, for the duration of 1000s. Upon loading, the indenter compresses the gel to a maximum stress, σ_m. For a period of time, t_f, the transient stress in the gel relaxes to a value of σ_f, the stress at failure. t_f can be defined as the

time to fracture and is the time if takes for the stress to relax from σ_m to σ_f. At σ_f, a signature of fracture occurs and the stress in the gel is relieved to a plateau stress of σ_{inf}.

As alluded to Figure 4.12, the details of the fracture event depend on the relative displacement at which it occurs, since large deformations can confine the elastic layer. The load-displacement graph of **Figure 5.3** demonstrates two different loading conditions in which the delayed fracture event is induced. The maximum displacements of two points of the neat gel are depicted. The indenter in each case is loaded onto the gel to a maximum load, held for 1000s, and unloaded. The dotted line represents loading conditions of the indenter when it is far from the bottom edge of the elastic layer ($\delta<h$), whereas the solid line designates applied displacements of the indenter close to undeformed thickness of the gel layer, h, ($\delta\approx h$). The fracture modes at these two different loading conditions are noted below.

5.3.1.1 Fracture at $\delta<h$

At stresses where the indenter is held at displacements far from the substrate ($\delta<h$), crack initiation occurs from a pre-existing surface flaw outside of the contact area. This behavior is noted in side-view images of the silicone sample in **Figure 5.4,** whose data correspond to the dotted line in **Figure 5.3**. As observed in **Figure 5.4(a),** a crack forms at the top half of the indenter after holding the indenter at 2 N. Retraction of the indenter leaves a silhouette of a Hertzian cone crack, as seen **Figure 5.4(b).** This

failure behavior is consistent with the experiments and simulations performed by Chai and Lawn[129] in which top-surface ring cracks were found to dominate crack initiation in very thick brittle coatings on complaint substrates utilizing a blunt indenter.

Based on these observations, a general failure mode can be used to describe the behavior of an indenter compressing on an elastomeric layer. **Figure 5.5** schematically illustrates this crack initiation behavior. (**Figure 5.5 (a)**) An indenter of radius *a,* is initially loaded to an elastic gel layer of thickness, *h.* (**Figure 5.5 (b)**) The sample is held at a constant stress and pre-present surface flaws are subjected to tensile stresses outside the contact zone. (**Figure 5.5 (c)**) At some point, a favorably located flaw, represented by the X, will initiate a crack. (**Figure 5.5 (d)**) A ring crack propagates incrementally downward in the rapidly weakening tensile field and the gel relaxes upward along the indenter. (**Figure 5.5 (e)**) The crack stops growing when there is no longer sufficient strain energy available to drive the crack. (**Figure 5.5 (f)**) Unloading of the indenter results in a Hertzian cone crack.

5.3.1.2 Fracture at $\delta \approx h$

At stresses where the indenter is held at displacements near the substrate ($\delta \approx h$), crack initiation is induced at the corner of the indenter. Corresponding to the data obtained from the solid line in **Figure 5.3**, **Figure 5.6** demonstrates the photographic evidence from the side-view camera of this response in a silicone gel compressed to a

σ_m of 1.26x10^7 Pa, which is equivalent to a load of 6 N. Initially, the gel is loaded and held to a maximum load of 6 N and relaxes for a time, t_f, as seen in **Figure 5.6(a)**. Note the evolution of a cone-like structure at the bottom of the indenter with time. At σ_f, a ring crack forms and propagates along the shaft of the indenter (**Figure 5.6(b)**). The formation of a ring crack column around the indenter is consistent to the observations of Shergold and Fleck in their puncture experiments[131, 132]. Retraction of the indenter leaves a silhouette of the crack as the volume of gel that was displaced returns to its original position (**Figure 5.6 (c)**).

An explanation of this behavior can be formed if we extend the general failure mode of an elastomeric layer to the highly confined volume of gel in these experiments. In these experiments, a top surface defect at the corner of the flat punch induces a ring crack to form, since the stresses are highest at those points of the indenter [63]. **Figure 5.7** demonstrates this behavior. (**Figure 5.7 (a)**) At first, an elastic silicone layer of thickness, *h,* is compressed by an indenter with a radius of 2a. The gel is held at a constant load. (**Figure 5.7 (b)**) Stresses at the point of contact are highest around the corner of the indenter, marked by Xs. (**Figure 5.7 (c)**) Eventually, a surface ring crack forms around the corner of the punch indenter and (**Figure 5.7 (d)**) the crack will propagate downward in the tensile field. (**Figure 5.7 (e)**) Since the crack cannot continue through the rigid substrate, the shape of the cracked material relaxes around the length of the indenter. (**Figure 5.7 (f)**) Unloading of the indenter results in a crack with a length, *l.*

The images of **Figure 5.6** and the above analysis strongly suggest that the behavior of the highly confined volume of elastic gel is therefore similar in nature of thin brittle coatings on a substrate, even though it has been noted that the substrate controls the stress level of the thin coating[129]. In work performed by Chai and Lawn [129], top ring cracks were observed in crack initiation of ultrathin brittle films when blunt indenters were used. This response is similar to the initiation of the crack by the corner of the indenter in our samples. Furthermore, though-thickness ring cracks were observed transversely along the entirety of thin ceramic films, where the radius of the ring crack in their samples was approximately equal to the radius of the area of contact[129]. In our samples, similar behavior is noted in **Figure 5.8,** where the average crack length, l_{avg}, of five samples is taken for each specific maximum stress, σ_{max}, plotted and normalized by the thickness, h, of the sample. Unfilled circles represent the gels with no additional sol fraction and filled circles represent those with sol in this graph. The data taken for this graph assumes that the overall fractured sample relaxes so that the crack tip can be imaged.

5.3.2 General Delayed Fracture Properties

Based on the above analysis, we now look at the specific properties which can be attributed to the delayed fracture response of elastomeric gels. We focus primarily on the gels in which failure occurs when $\delta \approx h$, since our data for these gels are

statistically significant. Several common characteristics are found among the gels when the applied maximum stress, σ_{max}, are compared to the failure characteristics identified in **Figure 5.2**.

Prior to failure, the amount of time for viscoelastic relaxation in the gels is shortened at higher loads. Such a characteristic is demonstrated in **Figure 5.9,** where time to failure is plotted against the maximum applied stress. The gel with no added sol fraction is represented by solid bars and the sample with 20% added sol is represented by the crosshatched ones. From this plot, it is evident that there is a decrease in the time to failure, t_f, as a larger maximum stress is applied in both gels. This trend indicates that the relaxation of the polymer chains in the network of the two gels is time dependent prior to fracture.

At and after fracture, a general correlation is also observed between the maximum stress applied, σ_{max}, to both the failure stress, σ_f, and the plateau stress, σ_{inf}, respectively. A linear relationship for these properties of the elastomers is shown in **Figures 5.10** and **5.11**. In these graphs, unfilled circles denote data for the neat gel, while crosses represent the modified gel. Two filled circles represent the samples from **Figure 5.3,** one that fails from a surface flaw and the other from the edge crack, and are highlighted for comparison. A dotted line is drawn on the plots, representing $\sigma_{max} = \sigma_f = \sigma_{inf}$, as a guide for the eye. This line indicates the expected behavior of a purely elastic solid in which there is no viscoelastic component contributing to stress relaxation or when there is no fracture that occurs.

From these plots, a predication can be made for the relaxation behavior and the stress released from delayed fracture of elastomeric gels in general. As shown in **Figure 5.10**, there is evidence from our measurements that relaxation occurs at a specific fractional value of its applied maximum stress; a ratio can therefore be determined for σ_f to σ_{max} by fitting a linear curve through the origin for each set of data. For our elastomer gels, this value ranges from approximately 10%-20%, as noted in **Table 5.1,** and implies that the majority of viscoelastic relaxation of our elastomeric gels is from the gel network. This property prior to fracture is similar to the behavior seen in alginate gels at large strains, where the maximum stress applied to these materials decayed to 0.5 of its original value after 500 s[48]. After fracture, **Figure 5.11** demonstrates that the total stress released from the resulting crack for each individual elastomer is nearly constant, since the resulting σ_{inf} increases proportionally to a greater applied σ_{max}. That is, a finite amount of stress can be released, since the maximum length the crack can propagate is from the bottom surface of the gel to its top surface. Further evidence of this behavior is supported from the crack lengths shown in **Figure 5.8,** which are also nearly constant for each individual gel sample at the varying maximum displacements. A resulting ratio of σ_{inf} to σ_{max} can also be determined for our gels in a similar manner described for σ_f/σ_{max} . Values of $\sigma_{inf}/\sigma_{max}$ are shown in **Table 5.1.** These general characteristics provide insight into mechanisms of fracture resistance and are useful in characterizing the effect of sol fraction in our systems.

5.3.3 Effect of Sol

The addition of sol to a silicone network changes the response of the gels at fracture. Although it has been shown in Chapter 4 that the modulus of a silicone decreases with increasing sol fraction, the addition of sol to a gel toughens it at stresses large enough to induce fracture.

A toughing effect is observed when comparing the delayed fracture characteristics noted in **Figure 5.2** and the crack lengths of the gels. For example, a comparison of failure times for the samples provides evidence that t_f decreases for each range of applied stresses when added sol exists in the gel, as demonstrated in **Figure 5.9.** One implication of this result is that the sol delays crack initiation by strengthening defects within the gel network. Furthermore, the statistical data in **Table 5.1** strongly suggests similar behavior. The contribution of strength from the sol to the network is observed when comparing the values of $\sigma_{inf}/\sigma_{max}$, the percentage of residual stress left after fracture, of the two samples. Despite a lower cross-link density in the gel with 20% sol fraction, this modified sample exhibits the greatest percent of residual stress. The difference between σ_f/σ_{max} and $\sigma_{inf}/\sigma_{max}$ also suggests toughening as well. As noted in the last column of **Table 5.1,** this value, which provides an indication of the fractional stress relaxation due to the formation of the crack, is larger for the neat gel. The amount of stress that is released from the fracture event in the modified gel with sol fraction is less than that of the neat elastomer. One explanation for this behavior is that the sol prevents the crack growth due to its incompressibility. Additional evidence

of crack blunting by the sol is illustrated in **Figure 5.8**, where the fraction of cracking in the gel after it has been unloaded is less in the modified gel.

5.3.4 Mechanisms for Fracture Resistance

Since the delayed failure event occurs in both gel systems, it is evident that fracture resistance of the material is primarily related to the strength of the polymer chain network. The mechanisms resisting crack initiation must therefore either absorb or dissipate energy from the system of polymer chains. Such mechanisms can be attributed to chain scission [115], entanglements[136], and viscous dissipation from the network.

The mechanisms resisting fracture contribute primarily to the value of time to failure, demarcated as t_f in **Figure 5.9,** in the delayed failure process. Resistance to failure in our case may result from a multiple-step process. Initially, the chains organize themselves to minimize the energy of the system as the maximum load is applied. As time progresses, there is viscoelastic loss from the strands in the network. The polymer chains are then stretched and a form of strain hardening occurs, where stress relaxation plateaus. This effect is supported by the results in **Figures 4.10** and **4.11**, which demonstrates the irreversibility of stress relaxation in the gel with successive loading cycles and the eventual weakening of the gel to fracture. The polymer chains or a subsection of the chains are possibly extended, creating resistance

to fracture [54]. Furthermore, entanglements with the gel act as effective cross-links [136] and chain pullout from surrounding section of the polymer matrix may occur before fracture is initiated [115].

The damage from applied stress can lead to fracture. The chains that lie in the fracture plane are ruptured, leading to the formation of a ring crack. This rupture behavior has been observed by Baumberger, et al. in hydrogels [115, 120], and is supported by the Lake and Thomas theory, which noted that both chains and bonds needed to be fully extended for rupture to occur.

In the modified gels, a surprising result from our experiments is that the added sol fraction creates greater resistance to fracture, even though it lowers the modulus of the gel at small strains. At stresses close to failure, the sol toughens the network prior to crack initiation and blunts crack growth. As noted before, the longer times to failure in **Figure 5.9** suggest that the sol prevents crack initiation. It is possible that the solvent-network motion prevents failure by providing easier access for chain pull-out from another fracture plane. This notion can be deduced from experiments performed by Baumberger , which found that high viscosity solvents will increase the energy required for failure in a soft solid [120]. Furthermore, the difference in crack lengths in **Figure 5.8** suggests that the sol fraction prevents crack growth. Elastic blunting of the crack may result [56], since the sol may be considered as an incompressible material. It is possible that the added sol fraction prevents the volume of gel to be displaced from underneath the indenter prior to fracture. As it is difficult to fully probe the effect of

solvent independent of the network, the role of the sol in relation to the network in a polymer gel needs to be explored with further experimentation.

5.4 CONCLUSIONS

A delayed indentation fracture response was observed and characterized in silicone gels under constant strain with a rigid flat punch probe. This response can be defined by a characteristic time to failure, which is the time it takes for a gel to fail catastrophically from the point of maximum loading.

Two modes of failure were observed, depending on the confinement of the elastic layer. When the indenter is held at displacements far from the substrate ($\delta<h$), a surface flaw initiates a ring crack that leads to the formation of a Hertzian cone crack. The crack in this case grows transversely until it reaches the edge of the weakening tensile field. When the indenter is held at displacements near the substrate ($\delta\approx h$), crack initiation is induced by the high tensile stresses around the corner of the flat punch probe. A ring crack is formed and the gel eventually relaxes along the shaft of the indenter to relieve the high stresses produced from loading. The overall fractured gel relaxes with retraction of the indenter and a crack length that is close to the thickness of the sample appears. The modes of fracture observed are similar those seen in thick and ultrathin brittle films [129].

From our analysis, the delayed fracture event is likely related to the strength of the polymer chain network. From our large deformation experiments in Chapter 4, fracture resistance mechanisms can be attributed to chain stretching [115], entanglements[136], and viscous dissipation from the network. The addition of sol also toughens the gel and creates resistance to fracture. An increase in added sol fraction leads to a larger load required for failure and results in shorter crack lengths after the fractured gel is allowed to relax. Crack blunting may occur due to the incompressibility of the sol or the movement of the polymer chains in the solvent.

5.5 ACKNOWLEDGEMENTS

Support to the author in the form of the National Physical Science Consortium Fellowship is acknowledged. The author also acknowledges Michelle Seitz for thoughtful discussions on this research.

	$\frac{\sigma_f}{\sigma_{max}}$	$\frac{\sigma_{inf}}{\sigma_{max}}$	$\frac{\sigma_f - \sigma_{inf}}{\sigma_{max}}$
No Sol	0.89	0.58	0.31
20% Sol	0.83	0.71	0.12

Table 5.1. Comparison of average fractional relaxation values for silicone samples.

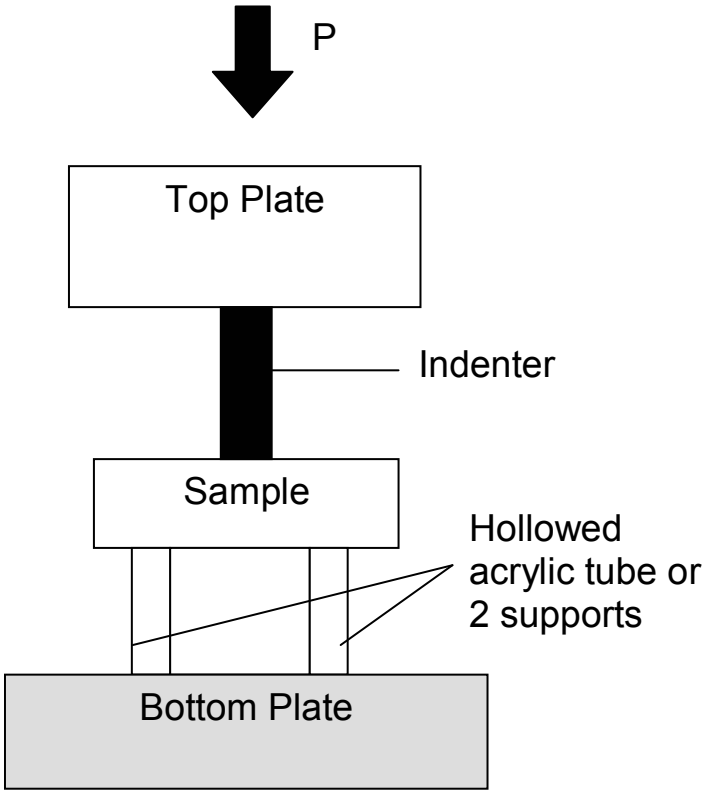

Figure 5.1. Common indentation geometry for soft solids. Note that the sample is not fully supported by a substrate.

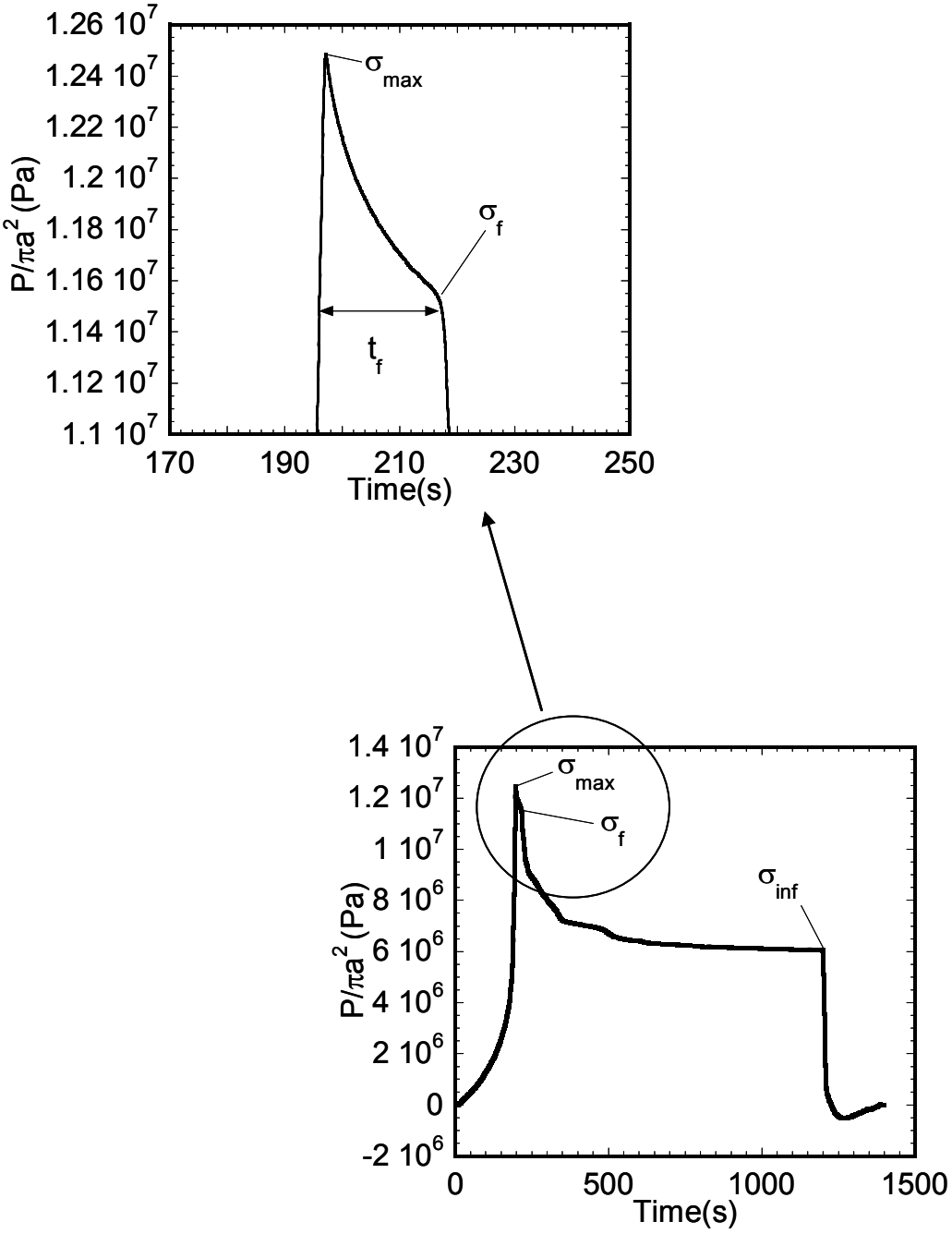

Figure 5.2. Typical delayed fracture response. The gel is loaded to a maximum stress, σ_{max}, and relaxes for a time, t_f. At σ_f, a crack forms and the gel eventually relaxes to a plateau stress, σ_{inf}.

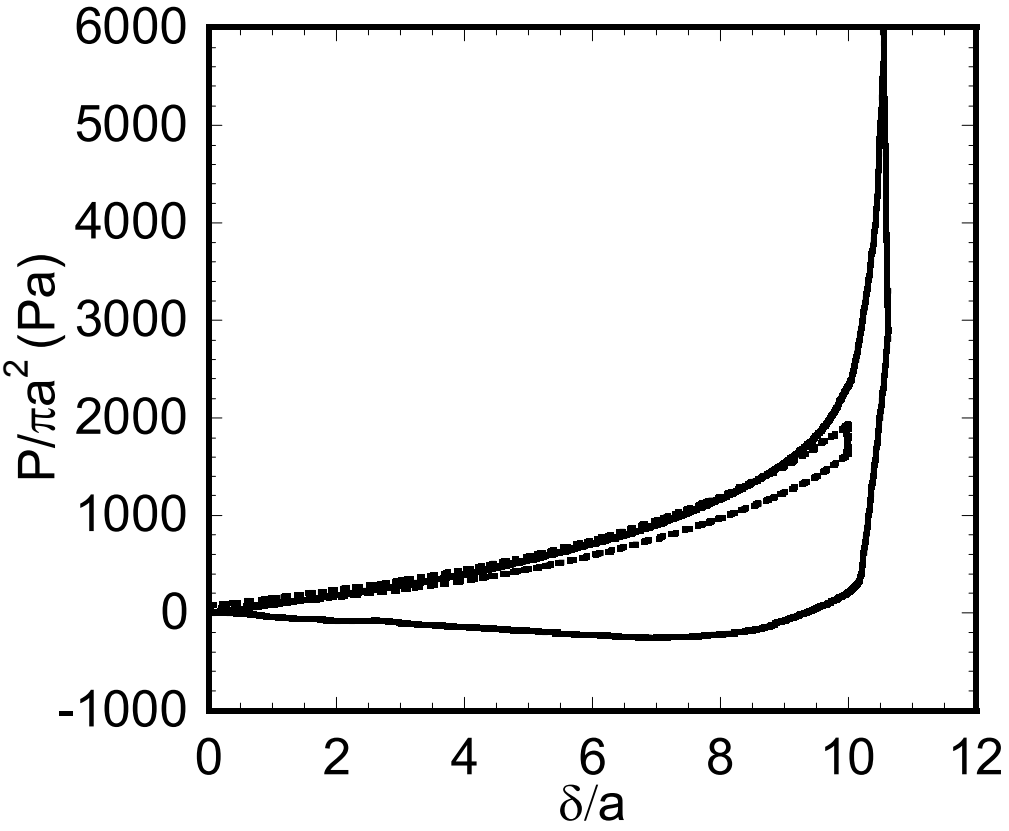

Figure 5.3. Load-displacement curves for a silicone with no added sol fraction. The solid line represents the response of the gel when the indenter is close to the substrate at maximum applied stress and corresponds to **Figure 5.2**. The dotted line designates delayed fracture behavior when the maximum displacement of the indenter is far from the substrate. The data were taken at two different points on the same gel.
.

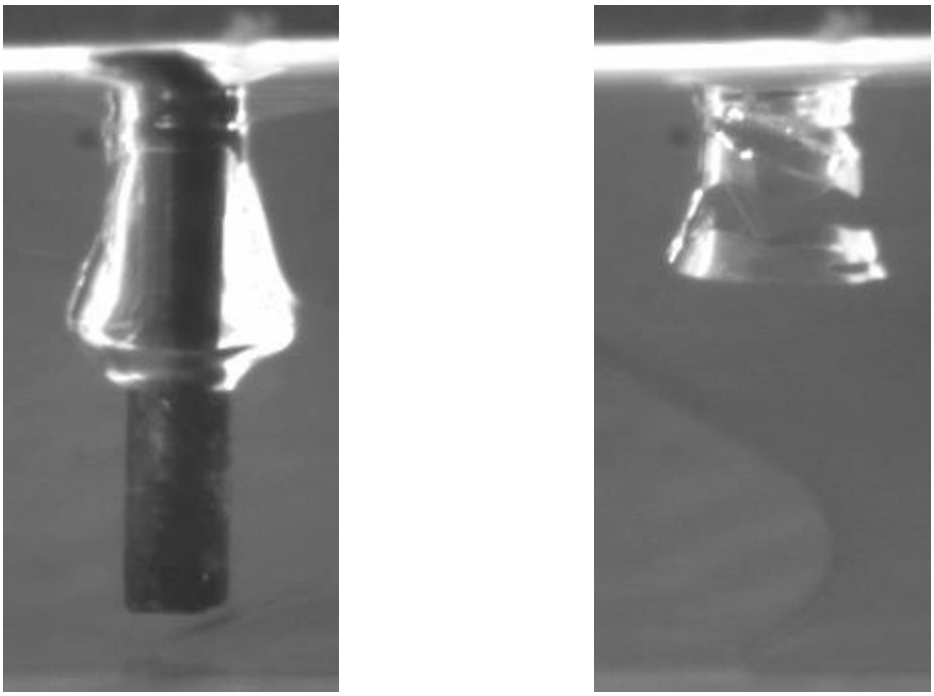

Figure 5.4. Observed failure behavior of gel when indenter is far from substrate. Side-view images are based on silicone with no added sol fraction. **(a)** Upon loading and holding the gel at 2 N, fracture of the gel occurs at the top half of the indenter. **(b)** Retraction of the indenter leaves a silhouette of a Hertzian cone crack. .

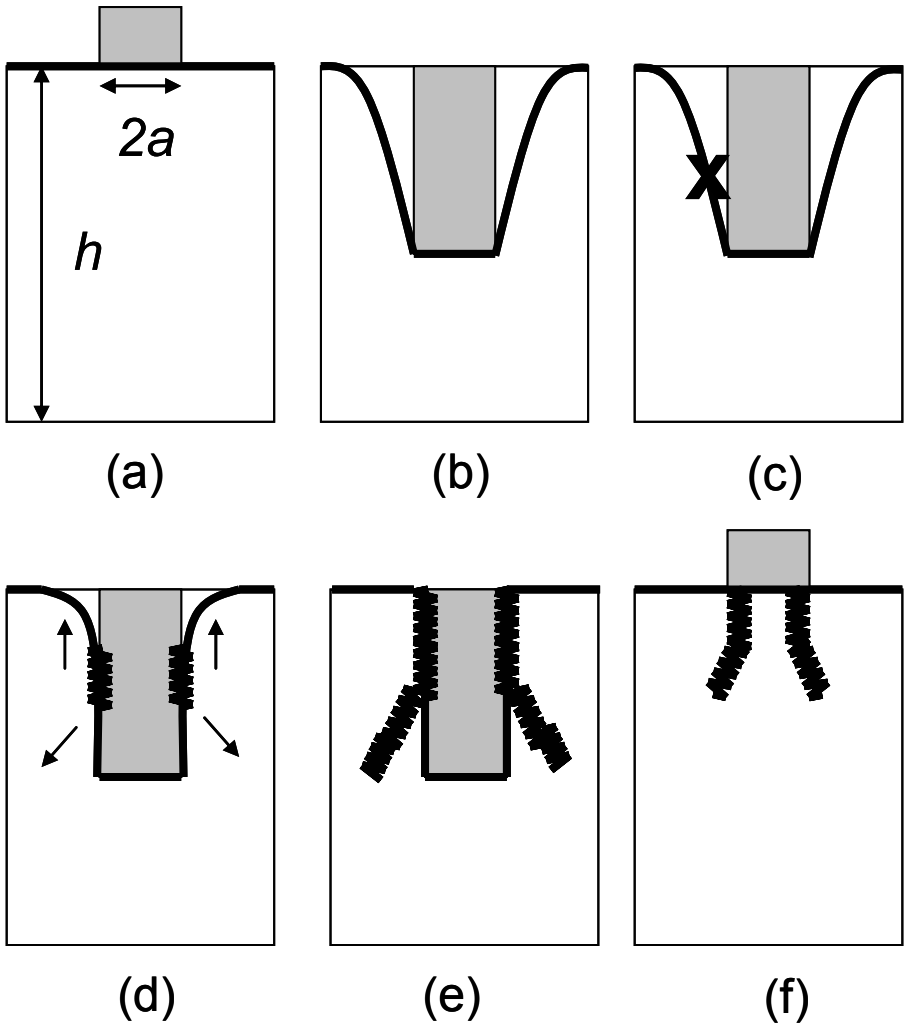

Figure 5.5. Schematic of flaw induced crack initiation behavior. **(a)** An indenter of radius a, is initially loaded to an elastic gel layer of thickness, h. **(b)** The sample is held at a constant stress. Pre-existing surface flaws are subjected to tensile stresses outside the contact zone. **(c)** At some point, a favorably located flaw, represented by the X, will initiate to crack. **(d)** The crack will propagate incrementally downward in the rapidly weakening tensile field. **(e)** Crack growth stops when there is no longer sufficient strain energy to drive it. The gel will relax around the indenter. **(f)** Unloading of the indenter results in a Hertzian cone crack.

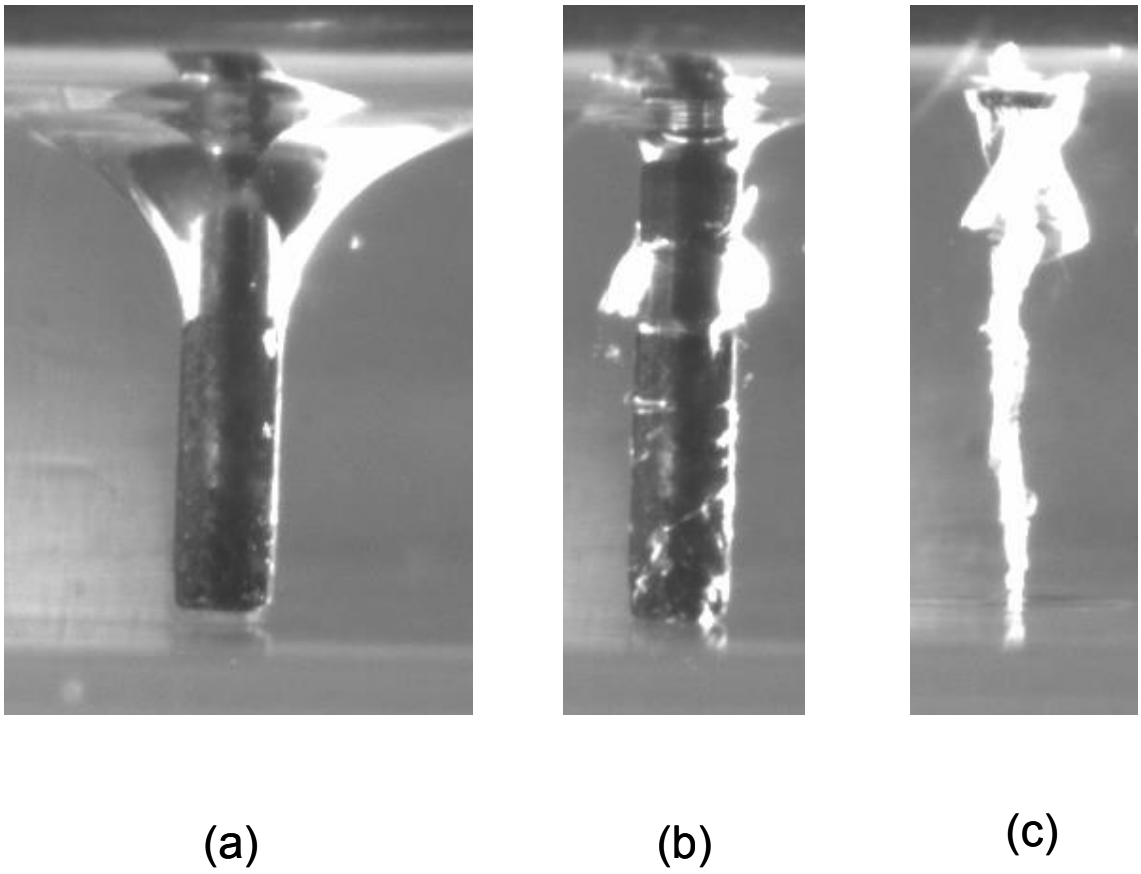

Figure 5.6. Observed failure behavior of gel when indenter is close to bottom substrate. Side view images are of a gel with 20% sol fraction and correspond to **Figure 5.2** **(a)** The gel is loaded and held to a maximum load of 6 N and relaxes for a time, t_f.. **(b)** At σ_f, a crack forms and propagates along shaft of indenter. **(c)** Retraction of indenter leaves a silhouette of crack.

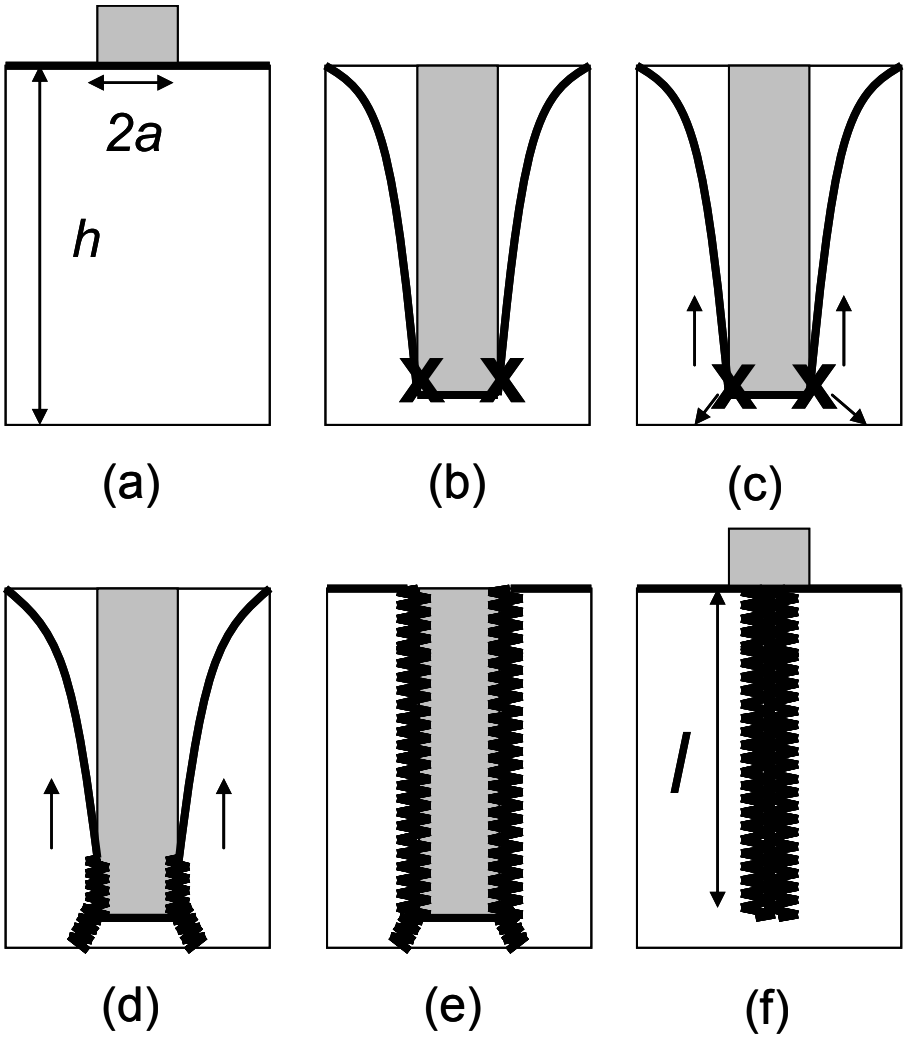

Figure 5.7. Schematic of edge induced crack initiation. **(a**) An elastic silicone layer of thickness, h, is compressed by an indenter with a diameter of 2a. **(b)** The gel is held at a constant load. Stresses at the point of contact are highest around the corner of the indenter, marked by Xs. **(c)** Eventually, a surface ring crack forms around the crack of the punch indenter. **(d)** The crack will propagate downward in the tensile field. **(e)** Since the crack cannot continue through the rigid substrate, the gel relaxes along the shaft of the indenter. **(f)** Unloading of the indenter results in crack with a length, l.

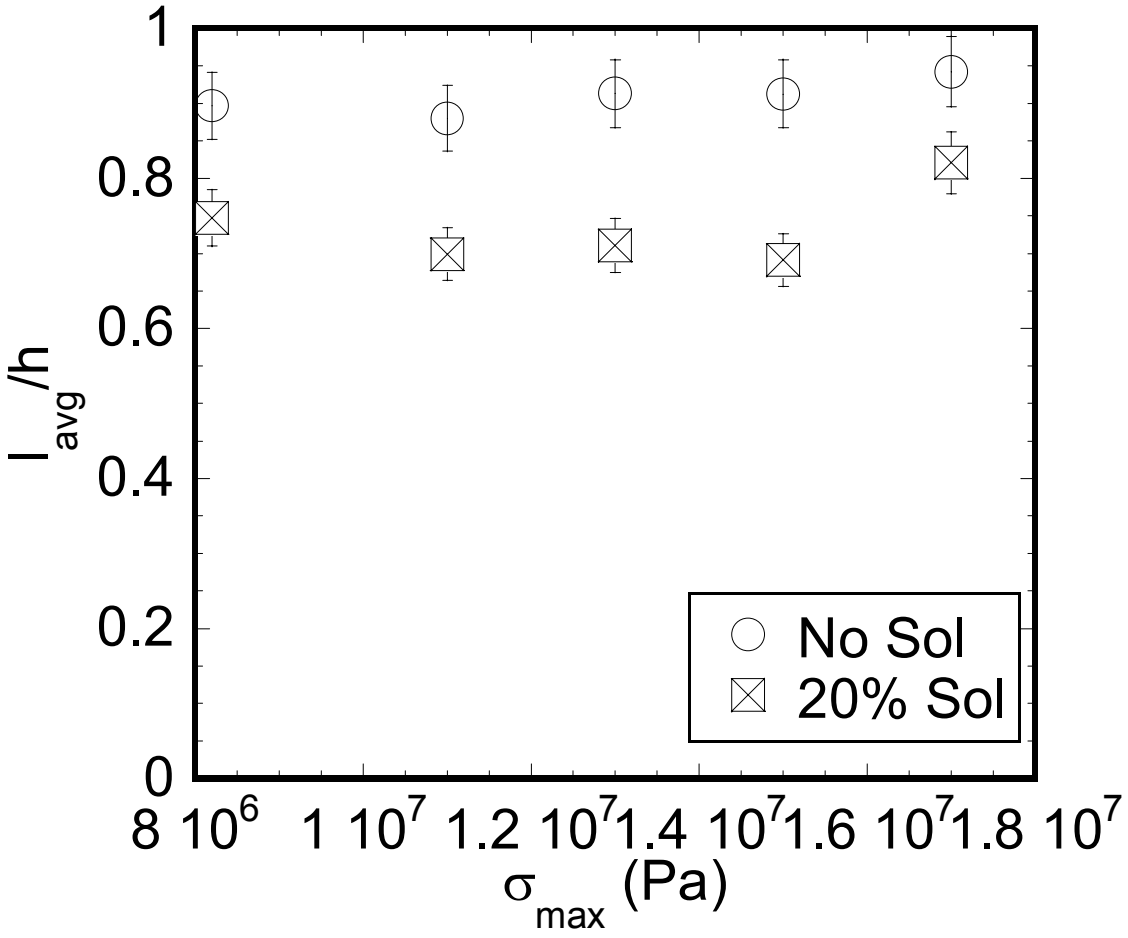

Figure 5.8. Normalized average crack length, l_{avg}/h as a function of maximum stress, σ_{max}. Unfilled circles (○) represent the gels with no additional sol fraction and the boxes with crosses represent those with sol. l is defined as the crack length from the top of the sample to the crack tip, as measured from **Figure 5.7(f)**. This value is normalized by the height of the sample, h, and assumes that the overall fractured sample relaxes so that the crack tip can be imaged.

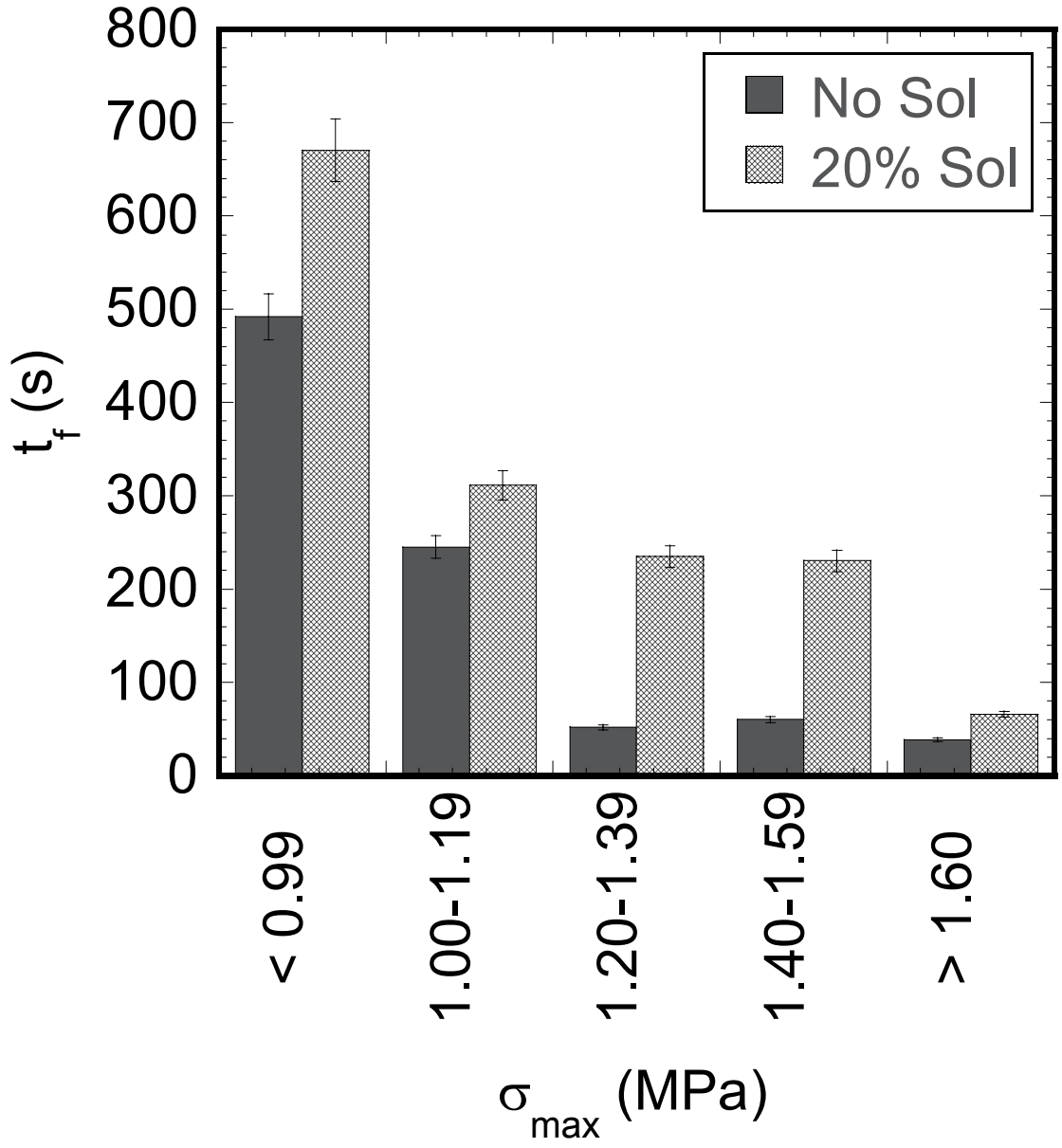

Figure 5.9. Relationship of time to failure, t_f, and applied maximum stress, σ_{max}. Filled bars represent samples with no sol fraction; cross-hatched bars represent silicones with 20% sol.

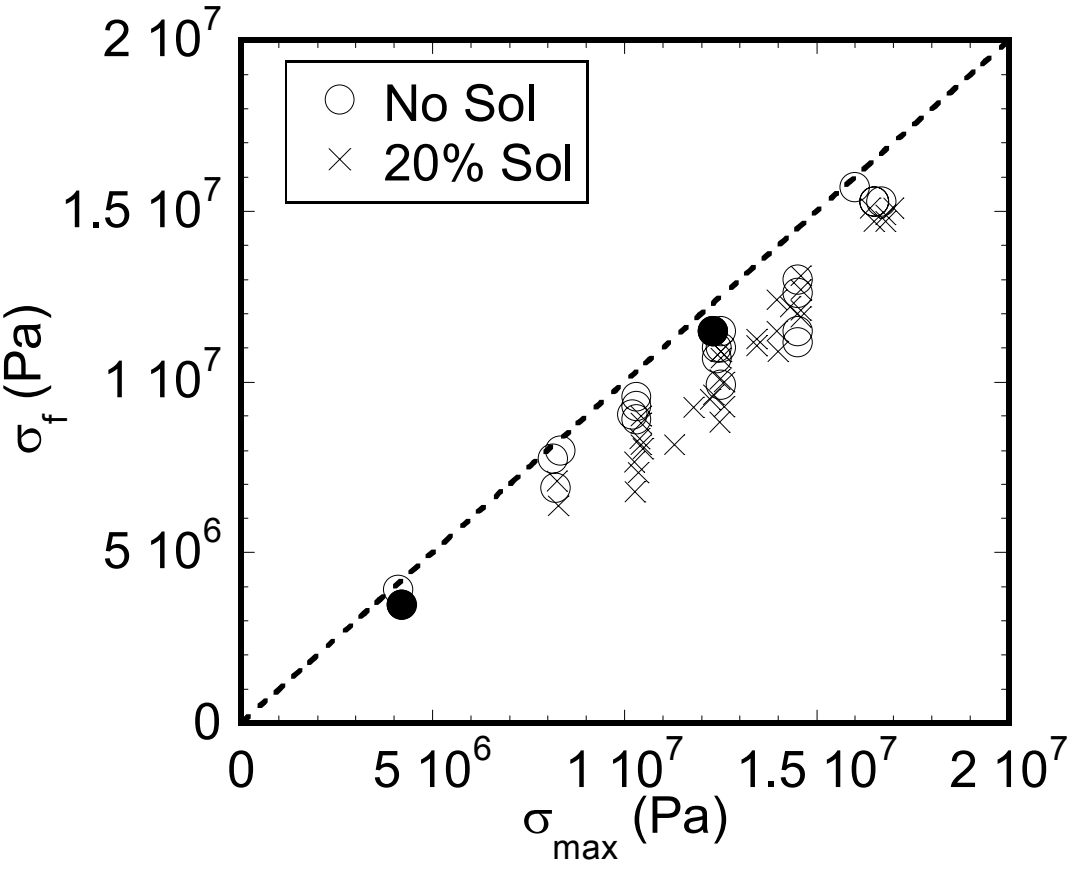

Figure 5.10. Stress at failure, σ_f as a function of applied maximum stress, σ_{max}. Unfilled circles (○) denote gels with no sol fraction and crosses (X) are those with added sol in this graph. Filled circles (●) represent the samples from **Figure 5.3**, which have no added sol fraction. The dashed line represents behavior expected for a purely elastic solid.

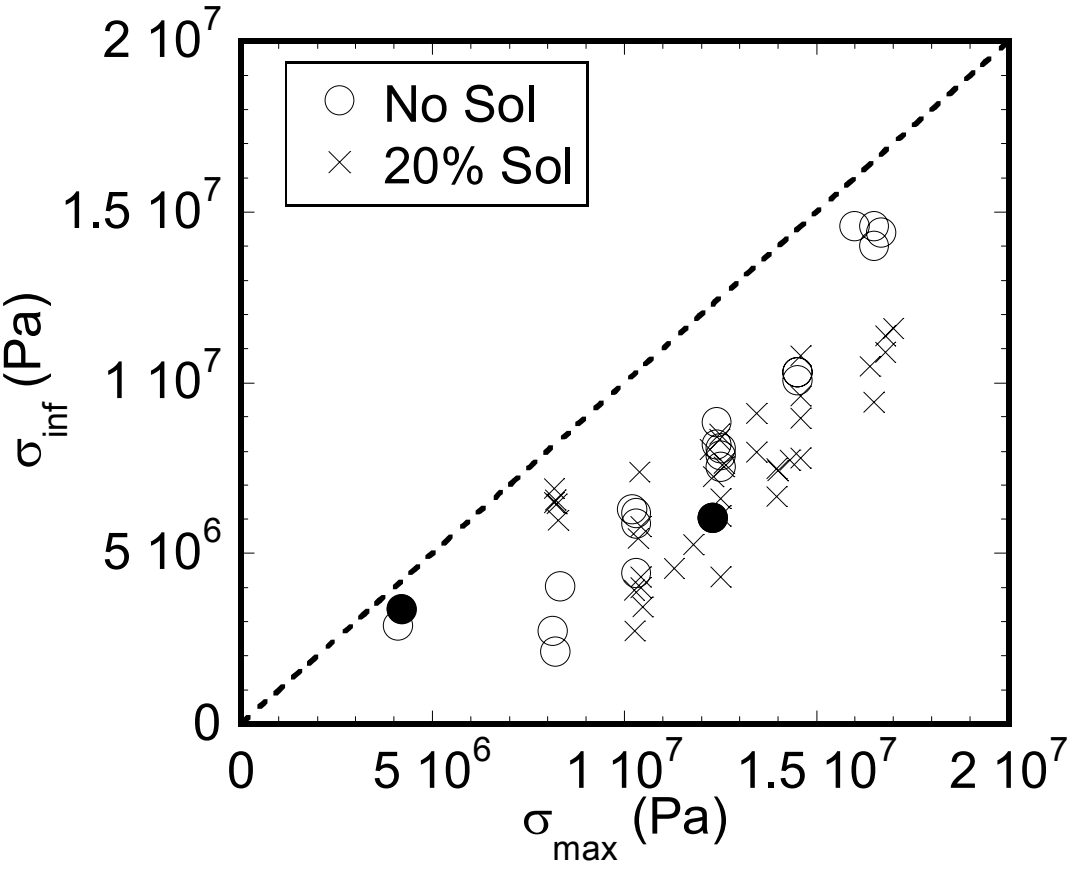

Figure 5.11. Plateau stress, σ_{inf} as a function of applied maximum stress, σ_{max}. Unfilled circles (○) represent gels with no sol fraction; crosses (X) are those with 20% sol. Filled circles (●) represent the gels from **Figure 5.3**, which have no sol fraction added to them.

CHAPTER 6

SUMMARY AND FUTURE WORK

CHAPTER 6

SUMMARY AND FUTURE WORK

6.1 SUMMARY OF THESIS

In this work, our goal was to explore the properties of cross-linked polymer gels from a mechanical perspective. Our work primarily focused on understanding the response of polymer gels over a range of stresses and at fracture using indentation techniques. Specifically, we developed novel experimental methods that allowed us to explore the effect of solvent in cross-linked gels at small and large stresses, as well as determine the mechanisms at failure of soft materials under compression. These techniques were a consequence of adapting existing theories in civil engineering, theoretical and applied mechanics, chemical engineering, and metallurgy to soft materials and indentation. The results of these methods and experiments are summarized in the following sections.

6.1.1 Solvent Flow and Linear Viscoelasticity

Initially, the effect of solvent on the response of gels was probed at small strains. In these experiments, a polymer gel was considered a form of porous media, where internal movement of the solvent within the gel network was similar to that of

water in a permeable soil. Alluding to the principles of soil consolidation [77] and Darcy's Law[137], a novel technique was presented that was ideally suited for characterizing the mechanical and transport properties of polymer gels in the linear elastic regime.

In this technique, a flat, circular punch and a flat, rectangular punch were used to probe the response of gels under oscillatory loading conditions. Solvent transport within the gel was assumed to be driven by gradients in hydrostatic pressure, giving rise to a dissipative response quantified by the phase lag between the punch displacement and the resulting load. By comparing results for different punch sizes, it was possible to differentiate between dissipation resulting from internal solvent flow and dissipation due to the viscoelastic character of the polymer network itself.

Use of the technique was illustrated with pNIPAM gels, a hydrogel that is often studied due its potential for biomedical applications [37]. This particular material was chosen due to the phase separation that occurs above its critical solution temperature of 35^{o}C. At temperatures below 35^{o}C, the elastic constants for the gel at small strains were shown to be independent of punch size and frequency. Above 35^{o}C, we were able to show that solvent transport through the gels was inhibited in comparison to the transport rate at low temperatures, where local phase separation was not observed. The experimental testing apparatus is sensitive to very small phase angles, and this technique could be applied to other heterogeneous gels.

6.1.2 Mechanical Characterization of Elastomeric Gels

The experimental investigations were extended to include the deformation behavior of elastomeric gels prior to fracture. By utilizing a flat punch probe indenter, silicone based gels were characterized to understand the influence of structure and geometry on their mechanical properties. These systems were selected because they were able to deform at high strains without failing, and could be potentially useful to model biological tissues

Tetra-functional end-linked silicone based systems with molecular weights ranging from 800 g/mol to 117,000 g/mol were chosen to determine the effect of molecular weight and structure on the mechanical properties of the system. Modulus measurements indicated that cross-linking dominated the small strain response of the silicones when molar mass strands in the network were below 28,000 g/mol. For strand molecular weights above this value, entanglements governed the elastic behavior and a plateau value of the shear modulus was obtained. However, this effect was not observed in the viscoelastic relaxation of these gels at high stresses. Longer chained networks led to a greater fractional relaxation due to a lower cross-link density. These results were supported by extraction data, which indicated that the amount of unintentional sol from unreacted PDMS correlates to the relaxation behavior of the silicone network.

The addition of sol to three base networks with molecular weights of 500 g/mol, 28,000 g/mol and 117,000 g/mol altered the mechanical properties of the

silicones when compared to the corresponding neat gels. At small strains, a decrease in modulus was noted as more sol fraction was added; however, the value of the modulus measured was found to be independent of the weight of the sol fraction added. At high stresses, the fractional relaxation of the gels is greatest for the samples with higher molecular weights. It was also noted that measurements of 500 g/mol silicone system were not reproducible.

Repeated stress-relaxation experiments of two gels further suggested that the gel network plays a relatively significant role in the elastic response of the sample at large stresses. A form of damage accumulation was observed, which could possibly lead to failure.

Characterization of these elastomeric gels ends with a model that considers geometric confinement of the elastic layer under large scale deformation. The degree of confinement is described by the ratio of the punch size to the sample thickness (a/h) and is dependent on the normalized displacement of the indenter into the sample (δ/h). Utilizing a Neohookean model for large strains, an indication of how stiff the material will become over a range of stresses is determined. At very large deformations, the confinement effect is magnified. The results from this model, as well as those presented from the experiments, provide insight into stresses which can lead to failure of the elastomeric gels.

6.1.3 Fracture Mechanisms and Polymer Gels

To complete the picture of the mechanical response of polymer gels under compression, we applied indentation fracture to our elastomeric gels using a blunt indenter. Based on the results from Chapter 4, we chose two model systems for comparison: one silicone network and a corresponding gel with added 20% sol fraction. Indentation fracture experiments were performed on these systems with a flat punch probe.

A delayed fracture response was characterized in both elastomeric gel systems. The typical delayed failure response occurs after the sample is compressed to a maximum stress and held at a constant displacement. Viscoelastic relaxation of the gel occurs until it catastrophically fails. The characteristic time it takes for crack initiation to occur is defined as the time to failure. The characteristic properties of delayed fracture are correlated to maximum stress applied.

Images and measurements of the gels indicated that delayed fracture is related to the effect of confinement in the elastic layer. When the indenter was far from the bottom of the gel and the elastic layer is very thick, surface flaws initiate fracture. A ring crack led to the formation of a Hertzian cone crack due to the stress fields in the gel. When the indenter was near the bottom surface of the gel and the elastic layer was confined underneath the probe, the high tensile stresses around the corner of the flat punch probe give way to the formation of a ring crack. The gel relaxes along the shaft of the indenter to relieve the high stress fields in this geometry. After the retraction of

the indenter, the resulting crack from the relaxed fractured gel is close to the thickness of the sample. These modes of fracture observed were similar those seen in thick and ultrathin brittle films [129].

Mechanisms leading to fracture resistance in the polymer chain network could be attributed to entanglements[136], and viscous dissipation from the network. The addition of sol was observed to toughen the gels, giving longer failure times and shortened resulting crack lengths. Crack blunting due to the incompressibility of the sol or an ease of movement of the polymer chains in the sol are possible. More experimentation is required to understand the effects of added sol fraction. These experiments provide the groundwork in predicting the mechanical response of soft, high deformable materials.

6.1.4 Main Points

From this research, a set of analytic tools based on a simple indentation technique has been provided to predict the mechanical response of polymer gels over a large range of stresses and at fracture. At small strains, the differentiation of solvent flow from viscoelasticity of a gel network was shown to be possible utilizing different punch sizes. At larger stresses and fracture, a delayed failure response of polymer gel layers was observed. The modes of failure are dependent on the geometry of the system. The addition of sol fraction in a gel was noted to toughen its network and play

an important role at these deformations. These results are useful in predicting the mechanical response of polymer gels when blunt indentation is considered. Further work in this area of research will improve the existing mechanical models and techniques applied to such materials.

6.2 RECOMMENDED FUTURE WORK

Based on the above results, a number of possible avenues for research can be taken to extend this work. These areas include further characterizing our existing systems, changing the geometry of our experiments, and applying our techniques to other soft material systems. Taking these opportunities will further increase our general knowledge of the mechanics involved when dealing with compressed gels and soft materials.

6.2.1 Further Characterization and Modeling of Gel Studies

One natural extension of this study is to further characterize our gels through experimentation and modeling. In doing so, we can create a more complete picture of our work and understand the limits of our models. In this section, we look to see how this can be done for our two chosen model systems using the flat punch probe geometry.

For the pNIPAM gels, indentation experiments conducted at stresses close to the failure stress would be useful. At room temperature, these experiments would complement the theories and models described by Hui, et al. [35] and Lin[64] for small strain behavior. From a mechanical perspective, indentation experiments on pNIPAM at stresses inducing fracture could also be compared to those of elastomer systems that were described in Chapter 5.

For the silicone gels, further characterization can lead us to gain a better understanding of the effect of sol fraction on an elastomeric network, as well as the stress fields within such a system. As noted in Chapter 5, it was evident that an added sol fraction led to tougher gels and a delayed fracture response. This behavior is also evident in **Figure 6.1**, where preliminary experiments indicate that a corresponding V31 gel with 40% sol fraction fails at higher stresses than those that were tested. This property was first observed when determining the range of stresses in which our gels would fail. It was noted that gels with 0% and 20% added sol fraction failed at maximum loads ranging between 4.0N to 8.0N, while gels with 40% added sol fraction did not fracture within the range of our load cell

To further explore the cause of this response, the de-coupling of network and solvent effects of the silicone gels is necessary at such high stresses. One method to do this is to perform fracture experiments on all the gels that were characterized in Chapter 4. Based on these experiments, we could determine how the cross-link density and molar mass of the polymer chains would affect the response at failure. These

experiments could be complemented by additional fracture studies performed after extraction of the sol component, as well as tests that vary the rate of loading on the sample. Results of these experiments would give us insight into the network response.

The stress fields of the indenter displaced in the gel could also be further modeled to determine how geometric confinement of the elastic layer affects fracture behavior. Modeling of stress fields of the flat punch indenter close to the substrate would provide us one method to determine network behavior in these types of geometries. Moreover, solvent effects at these large deformations could be modeled as an extension of the existing small strain studies performed by Lin, et al[64]. These studies could be compared to large deformation and failure experiments of silicone gel thin films, as well as birefringence studies of the elastic layers of varying thicknesses.

Further characterization and modeling of these materials lays the groundwork for general models of soft systems over a large range of stress and a range of thicknesses. These models would be invaluable in situations where the prediction of a soft material is necessary, whether it involves utilizing a hydrogel for dental sutures or determining the response of a silicone network that has not fully cured, and would extend the models of indentation fracture to include other soft materials.

6.2.2 Indentation Studies in Other Geometries

Another extension of our experiments is to apply alternate indenter geometries to our compression tests. Common to our experiments was the utilization of a circular, flat punch probe with a contact radius of 0.39 mm to perform indentation. Elements of this idea were integrated in Chapter 3, when probing the transport properties of hydrogels. However, our attempts to move away from the flat probe punch were unsuccessful due to the inhomogeneity of the gels and the alignment of the indenter. An interesting approach to the small strain and fracture studies is to utilize indenters with smaller punch radii.

One possibility is to use circular, punch probes with contact radii that are significantly less than 0.39 mm. In determining internal transport of hydrogels, a smaller contact area would decrease the relaxation time of the gel, as noted in Equation (3.9) lessening the distance of travel of the solvent underneath the punch. This solution would possibly resolve the issue of a discernable phase angle when comparing punch sizes. Furthermore, the homogeneity of the pore size in a gel would be less of a concern. For the fracture experiments, the use of a smaller punch radius would resolve the issues of reaching the limits of our load cell, which were problematic when a corresponding gel of our samples with 40% sol fraction was tested. A smaller contact area would decrease the maximum load required to fracture a gel; however, care would have to be taken to prevent the indenter from bowing. For our small strain experiments

and for softer polymer gels, mechanical measurements could be made from punch sizes that were on the order of those used in nanoindentation.

To minimize the contact radius of an indenter, another possibility is to use a 'sharp' indenter. By definition, the circular, flat punch probe used in our experiments is a blunt indenter. The indenter would become a 'sharp' contact at the limits of Equation (2.31), where a stress singularity is formed as the contact pressure increases and the indenter size decreases. The behavior of our materials was analogous to the studies of thick brittle coatings performed by Chai and Lawn [129]. It would be interesting to see if a blunt contact would behave in a similar manner as a sharp indenter [130].

Utilization of a sharp indenter in large scale deformation and fracture experiments on an elastic substrate would then allow us to see if plastic-like behavior ever occurs in these and other soft material systems. Characterization of materials in this geometry has been performed on metals and ceramics [74] but has yet to be done on polymer gels and other soft materials. These studies would open up a whole new understanding of the fracture behavior of soft materials.

6.2.3 Compression Studies of Other Materials

As a more complete picture of our chemically cross-linked model systems is formed, an interesting aspect of our research would be to apply our indentation experiments, particularly the large stresses and fracture studies, to other highly

compliant materials. Alternate materials that are well-suited for this geometry include physically cross-linked gels, double network hydrogels, and biological tissues.

The use of physically cross-linked gels would allow us to further understand the nature of large scale deformation and fracture in these types of networks. One such system of interest in our experiments are thermoreversible, self-assembling acrylic triblock copolymer gels [9, 58]. In these systems, a gel is formed by dissolving the midblock with a selected solvent. A polymer network is formed from the self-aggregation of the endblocks and the bridging of midblocks between these domains. At very high stresses and fracture, it would be expected that the gels may fail as a result of viscoplastic chain pull-out, as noted by Baumberger, et al. [115]. However, it has been has been shown that the degree of midblock stretching increases for gels with relatively large aggregation numbers and short midblocks[9]. Further investigations on such materials would lead to a better understanding of the mechanical response of physically cross-linked polymer gels. Moreover, an understanding of triblock hydrogels, such as those with poly(lactide) endblocks, would be well-suited as tissue engineering models, since their modulus is similar to that of soft tissue[138, 139].

Indentation fracture experiments would also be of interest in interpenetrating network hydrogels. Double network hydrogels can be made from a two-step polymerization process, where a tightly-cross-linked network is formed first and followed by the synthesis of a loosely-cross-linked network[139]. The resulting gels that are formed are very tough with fracture strengths of 17 MPa[140]. In these gels,

it has been noted that the mechanical strength is not simply attributed to chemical cross-linking or physical entanglements between the two networks, since double network gels with loosely cross-linked networks exhibited greater strength[140]. Instead, the molecular weight of the second linear polymer chain in these networks determines the strength of the system, since these polymer chains are noted to entangled within themselves[141]. A comparative study of indentation fracture between these interpenetrating systems and the silicone gels would allow us to understand the effect of unreacted PDMS on our systems. In the case of our gels, the unreacted PDMS could be treated as an interpenetrating network.

An application of indentation experiments to biological tissue is another avenue of research. One extension of our research is to apply the indentation fracture experiments to mammalian skin. Since our silicone gels have Young's moduli that are close to the values of skin obtained by Shergold and Fleck[131, 132], we can utilize our experiments on soft tissue and understand their behavior prior to fracture. These experiments would complement existing research on the puncture mechanisms of skin[132] by utilizing a method that is able to control the rate of penetration in the material. Such experiments would benefit the medical community and biomedical research.

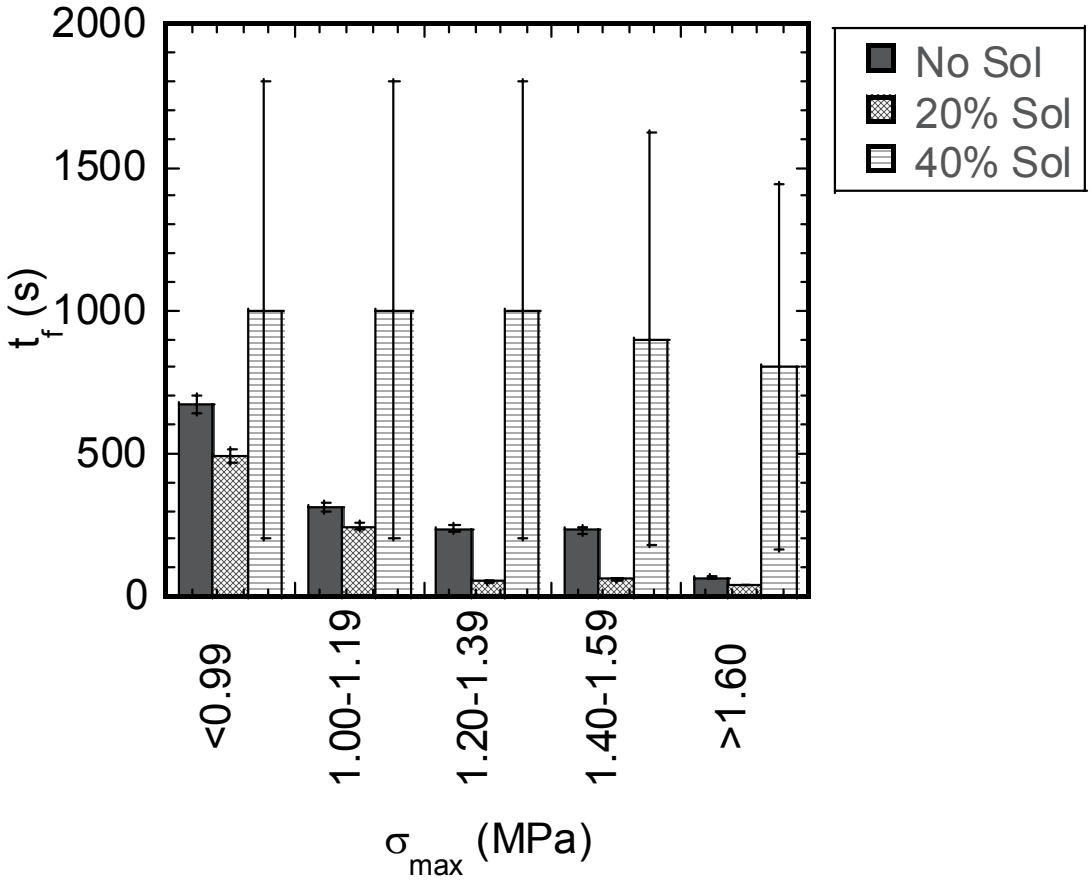

Figure 6.1. Time of failure with increasing sol fraction in gel.

APPENDIX A

Derivation of Equation (3.31)

To determine the phase angle over a continuous frequency spectrum, we begin by rewriting Equation (3.29) in the following way:

$$I(\Omega) = i\Omega\int_0^\infty \left[1 - erf\left(f\left(\kappa\right)\right)\right]e^{-i\Omega T}d\kappa = -\int_0^\infty \left[1 - erf\left(f\left(\kappa\right)\right)\right]de^{-i\Omega\kappa} \qquad \text{(A.1)}$$

Integration of Equation (A.1) by parts gives the following expression:

$$I\left(\Omega\right) = -\left[1 - erf\left(f\left(\kappa\right)\right)\right]e^{-i\Omega\kappa}\Big|_0^\infty + \int_0^\infty e^{-i\omega\kappa}d\left[1 - erf\left(f\left(\kappa\right)\right)\right] \qquad \text{(A.2)}$$

With $d\left[erf\left(f\left(\kappa\right)\right)\right] = \frac{2}{\sqrt{\pi}}e^{-\left(f(\kappa)\right)^2}df\left(\kappa\right)$, we have:

$$I(\Omega) = 1 - \frac{2}{\sqrt{\pi}}\int_0^\infty e^{-i\Omega\kappa}e^{-f(\kappa)^2}f'(\kappa)d\kappa\,, \qquad \text{(A.3)}$$

with *f′* defined as the differential of *f*.

Equation (A.3) is a general expression relating *I(Ω)* to *f(κ)*. In order to obtain an approximate relationship for *I(Ω)* for a circular punch in contact with an elastic half space, we retain only the first term in Equation (3.26) for *f(κ)*, to obtain the following:

$$I(\Omega) \cong 1 - \frac{1}{\sqrt{\pi}} \int_0^\infty \frac{e^{-i\Omega\kappa} e^{-\kappa}}{\sqrt{\kappa}} d\kappa = 1 - \frac{2}{\sqrt{\pi}} \int_0^\infty e^{-(1+i\Omega)x^2} dx = 1 - \frac{1}{\sqrt{1+i\Omega}}. \qquad \text{(A.4)}$$

With $1 + i\Omega = \mathrm{Re}^{i\theta}$, Equation(A.4) becomes:

$$I(\Omega) \cong 1 - R^{-1/2} \left[\cos\frac{\theta}{2} - i \sin\frac{\theta}{2} \right]. \qquad \text{(A.5)}$$

With $R = \sqrt{1+\Omega^2}$, $\sin(\theta/2) = \sqrt{(1-\cos\theta)/2}$, $\cos(\theta/2) = \sqrt{(1+\cos\theta)/2}$ and $\cos\theta = 1/\sqrt{1+\Omega^2}$, we obtain:

$$I(\Omega) = 1 - \frac{\left(1+\Omega^2\right)^{-1/4}}{\sqrt{2}} \left[\sqrt{\left(1 + \frac{1}{\sqrt{1+\Omega^2}}\right)} - i\sqrt{\left(1 - \frac{1}{\sqrt{1+\Omega^2}}\right)} \right]. \qquad \text{(A.6)}$$

Equation (3.31) for the phase angle is obtained by substitution of Equation (A.6) into Equation (3.28).

REFERENCES

1. Hilts, P.J., *Maker of implants balked at testing, its records show*, in *The New York Times*. 1992: New York, NY. p. A1.

2. Marotta, J.S., et al., *Silicone gel breast implant failure: Evaluation of properties of shells and gels for explanted prostheses and meta-analysis of literature rupture data.* Annals of Plastic Surgery, 2002. **49**(3): p. 227-242.

3. Sass, S.L., *The Substance of Civilization: Materials and Human History from the Stone Age to the Age of Silicon*. 1998, New York: Arcade Publishing.

4. Qiu, L.Y. and Y.H. Bae, *Polymer architecture and drug delivery.* Pharmaceutical Research, 2006. **23**(1): p. 1-30.

5. Bischoff, R. and S.E. Cray, *Polysiloxanes in macromolecular architecture.* Progress in Polymer Science, 1999. **24**(2): p. 185-219.

6. Likos, C.N., *Soft matter with soft particles.* Soft Matter, 2006. **2**(6): p. 478-498.

7. Suematsu, K., *Recent progress in gel theory: Ring, excluded volume, and dimension*, in *Molecular Simulation Fracture Gel Theory*. 2002. p. 137-214.

8. de Gennes, P.G., *Scaling Concepts in Polymer Physics*. 1979, Ithaca, NY: Cornell University Press.

9. Seitz, M.E., et al., *Self-Assembly and Stress Relaxation in Acrylic Triblock Copolymer Gels.* Macromolecules, 2007. **40**(4): p. 1218-1226.

10. Brinker, C.J., *Porous inorganic materials.* Current Opinion in Solid State & Materials Science, 1996. **1**(6): p. 798-805.

11. Ulijn, R.V., et al., *Bioresponsive hydrogels.* Materials Today, 2007. **10**(4): p. 40-48.

12. Young, R.J. and P.A. Lovell, *Introduction to Polymers*. Second ed. 1991, Cheltenham, U.K.: Stanley Thornes Ltd.

13. Wichterle, O. and D. Lim, *Hydrophilic Gels for Biological Use.* Nature, 1960. **185**(4706): p. 117-118.

14. N. A. Peppas, J.Z.H.A.K.R.L., *Hydrogels in Biology and Medicine: From Molecular Principles to Bionanotechnology.* Advanced Materials, 2006. **18**(11): p. 1345-1360.

15. Corkhill, P.H., C.J. Hamilton, and B.J. Tighe, *Synthetic hydrogels VI. Hydrogel composites as wound dressings and implant materials.* Biomaterials, 1989. **10**(1): p. 3-10.

16. Zhang, S., *Hydrogels: Wet or let die.* Nat Mater, 2004. **3**(1): p. 7-8.

17. Mart, R.J., et al., *Peptide-based stimuli-responsive biomaterials.* Soft Matter, 2006. **2**(10): p. 822-835.

18. Eastoe, J. and A. Vesperinas, *Self-assembly of light-sensitive surfactants.* Soft Matter, 2005. **1**(5): p. 338-347.

19. W. Frey, D.E.M.A.C., *Dynamic Addressing of a Surface Pattern by a Stimuli-Responsive Fusion Protein.* Advanced Materials, 2003. **15**(3): p. 248-251.

20. Gil, E.S. and S.M. Hudson, *Stimuli-responsive polymers and their bioconjugates.* Progress in Polymer Science, 2004. **29**(12): p. 1173-1222.

21. Miyata, T., T. Uragami, and K. Nakamae, *Biomolecule-sensitive hydrogels.* Advanced Drug Delivery Reviews, 2002. **54**(1): p. 79-98.

22. Chalk, A.J. and J.F. Harrod, *Homogeneous catalysis. II. The mechanism of the hydrosilation of olefins catalyzed by Group VIII metal complexes.* Journal of the American Chemical Society, 1965. **87**(1): p. 16-21.

23. Lake, G.J. and P.B. Lindley, *Mechanical Fatigue Limit for Rubber.* Journal of Applied Polymer Science, 1965. **9**(4): p. 1233-&.

24. Larsen, A.L., et al., *Elastic properties of nonstoichiometric reacted PDMS networks.* Macromolecules, 2003. **36**(26): p. 10063-10070.

25. Obukhov, S.P., M. Rubinstein, and R.H. Colby, *Network Modulus and Superelasticity.* Macromolecules, 1994. **27**(12): p. 3191-3198.

26. Gottlieb, M., et al., *Equilibrium Modulus of Model Poly(Dimethylsiloxane) Networks.* Macromolecules, 1981. **14**(4): p. 1039-1046.

27. Andrady, A.L., et al., *Model Networks of End-Linked Polydimethylsiloxane Chains .12. Dependence of Ultimate Properties on Dangling-Chain Irregularities.* Journal of Applied Polymer Science, 1981. **26**(6): p. 1829-1836.

28. Valles, E.M. and C.W. Macosko, *Structure and Viscosity of Poly(Dimethylsiloxanes) with Random Branches.* Macromolecules, 1979. **12**(3): p. 521-526.

29. Valles, E.M. and C.W. Macosko, *Properties of Networks Formed by End Linking of Poly(Dimethylsiloxane).* Macromolecules, 1979. **12**(4): p. 673-679.

30. Gent, A.N. and C.T.R. Pulford, *Micromechanics of Fracture in Elastomers.* Journal of Materials Science, 1984. **19**(11): p. 3612-3619.

31. Flory, P.J., *Principles of Polymer Chemistry*. 1953, Ithaca, NY: Cornell University Press.

32. Ahagon, A. and A.N. Gent, *Threshold fracture energies for elastomers.* Journal of Polymer Science, 1975. **13**: p. 1903-1911.

33. Heinrich, G., M. Kluppel, and T.A. Vilgis, *Reinforcement of elastomers.* Current Opinion in Solid State & Materials Science, 2002. **6**(3): p. 195-203.

34. Yoo, S.H., C. Cohen, and C.Y. Hui, *Mechanical and swelling properties of PDMS interpenetrating polymer networks.* Polymer, 2006. **47**(17): p. 6226-6235.

35. Hui, C.-Y., et al., *A contact mechanics method for characterizing the elastic properties and permeability of gels.* Journal of Polymer Science Part B-Polymer Physics, 2005.

36. Scherer, G.W., *Influence of viscoelasticity and permeability on the stress response of silica gel.* Langmuir, 1996. **12**(5): p. 1109-1116.

37. Gotoh, T., Y. Nakatani, and S. Sakohara, *Novel synthesis of thermosensitive porous hydrogels.* Journal of Applied Polymer Science, 1998. **69**(5): p. 895-906.

38. Jones, R.A.L., *Soft Condensed Matter*. 2002, New York, NY: Oxford University Press, Inc.

39. Rubinstein, M. and R.H. Colby, *Self-Consistent Theory of Polydisperse Entangled Polymers - Linear Viscoelasticity of Binary Blends.* Journal of Chemical Physics, 1988. **89**(8): p. 5291-5306.

40. Colby, R.H. and M. Rubinstein, *2-Parameter Scaling for Polymers in Theta-Solvents.* Macromolecules, 1990. **23**(10): p. 2753-2757.

41. Rubinstein, M. and R.H. Colby, *Elastic-Modulus and Equilibrium Swelling of near-Critical Gels.* Macromolecules, 1994. **27**(12): p. 3184-3190.

42. Langley, N.R., *Elastically Effective Strand Density in Polymer Networks.* Macromolecules, 1968. **1**(4): p. 348-352.

43. Everaers, R., *Entanglement effects in defect-free model polymer networks.* New Journal of Physics, 1999. **1**: p. 12.1-12.54.

44. Patel, S.K., et al., *Elastic-Modulus and Equilibrium Swelling of Poly(Dimethylsiloxane) Networks.* Macromolecules, 1992. **25**(20): p. 5241-5251.

45. Graessley, W.W. and S.F. Edwards, *Entanglement interactions in polymers and the chain contour concentration.* Polymer, 1981. **22**(10): p. 1329-1334.

46. Graessley, W.W., *Entangled Linear, Branched and Network Polymer Systems - Molecular Theories.* Advances in Polymer Science, 1982. **47**: p. 67-117.

47. Rubenstein, M. and R.H. Colby, *Polymer Physics*. 2003, Oxford: Oxford University Press.

48. Webber, R.E. and K.R. Shull, *Strain Dependence of the Viscoelastic Properties of Alginate Hydrogels.* Macromolecules, 2004. **37**(16): p. 6153-6160.

49. Batra, A., C. Cohen, and L. Archer, *Stress relaxation of end-linked polydimethylsiloxane elastomers with long pendent chains.* Macromolecules, 2005. **38**(16): p. 7174-7180.

50. Winter, H.H. and M. Mours, *Rheology of polymers near liquid-solid transitions*, in *Neutron Spin Echo Spectroscopy Viscoelasticity Rheology*. 1997. p. 165-234.

51. Crosby, A.J., et al., *Rheological properties and adhesive failure of thin viscoelastic layers.* Journal of Rheology, 2002. **46**(1): p. 273-294.

52. Tanaka, Y., Fukao, and Y. Miyamoto, *Fracture energy of gels.* The European Physical Journal E, 2000. **3**: p. 395-401.

53. Rivlin, R.S. and A.G. Thomas, *Rupture of rubber. I. Characteristic energy for tearing.* Journal of Polymer Science 1953. **10**: p. 291.

54. Lake, G.J. and A.G. Thomas, *Strength of Highly Elastic Materials.* Proceedings of the Royal Society of London Series a-Mathematical and Physical Sciences, 1967. **300**(1460): p. 108-&.

55. de Gennes, P.G., *Soft Adhesives.* Langmuir, 1996. **12**(19): p. 4497-4500.

56. Hui, C.Y., et al., *Crack blunting and the strength of soft elastic solids.* Proceedings of the Royal Society A: Mathematical, Physical and Engineering Sciences, 2003. **459**(2034): p. 1489-1516.

57. Rubinstein, M. and R.H. Colby, *Elastic Modulus and Equilibrium Swelling of Near-Critical Gels.* Macromolecules, 1994. **27**(12): p. 3184-3190.

58. Drzal, P.L. and K.R. Shull, *Origins of mechanical strength and elasticity in thermally reversible, acrylic triblock copolymer gels.* Macromolecules, 2003. **36**(6): p. 2000-2008.

59. Strobl, G., *The Physics of Polymers: Concenpts for Understanding their Structures and Behaviors*. 1996, Berlin: Springer-Verlag.

60. Noda, I., et al., *Thermodynamic Properties of Moderately Concentrated Solutions of Linear Polymers.* Macromolecules, 1981. **14**: p. 668-676.

61. Geissler, E. and A.M. Hecht, *The Poisson Ratio in Polymer Gels.* Macromolecules, 1980. **13**(5): p. 1276-1280.

62. Hui, C.-Y., et al. *A Contact Mechanics Method for Characterizing the Elastic Properties and Permeability of Gels*. in *27th Annual Meeting of the Adhesion Society, Inc.* 2003. Wilmington, NC.

63. Johnson, K.L., *Contact Mechanics*. 1985, Cambridge: Cambridge University Press.

64. Lin, Y.Y. and B.W. Hu, *Load relaxation of a flat rigid circular indenter on a gel half space.* Journal of Non-Crystalline Solids, 2006. **352**(38-39): p. 4034-4040.

65. Maugis, D. and M. Barquins, *Fracture Mechanics and Adherence of Viscoelastic Bodies.* Journal of Physics D-Applied Physics, 1978. **11**(14): p. 1989-&.

66. Shull, K.R., *Contact mechanics and the adhesion of soft solids.* Materials Science & Engineering R-Reports, 2002. **36**(1): p. 1-45.

67. Lin, Y.Y. and H.Y. Chen, *Effect of large deformation and material nonlinearity on the JKR (Johnson-Kendall-Roberts) test of soft elastic materials.* Journal of Polymer Science Part B-Polymer Physics, 2006. **44**(19): p. 2912-2922.

68. Lin, W.-C. and K.R. Shull, *Contact measurement of internatl fluid flow within poly(n-isopropyl acrlyamide gels).* Journal of Chemical Physics, 2007. **submitted**.

69. Fabbroni, E.F., K.R. Shull, and M.C. Hersam, *Adhesive and mechanical properties of soft nanocomposites: Model studies with blended latex films.*

Journal of Polymer Science Part B-Polymer Physics, 2001. **39**(24): p. 3090-3102.

70. Crosby, A.J., *Deformation and Failure of Thin Viscoelastic Adhesives*, in *Materials Science and Engineering*. 2000, Northwestern University: Evanston, IL.

71. Shull, K.R., et al., *Axisymmetric adhesion tests of soft materials.* Macromolecular Chemistry and Physics, 1998. **199**(4): p. 489-511.

72. Lawn, B., *Fracture of Brittle Solids - Second Edition*. Cambridge Solid State Series. 1975, Cambridge: Cambridge University Press.

73. Lawn, B.R., E.R. Fuller, and S.M. Wiederhorn, *Strength Degradation of Brittle Surfaces - Sharp Indenters.* Journal of the American Ceramic Society, 1976. **59**(5-6): p. 193-197.

74. Lawn, B. and R. Wilshaw, *Indentation Fracture - Principles and Applications.* Journal of Materials Science, 1975. **10**(6): p. 1049-1081.

75. Ostojic, P. and R. Mcpherson, *A Review of Indentation Fracture Theory - Its Development, Principles and Limitations.* International Journal of Fracture, 1987. **33**(4): p. 297-312.

76. Tanaka, T., L.O. Hocker, and G.B. Benedek, *Spectrum of light scattered from a viscoelastic gel.* Journal of Chemical Physics, 1973. **59**: p. 5151-5159.

77. Biot, M.A., *General Theory of Three-Dimensional Consolidation.* Journal of Applied Physics, 1941. **12**: p. 155-164.

78. Davson, H., *Physiology of the Eye*. Fifth Edition ed. 1990, New York: Pergamon Press, Inc. 184,100.

79. Makino, K., J. Hiyoshi, and H. Ohshima, *Effects of thermosensitivity of poly (N-isopropylacrylamide) hydrogel upon the duration of a lag phase at the beginning of drug release from the hydrogel.* Colloids and Surfaces B: Biointerfaces, 2001. **20**(4): p. 341-346.

80. Andersson, M., A. Axelsson, and G. Zacchi, *Diffusion of glucose and insulin in a swelling N-isopropylacrylamide gel.* International Journal of Pharmaceutics, 1997. **157**(2): p. 199-208.

81. Tan, C.L.-L., *Beauty 'Patches'*, in *Wall Street Journal*. 2005: New York, NY. p. D4.

82. Hecht, A.M., E. Geissler, and A. Chosson, *Dynamic light scattering by gels under hydrostatic pressure.* Polymer, 1981. **22**(7): p. 877-881.

83. Geissler, E. and A.M. Hecht, *The Poisson Ratio in Polymer Gels .2.* Macromolecules, 1981. **14**(1): p. 185-188.

84. Scherer, G.W., *Bending of Gel Beams - Method for Characterizing Elastic Properties and Permeability.* Journal of Non-Crystalline Solids, 1992. **142**(1-2): p. 18-35.

85. Andersson, M., A. Axelsson, and G. Zacchi, *Determination of the Pore-Size Distribution in Gels.* Bioseparation, 1995. **5**(2): p. 65-72.

86. Andersson, M., A. Axelsson, and G. Zacchi, *Swelling kinetics of poly(N-isopropylacrylamide) gel.* Journal of Controlled Release, 1998. **50**(1-3): p. 273-281.

87. Zhang, X.Z., et al., *Thermosensitive poly(N-isopropylacrylamide-co-acrylic acid) hydrogels with expanded network structures and improved oscillating swelling-deswelling properties.* Langmuir, 2002. **18**(6): p. 2013-2018.

88. Hirokawa, Y. and T. Tanaka, *Volume Phase-Transition in a Non-Ionic Gel.* Aip Conference Proceedings, 1984(107): p. 203-208.

89. Otake, K., et al., *Thermal analysis of the volume phase transition with N-isopopylacrylamide gels.* Macromolecules, 1990. **23**(1): p. 283-289.

90. Inomata, H., S. Goto, and S. Saito, *Phase transition of N-substituted acrylamide gels.* Macromolecules, 1990. **23**(22): p. 4887-4888.

91. Horkay, F., A.M. Hecht, and E. Geissler, *Fine structure of polymer networks as revelad by solvent swelling.* Macromolecules, 1998. **31**: p. 8851-8856.

92. Hirotsu, S., *Phase-Transition of a Polymer Gel in Pure and Mixed-Solvent Media.* Journal of the Physical Society of Japan, 1987. **56**(1): p. 233-242.

93. Messersmith, P. and F. Znidarsich. *Synthesis and LCST Behavior of Thermally Responsive Poly (N-Isopropylacrylamide)/Layered Silicate Nanocomposites*. in *Materials Research Society Symposium Proceedings*. 1997.

94. Webber, R.E., et al., *Effects of geometric confinement on the adhesive debonding of soft elastic solids.* Physical Review E, 2003. **68**(2): p. -.

95. Scherer, G.W. and R.M. Swiatek, *Measurement of Permeability .2. Silica-Gel.* Journal of Non-Crystalline Solids, 1989. **113**(2-3): p. 119-129.

96. Adam, M. and M. Delsanti, *Dynamical properties of polymer solutions in good solvent by Rayleigh scattering experiments.* Macromolecules, 1977. **10**(6): p. 1229.

97. Rossmurphy, S.B. and S. Todd, *Ultimate Tensile Measurements of Filled Gelatin Gels.* Polymer, 1983. **24**(4): p. 481-486.

98. Lelievre, J., I. Mirza, and J.M. Tang, *Measurement of the Tensile Failure of Gels.* Journal of Texture Studies, 1992. **23**(3): p. 349-358.

99. McEvoy, H., S.B. Ross-Murphy, and A.H. Clark, *Large deformation and ultimate properties of biopolymer gels: 2. Mixed gel systems.* Polymer, 1985. **26**(10): p. 1493-1500.

100. McEvoy, H., S.B. Rossmurphy, and A.H. Clark, *Large Deformation and Ultimate Properties of Bio-Polymer Gels .1. Single Bio-Polymer Component Systems.* Polymer, 1985. **26**(10): p. 1483-1492.

101. Cox, M.A., et al., *Mechanical characterization of anisotropic planar biological soft tissues using large indentation: A computational feasibility study.* Transactions of the ASME, 2006. **128**: p. 428-436.

102. Rossmurphy, S.B., *Rheological Characterization of Polymer Gels and Networks.* Polymer Gels and Networks, 1994. **2**(3-4): p. 229-237.

103. Ebenstein, D.M. and L.A. Pruitt, *Nanoindentation of soft hydrated materials for application to vascular tissues.* Journal of Biomedical Materials Research Part A, 2004. **69A**(2): p. 222-232.

104. Ozkan, N., H. Xin, and X.D. Chen, *Application of a depth sensing indentation hardness test to evaluate the mechanical properties of food materials.* Journal of Food Science, 2002. **67**(5): p. 1814-1820.

105. Hein, D.R., et al., *Atomistic simulations of end-linked poly(dimethylsiloxane) networks: Structure and relaxation.* Macromolecules, 2004. **37**: p. 3857-3864.

106. Wong, C.P., *Thermal-mechanical enhanced high-performance silicone gels and elastomeric encapsulants in microelectronics packaging.* IEE transactions on components, packaging, and manufacturing technology - Part A, 1995. **18**(2): p. 270-273.

107. Takahashi, H., Y. Ishimuro, and H. Watanabe, *Viscoelastic behavior of scarcely crosslinked poly(dimethyl siloxane) gel.* Journal of the Society of Rheology, Japan, 2006. **34**(3): p. 135-145.

108. Allen, G., P.L. Egerton, and D.J. Walsh, *Model Polyurethane Networks.* Polymer, 1976. **17**(1): p. 65-71.

109. Pearson, D.S. and W.W. Graessley, *Elastic Properties of Well-Characterized Ethylene-Propylene Co-Polymer Networks.* Macromolecules, 1980. **13**(4): p. 1001-1009.

110. Dossin, L.M. and W.W. Graessley, *Rubber Elasticity of Well-Characterized Polybutadiene Networks.* Macromolecules, 1979. **12**(1): p. 123-130.

111. Rubinstein, M. and S. Panyukov, *Elasticity of polymer networks.* Macromolecules, 2002. **35**(17): p. 6670-6686.

112. Kawamura, T., K. Urayama, and S. Kohjiya, *Multiaxial deformations of end-linked poly (dimethylsiloxane) networks. III. Effect of entanglement density on*

strain-energy density function. Journal of Polymer Science Part B-Polymer Physics, 2002. **40**(24): p. 2780-2790.

113. Granick, S., et al., *Stress-Relaxation and Dynamic Viscoelastic Properties of End-Linked Poly(Dimethyl Siloxane) Networks Containing Unattached Poly(Dimethyl Siloxane).* Journal of Polymer Science Part B-Polymer Physics, 1981. **19**(11): p. 1745-1757.

114. Okumura, K., *Toughness of double elastic networks.* Europhysics Letters, 2004. **67**(3): p. 470-476.

115. Baumberger, T., C. Caroli, and D. Martina, *Fracture of a biopolymer gel as a viscoplastic disentanglement process.* European Physical Journal 2006.

116. Gent, A.N. and J. Schultz, *Effect of wetting liquids on strength of adhesion of viscoelastic materials.* Journal of Adhesion, 1972. **3**(4): p. 281-294.

117. Gent, A.N. and R.P. Petrich, *Adhesion of Viscoelastic Materials to Rigid Substrates.* Proceedings of the Royal Society of London Series a-Mathematical and Physical Sciences, 1969. **310**(1502): p. 433-&.

118. Thomas, A.G., *Rupture of rubber. II. The strain concentration at an incision.* Journal of Polymer Science, 1955. **18**(88): p. 177-188.

119. H. W. Greensmith, A.G.T., *Rupture of rubber. III. Determination of tear properties.* Journal of Polymer Science, 1955. **18**(88): p. 189-200.

120. Baumberger, T., C. Caroli, and D. Martina, *Solvent control of crack dynamics in a reversible hydrogel.* Nature Materials, 2006. **5**(7): p. 552-555.

121. Brown, H.R., *The Adhesion between Polymers.* Annual Review of Materials Science, 1991. **21**: p. 463-489.

122. Lenhart, J.L. and P.J. Cole, *Adhesion properties of lightly crosslinked solvent-swollen polymer gels.* Journal of Adhesion, 2006. **82**(10): p. 945-971.

123. Taub, M.B. and R.H. Dauskardt, *Adhesion of pressure sensitive adhesives with applications in transdermal drug delivery*, in *Mater. Res. Soc. Proc.*, S. Mallapragada, et al., Editors. 2001: Warrendale, PA.

124. Carlsson, L.A., et al., *Crack path in foam cored DCB sandwich fracture specimens.* Composites Science and Technology, 2005. **65**(15-16): p. 2612-2621.

125. Crosby, A.J. and K.R. Shull, *Debonding mechanisms of PSAs.* Adhesives Age, 1999. **42**(7): p. 28-+.

126. Crosby, A.J., et al., *Deformation and failure modes of adhesively bonded elastic layers.* Journal of Applied Physics, 2000. **88**(5): p. 2956-2966.

127. Flanigan, C.M., A.J. Crosby, and K.R. Shull, *Structural development and adhesion of acrylic ABA triblock copolymer gels.* Macromolecules, 1999. **32**(21): p. 7251-7262.

128. Shull, K.R., *Fracture and adhesion of elastomers and gels: Large strains at small length scales.* Journal of Polymer Science Part B-Polymer Physics, 2006. **44**(24): p. 3436-3439.

129. Chai, H. and B.R. Lawn, *Fracture mode transitions in brittle coatings on compliant substrates as a function of thickness.* Journal of Materials Research, 2004. **19**(6): p. 1752-1761.

130. Chai, H. and B.R. Lawn, *Failure of brittle layers on polymeric substrates from Vickers indentation.* Scripta Materialia, 2006. **55**(4): p. 335-338.

131. Shergold, O.A. and N.A. Fleck, *Mechanisms of deep penetration of soft solids, with application to the injection and wounding of skin.* Proceedings of the Royal Society of London 2004. **A**(460): p. 3037-3058.

132. Shergold, O.A. and N.A. Fleck, *Experimental investigation into the deep penetration of soft solids by sharp and blunt punches, with application to the piercing of skin.* Transactions of the ASME, 2005. **127**: p. 838-848.

133. Nguyen, C. and T. Vu-Khanh, *Mechanics and mechanisms of puncture of elastomer membranes.* Journal of Materials Science, 2004. **39**(24): p. 7361-7364.

134. Jones, D.W., E.J. Sutow, and B.S. Graham, *Gel strength and rate of gelation of soft polymers.* Dental Materials, 1991. **7**(2): p. 138-144.

135. van Vliet, T. and P. Walstra, *Large deformation and fracture behavior of gels.* Faraday Discussions, 1995. **101**: p. 359-370.

136. Mazich, K.A., et al., *Threshold Fracture of Lightly Cross-Linked Networks.* Macromolecules, 1991. **24**(10): p. 2766-2769.

137. Scherer, G.W., *Viscoelasticity and permeability of silica gels.* Faraday Discussions, 1995(101): p. 225-234.

138. Agrawal, S.K., et al., *Rheological characterization of biocompatible associative polymer hydrogels with crystalline and amorphous endblocks.* Journal of Materials Research 2006. **21**(8): p. 2118-2125

139. Tanaka, Y., et al., *Determination of fracture energy of high strength double network hydrogels.* Journal of Physical Chemistry B, 2005. **109**(23): p. 11559-11562.

140. Gong, J.P., et al., *Double-network hydrogels with extremely high mechanical strength.* Advanced Materials, 2003. **15**(14): p. 1155-+.

141. Tsukeshiba, H., et al., *Effect of polymer entanglement on the toughening of double network hydrogels.* Journal of Physical Chemistry B, 2005. **109**(34): p. 16304-16309.

VITAE

Wei-Chun Lin spent most of her infant life sleeping in the oceanography lab of University of California Berkeley, while her father ran experiments in graduate school. Growing up in Boca Raton, Florida, her curiosity led her to science projects that involved throwing her stuffed animals off the roof of her family's home to determine what types of parachutes were best for slowing down falling objects. Her mother was not always pleased with her experiments.

Wei-Chun always knew she was destined for graduate school when her parents nicknamed her Chau-Jean, which means "little scholar" in Chinese. She received her Bachelors of Science in Materials Science and Engineering at Cornell University in Ithaca, New York, where she was a Cornell Presidential Research Scholar, and attended Northwestern University in Evanston, Illinois for her Doctorate in Philosophy in the same subject area. Her advisor in graduate school was Dr. Kenneth R. Shull. She will postdoc at Ecole Supérieure de Physique et de Chimie Industrielles (ESPCI) under Dr. Costantino Creton in Paris, France.